Kaho'olawe Island Conveyance Commission
Consultant Report No. 4

The Spatial Variability of Near-Surface Soil Hydraulic Properties for Kaho'olawe: A Preliminary Investigation

By:
Thomas W. Giambelluca
Keith Loague

Final Report to the *Kaho'olawe Island Conveyance Commission* "The Spatial variability of near-surface soil hydraulic properties for Kaho'olawe: A preliminary investigation"

by*

Thomas W. Giambelluca, Principal Investigator
Department of Geography
University of Hawaii, Honolulu

* prepared by: Keith Loague
Department of Soil Science
University of California, Berkeley

TABLE OF CONTENTS

APPENDICES:

INTRODUCTION

The Hawaiian island of Kaho'olawe has experienced widespread landscape degradation due to extended periods of overgrazing and military activity. Before environmental management practices can be implemented to arrest the surface erosion problem on Kaho'olawe the near-surface hydrology of the island needs to be characterized. To understand the hydrologic response characteristics of Kaho'olawe the parameters that control rainfall-runoff processes must be estimated. Before this study there was no such existing data.

Most likely, overland flow is currently the dominant factor in massive erosion losses on Kaho'olawe. Overland flow results from excess rainfall. The infiltration characteristics of land surfaces are controlled by the near-surface saturated hydraulic conductivity. In this effort we conducted a field investigation to acquire a relatively large new saturated hydraulic conductivity data set for Kaho'olawe. In the following section the anatomy of an access, designed to facilitate our field study, is described.

Anatomy of an access

The field study reported in this paper was conducted during two trips to Kaho'olawe. Each of these trips is referred to in this report as an access. The first access took place August 18th through 20th, 1991; the second access took place June 11th through 14th, 1992. The anatomy of an access is described in the remainder of this section.

The field study team departs for Kaho'olawe at about 4 a.m. from two locations on the island of Maui. The majority of the team leaves from Maalaea in a 35-foot commercial fishing boat; the crossing takes approximately one hour. This group brings the study equipment, food, water, and everything else needed for the stay on the island. The remainder of the team leaves from Makena in a PKO zodiac (rubber boat). The zodiac crew arrives at Kaho'olawe first and meets the boat crew approximately 200 m offshore from Hakioawa, where the team members and equipment are transferred. The zodiac then moves to the reef where people enter the surf and swim all the equipment and supplies (in waterproof bags) to shore. Several zodiac trips are required to down-load the boat. On the second access, three trips were required with the boat between Maalea and Hakioawa to transport everyone to the island as other activities were scheduled besides the effort reported here. Once the unloading is completed, the boat departs and the zodiac is beached at Hakioawa. At the end of an access the entire procedure is repeated, in reverse, with the boat arriving at 6 a.m.

On the island everyone camped at Hakioawa; PKO members prepared meals and organized all activities. During the data collection exercises the field study team was accompanied by U.S. Navy EOD (Emergency Ordnance Disposal) personnel. Despite the fact that sections of the island have been swept several times (since 1981), spent ordnance (occasionally undetonated) is still quite prevalent. The equipment and water necessary to conduct the experiments, along with food, was carried by the field study team.

OBJECTIVE

The objective of our two Kaho'olawe accesses was to make measurements of saturated hydraulic conductivity at as many locations, representing different land covers, as possible in relatively short periods of time. The data reported here are the first of their kind for this generally inaccessible island. The saturated hydraulic conductivity measurements, from 110 locations across Kaho'olawe, are currently being employed in a larger study, to be described in a two-part paper (Loague et al., 1992a,b) discussing (i) the distributed nature of near-surface soil-hydraulic properties, and (ii) a quasi-physically based rainfall-runoff model simulations of Horton overland flow for Kaho'olawe.

LAND COVER

Land cover classifications, for Kaho'olawe are shown in Figure 1 and listed in Table 1. The eighteen different land cover classifications in Figure 1 were based upon air photo interpretations. Illustrated here in black and white, Figure 1 was generated as a color map, using a geographic information system (GIS) approach, to show the regional scale variations in land cover. In this effort we use land cover as a surrogate for near-surface soil hydraulic property distributions in space. Relationships between sparse (yet precious) soil-hydraulic property measurements and land cover are established and extrapolated.

METHODS

The methods used in this study are easily divided into field measurements and data analysis. To make surface estimates of saturated hydraulic conductivity in the field we employed disk permeameters; soil-water contents needed for these estimates were made using time-domain reflectometry. Two statistical approaches were used for analysis of the saturated hydraulic conductivity data: classical and geostatistical methods. In the following sections the disk permeameter, time-domain reflectometry, and geostatistical methods are briefly reviewed.

Field Measurements

Disk Permeameter

Saturated hydraulic conductivity was measured at selected sites across Kaho'olawe using four CSIRO disk permeameters. The saturated hydraulic conductivity (K_s) estimates are based upon the following relationship:

$$K_s = \frac{q}{\pi r^2} - \frac{4 b S^2}{\pi r (\theta_n - \theta_i)} \qquad (1)$$

where, q is the flow rate [L^3/T], π is 3.1416, r_0 is the radius of permeameter ring [L], b is a constant (0.55), S_0 is sorptivity [$L/T^{1/2}$], θ_i is the volumetric soil-water content at the start of the measurement [dimensionless], and θ_n is the volumetric soil-water content at the end of the measurement [dimensionless]. The sorptivity is calculated from the early-time data by plotting $Q/\pi r^2$ versus the square root of time, where $Q[L^3]$ is the cumulative volume of water used in the measurement. The theory and design of the CSIRO disk permeameter is discussed by Perroux and White (1988).

Time Domain Reflectometry (TDR)

Volumetric soil-water content was measured, via the TDR approach, at the start (θ_i) and end (θ_n) of each disk permeameter measurement using the Trase System 1 (Soilmoisture, 1990). The Trase System 1 is a time domain reflectometry (TDR) approach to making indirect soil-water content measurements. TDR is an in situ technique for estimating near-surface soil-water contents via the electro-magnetic properties of the soil. The reader interested in a detailed review of TDR is directed to Davis and Annan (1977) and Topp et al. (1980).

Data Analysis

Geostatistics

The theory of regionalized variables (Journel and Huijbregts, 1978; de Marsily, 1986), was pioneered by Matheron (1971). A regionalized variable is a set of measurements and should be interpreted as a particular realization of a certain random function. Any hydrologic variable distributed in space and/or time may be considered a regionalized variable (Loague and Gander, 1990). The primary application of geostatistics is for making estimates of regionalized variables at unsampled locations. Kriging is a method of interpolation and spatial averaging with sparse data. The technique uses the structural properties of the existing data. Kriging gives the optimal unbiased estimate for a regionalized variable. In addition to the unbiased estimate, kriging provides an estimation variance. The square root of this variance is the kriging standard deviation, which is one measure of the reliability of the interpolation. Both semivariance and generalized covariance techniques, discussed below, can be employed to develop spatial structure models for kriging.

Semivariance $\gamma(\mathbf{h})$ expresses the distribution of variance as a function of separation between the spatially dependent components of a random function. A plot of $\gamma(\mathbf{h})$ versus h (the separation distance) is a semivariogram (see Figure 3). If the semivariogram is a function of distance alone, it is isotropic; however, if it is also a function of direction, it is anisotropic. The dimensions of a semivariogram are those of the measured variable squared. By definition, $\gamma(\mathbf{h}) = 0$ where $h = 0$. However, a nugget is often found in an experimental semivariogram. This discontinuity at the origin is due either to spatial variability at a scale smaller than the spacing of the data, or to measurement error. The semivariogram may reach a limiting value called the sill that is equal to the variance of the data. The distance between the origin and the point at which the sill is reached is called the range. Observations separated by distances greater than the range are not correlated. If measurements are totally without correlation, the experimental semivariogram will exhibit a pure nugget effect.

A regional variable is described by the drift and covariance structure of the observed data. The drift is the deterministic component that represents slowly decaying continuous features. The covariance is the spatially fluctuating random variable with zero expectation. The theory of regionalized variables has a troublesome paradox. To estimate a semivariogram requires knowledge of the drift, but the semivariogram itself must be known to determine the drift. Both the semivariogram and the drift must be estimated from the data. If the drift is constant, then the semivariogram can be estimated directly from the data without bias. In general, however, the drift may not be a constant. A method that was developed by Matheron (1973) and further expanded by Delfiner (1976) circumvents the paradox mentioned here by eliminating the need to estimate the drift. In this method the spatial process is viewed as an intrinsic random function (IRF) that may achieve stationarity by filtering. An IRF that requires a kth-order increment to achieve stationarity is denoted by k-IRF.

Increments of order zero, one, and two filter out constant, linear, and quadratic drifts, respectively. The conditions that filter out drift are summarized by Loague and Gander (1990). In this study we use semivariance and generalized covariance techniques to characterize the spatial variability of surface saturated hydraulic conductivity (and sorptivity) values for the Kaho'olawe data sets.

DATA SUMMARY

The saturated hydraulic conductivity (and sorptivity) values determined for the 110 Kaho'olawe measurement sites (Figure 2) are given in Table 2. The general selection of the measurement sites was based upon our desire to represent the spatial variations in land cover, taken loosely as a surrogate for saturated hydraulic conductivity, and strict time constraints. At each of the 110 sites, representation of small-scale variability dictated the location of the measurement. It was not possible to establish multiple measurement sites for all the land-cover classifications listed in Table 1 due to the time limitations of the two Kaho'olawe accesses. Therefore, we grouped the 18 classifications in Table 1 into the three revised land-cover classifications listed in Table 3. The land-cover classifications in Table 3 are used to group the estimates of saturated hydraulic conductivity (and sorptivity) into three classes.

Inspection of Table 2 shows that there is tremendous variability in the saturated hydraulic conductivity (and sorptivity) measurements across Kaho'olawe; the maximum and minimum values being 4.2×10^{-3} m/s and 1.9×10^{-8} m/s, respectively. The mean (harmonic) saturated hydraulic conductivity value for the 110 estimates is 1.5×10^{-6} m/s. The uncertainty in these estimates (represented by the standard deviation is 4.3×10^{-4} m/s. The coefficient of variation (standard deviation/arithmetic mean) for the entire saturated hydraulic

conductivity data set is a fairly large 3.6; therefore, the average value is unlikely to be a representative "effective value" for the island.

RESULTS

The statistical characteristics of the 110 saturated hydraulic conductivity and sorptivity estimates, based upon the land cover classifications in Table 3, are given in Tables 4 and 5, respectively. The spatial structure of saturated hydraulic conductivity (and sorptivity) across Kaho'olawe, based upon the 110 estimates for each parameter, is represented by the two-dimensional directional semi-variograms shown in Figure 4 and the generalized covariance parameters given in Table 6.

Perusal of the results in Tables 4 through 6 and Figure 4 leads to the following generalized comments:

(i) The average saturated hydraulic conductive value are greatest for the grass and smallest for the exposed surface land covers, as should be expected.

(ii) There is considerable uncertainty in the saturated hydraulic conductivity estimates for three land covers; coefficients of variation of 5.3, 1.4, and 1.9 for the A, B, and C land covers, respectively.

(iii) The range in saturated hydraulic conductivity estimates for the exposed surface land cover (A) is almost five orders of magnitude; for the other two land covers (B and C) and the combination of B and C (vegetated surfaces) the range is much smaller.

(iv) The sorptivity data for all three land covers is very similar; the uncertainties are much smaller than for the saturated hydraulic conductivity estimates.

(v) There appears to be no spatial structure for either the saturated hydraulic conductivity or sorptivity data.

DISCUSSION AND CONCLUSIONS

The field study undertaken for this study was highly successful, providing a new and unique data set of near-surface soil hydraulic property information for Kaho'olawe. The large variability (within and between land covers) and uncertainty in the saturated hydraulic conductivity data provide physically-based process evidence that hydrologic response is extremely variable on Kaho'olawe. It was not possible in this study to do any spatial interpolation of the Kaho'olawe data with geostatistical methods (kriging) as there was no structure in the data.

The saturated hydraulic conductivity (and sorptivity data) reported here will facilitate the simulation of rainfall-runoff response for Kaho'olawe for different size events with a quasi-physically based rainfall-runoff model (see Loague, 1990) of Hortonian overland flow (this is an ongoing effort; see Loague et al., 1992a,b). The rainfall-runoff simulations will subsequently enable us to simulate landscape evolution processes under alternative environmental management strategies focused upon the restoration of Kaho'olawe through revegetation and erosion reduction.

ACKNOWLEDGMENTS

The work described here could not have been undertaken without the invitation and cooperation of the Protect Kaho'olawe 'Ohana (PKO). We are extremely grateful to those who worked with us on Kaho'olawe. The first access team was Rod Adlawan (O'ahu), Dan Holmes (Maui), Kim Kanoa (O'ahu), Kalani Pruzt (O'ahu), Craig Rowland (O'ahu), and Steven Vana (O'ahu). The second access team was Fiona Dempster (O'ahu), Dan Holmes (Maui), Mike Kamaka (O'ahu), Mike Parke (O'ahu), Dave Penn (O'ahu), and Kalikiano Rose (Maui). The U.S. Navy supported us on both of our accesses; in particular we would like to thank Lieutenant Veronon Young (O'ahu) for his assistance. We are also grateful to Dick Green from the University of Hawaii for the loan of some equipment on the second access. The analysis reported here was performed by Keith Loague, Anh Nguyen, and D'Artagnon Lloyd, at the University of California, Berkeley. The land cover map was generated by Yuan Qing Li, Fang Tao, and Yuhao Wang from the Department of Geography at the University of Hawaii. The figures were drafted by Frank Murillo (Berkeley). Finally, we wish to extend our heartfelt *Mahalo Nui Loa* to Keoni Fairbanks (Maui), Davianna McGregor (O'ahu), Rendall Tong (O'ahu), Hardy Spoehr (O'ahu), and Uncle Les (Maui), for their awesome assistance. This effort was supported by the Kaho'olawe Island Conveyance Commission.

REFERENCES

Davis, J.L. and A.P. Annan. Electromagnetic detection of soil moisture: Progress Report I. *Can. J. Remote Sens. 3*, 76–86. 1977.

Delfinger, P. Linear estimation of non-stationary spatial phenomena, in *Advanced Geostatistics in the Mining Industry*, edited by M. Gvarascio et al., pp. 49–68, D. Reidel, Hingham, Mass. 1976.

de Marsily, G. Quantitative Hydrogeology: Groundwater Hygrology for Engineers, pp. 284–337, Academic, San Diego, Calif. 1986.

Journel, A.G., and Ch. J. Huijbregts. Mining and Geostatistics, 600 pp., Academic, San Diego, Calif. 1978.

Loague, K., and G.A. Gander. R-5 revisited: 1. Spatial variability of infiltration on a small rangeland catchment. *Water Resour. Res., 26*, 957–971. 1990.

Loague, K., T.W. Giambelluca, B. Sakata, D. Lloyd, and A. Nguyen. The implication of land use on hydrologic relationships; Kaho'olawe, Hawaii: 1. Background, Field study, and spatial analysis. *Water Resources Research* (now in preparation), 1992a.

Loague, K., A. Nguyen, D. Lloyd, and T.W. Giambelluca. The implication of land use on hydrologic relationships; Kaho'olawe, Hawaii: 1. Simulation of Horton overland flow generation areas. *Water Resources Research* (now in preparation), 1992b.

Loague, K. R-5 revisited: 2. Reevaluation of a quasi-physically based rainfall-runoff model with supplemental information. *Water Resources Research*, 26, 973–987, 1990.

Matheron, G. *The Theory of Regionalized Variables and its Applications*, Les Cahiers du Centre de Morphologie Mathematique, Fasc. 5, CG Fontainebleau. 1971.

Matheron, G. The intrinsic random functions and their applications, *Adv. Appl. Probl., 5*, 439–468. 1973.

Perroux, K.M., and I. White. Designs for disk permeameters. *Soil Science Society America,* 52:1205–1215. 1988.

Soilmoisture. TRASE System 1: Operating Instructions, 53 pp., Santa Barbara, Calif. 1990

Topp, G.C., J.L. Davis, and A.P. Annan. Electromagnetic determination of soil water content: Measurements in coaxial transmission lines. *Water Resources Research, 16* 574–582. 1980.

LIST OF TABLES

Table 1. Land cover classifications for Kaho'olawe as shown on Figure 4.

Land cover class	Description	Percentage of Island
1	Exposed soil or subsoil – dark color*	0.5
2	Exposed or subsoil – medium color	19.9
3	Gullied-exposed soil or subsoil – medium color	0.1
4	Exposed soil or subsoil – light color	4.6
5	Gullied – exposed soil or subsoil – light color	0.8
6	Sea cliff – exposed soil or subsoil – light color	0.6
7	Shrubs and trees – high density	8.0
8	Sea cliff – shrubs and trees – high density	0.4
9	Shrubs and trees – medium density	46.6
10	Gullied – shrubs and trees – medium density	0.2
11	Sea cliff – shrubs and trees – medium density	0.7
12	Shrubs and trees – low density	11.6
13	Gullied – shrubs and trees – low density	0.2
14	Sea cliff – shrubs and trees – low density	1.3
15	Grass	3.8
16	Gullied – grass	0.2
17	Sea cliff – grass	0.3
18	Beach	0.2

* Color is keyed to Figure 1.

Table 2. Saturated hydraulic conductivity and sorptivity estimates from two Kaho'olawe accesses.

Measurement[1] Number	Location[2]; x,y (m)	Saturated Hydraulic Conductivity, K_s (m/s)	Sorptivity, S ($m\ s^{-1/2}$)	Land cover classification[3]
1	17200,11975	8.7E-6*	1.8	C
2	17210,11975	2.6E-5	1.6	C
3	17000,11700	1.5E-5	1.0	A
4	17010,11700	5.5E-5	1.5	A
5	16675,11475	6.1E-5	1.1	A
6	16685,11475	1.1E-5	0.7	A
7	15875,10925	1.0E-5	1.1	A
8	15885,10925	4.5E-6	0.7	B
9	15950,10925	5.3E-5	1.1	A
10	15960,10925	8.9E-6	0.5	A
11	15900,10900	4.9E-5	1.8	C
12	15910,10900	1.4E-4	1.5	C
13	15825,11150	1.9E-5	0.7	A
14	15835,11150	1.0E-5	1.0	A
15	15775,10375	1.9E-5	0.8	C
16	15785,10375	3.1E-5	0.9	C
17	15765,10375	8.4E-6	1.2	C
18	15775,10365	1.2E-5	2.0	C
19	15775,10385	7.0E-6	1.7	C
20	15765,10385	7.8E-4	1.6	C
21	15785,10385	2.2E-5	1.4	C
22	15765,10365	1.3E-5	1.3	C
23	15785,10365	3.5E-5	1.2	C
24	15765,10395	4.3E-5	0.9	C
25	15775,10395	1.2E-5	1.3	C
26	15785,10395	8.9E-5	1.6	C
27	15525,8600	2.4E-5	0.1	A
28	15535,8600	3.6E-7	0.3	A
29	16585,9595	7.8E-5	1.7	C
30	16600,9600	1.2E-3	0.7	C

Table 2 — continued

Measurement[1] Number	Location[2]; x,y (m)	Saturated Hydraulic Conductivity, K_s (m/s)	Sorptivity, S ($m\ s^{-1/2}$)	Land cover classification[3]
31	16615,9610	2.7E-7	0.3	A
32	16620,9620	3.3E-6	0.3	A
33	16595,9595	1.0E-4	0.9	C
34	16610,9600	1.9E-5	2.0	C
35	16695,10025	1.2E-5	1.6	A
36	16700,10025	9.9E-6	1.1	A
37	16700,10030	4.3E-6	1.6	B
38	16705,10025	5.2E-5	1.4	A
39	16635,11095	4.6E-6	1.6	A
40	16645,11080	2.4E-5	0.6	A
41	16640,11075	2.5E-5	1.3	A
42	4055,4750	7.7E-4	0.9	C
43	4050,4735	9.1E-4	0.1	B
44	4055,4735	1.6E-4	0.8	B
45	4065,4750	3.5E-4	0.9	C
46	4060,4735	3.0E-4	0.8	B
47	4065,4735	7.4E-4	1.6	B
48	4685,2155	1.4E-4	2.3	B
49	4685,2140	2.0E-5	1.2	B
50	4705,2175	4.9E-6	0.8	C
51	4680,2155	5.3E-5	2.3	B
52	4705,2170	1.5E-5	1.6	B
53	4715,2170	2.1E-5	1.0	A
54	6625,3965	3.6E-6	0.9	B
55	6595,3970	1.8E-5	1.3	A
56	6590,3985	1.7E-5	1.2	C
57	6615,3960	1.6E-5	1.3	B
58	6585,3975	2.9E-5	1.0	B
59	6595,3975	1.6E-5	0.3	C
60	9135,6035	3.0E-5	1.8	B
61	9135,6030	2.6E-5	0.7	A

Table 2 — continued

Measurement[1] Number	Location[2]; x,y (m)	Saturated Hydraulic Conductivity, K_s (m/s)	Sorptivity, S ($m\ s^{-1/2}$)	Land cover classification[3]
62	9145,6035	1.9E-8	0.9	A
63	9140,6035	6.5E-5	1.8	B
64	9140,6030	2.7E-5	0.7	A
65	9145,6040	1.2E-5	1.1	A
66	8920,5975	6.9E-6	1.1	A
67	8905,5940	4.6E-6	0.8	A
68	8925,5955	3.3E-5	1.6	A
69	8920,5980	1.1E-5	0.6	A
70	8905,5935	5.0E-4	0.7	C
71	8925,5960	5.1E-5	1.1	A
72	15980,8640	8.7E-5	1.5	A
73	15995,8640	2.7E-5	0.6	A
74	16020,8640	3.3E-6	0.5	A
75	16035,8640	3.1E-5	1.1	A
76	15965,8640	3.1E-5	0.9	A
77	15950,8640	5.8E-7	0.4	A
78	16015,8640	4.2E-3	0.8	A
79	16040,8640	1.1E-5	0.6	A
80	12415,6205	7.9E-6	0.6	A
81	12420,6205	2.8E-6	0.4	A
82	12415,6200	8.2E-5	1.4	A
83	12420,6195	2.7E-5	1.1	A
84	12425,6205	4.2E-5	1.3	A
85	12420,6200	2.1E-5	1.2	C
86	14110,6920	2.0E-6	1.7	A
87	14140,6940	4.8E-5	1.2	A
88	14125,6930	4.2E-5	1.1	A
89	14150,6950	4.0E-5	0.9	C
90	14120,6920	2.6E-4	0.8	A
91	14150,6940	5.4E-5	1.0	C
92	14135,6930	4.7E-7	0.8	A

Table 2 — continued

Measurement[1] Number	Location[2]; x,y (m)	Saturated Hydraulic Conductivity, K_s (m/s)	Sorptivity, S ($m\ s^{-1/2}$)	Land cover classification[3]
93	14160,6950	9.6E-6	0.9	C
94	14115,6930	5.7E-7	0.6	A
95	15755,5300	3.8E-5	0.2	C
96	15750,5310	1.2E-4	0.6	C
97	15750,5315	8.0E-6	0.9	C
98	15765,5320	2.4E-5	2.0	C
99	15135,8110	6.0E-5	1.0	C
100	16120,8100	4.6E-5	0.9	C
101	15125,8110	2.5E-5	0.6	A
102	15135,8130	2.7E-5	2.0	C
103	15935,8510	2.0E-5	1.5	A
104	15965,8515	8.9E-5	1.7	C
105	15945,8510	5.7E-5	1.3	B
106	15955,8510	1.4E-4	1.6	C
107	15940,8510	5.5E-5	2.2	C
108	15970,8515	2.7E-4	0.7	B
109	15950,8510	1.6E-4	1.0	C
110	15960,8510	7.4E-5	1.4	C
Harmonic mean		1.5E-6	0.8	
Arithmetic mean		1.2E-4	1.1	
Geometric Mean		2.5E-5	1.0	
Standard Deviation		4.3E-4	0.5	
Maximum value		4.2E-3	2.3	
Minimum value		1.9E-8	0.1	
Median		2.6E-5	1.1	

[1] Measurements 1–28; August 18–20, 1991; measurements 29–110; June 11–14, 1992
[2] See Figure 2
[3] See Table 3
* 8.7E-6 = 8.7×10^{-6}

Table 3. Land cover classification used to group saturated hydraulic conductivity (K_s) and sorptivity (S) estimates.

Land Cover	Description	Percentage of Island	Used to represent classifications in Table 1
A	Exposed soil or subsoil	26.5	1–6
B	Shrubs and trees	69.0	7–14
C	Grass	4.5	15–18

Table 4. Statistical characteristics of saturated hydraulic conductivity estimates based upon land cover.

Land Cover[1]	Saturated Hydraulic Conductivity			
	number of measurements	mean values* (m/s)	standard deviation (m/s)	maximum and minimum values (m/s)
A	51	7.3E-7* 1.1E-4** 1.3E-5*** 2.0E-5****	5.8E-4	4.2E-3 1.9E-8
B	17	1.6E-5 1.7E-4 5.0E-5 1.6E-5	2.4E-4	9.2E-4 3.6E-6
C	42	2.3E-5 1.3E-4 4.5E-5 4.0E-5	2.5E-4	1.2E-3 4.9E-6
vegetated surfaces (B,C)	59	2.1E-5 1.4E-4 4.6E-5 4.0E-5	2.5E-4	1.2E-3 3.6E-6

[1] See Tables 1–3 and Figures 1 and 2.

* Harmonic mean; **arithmetic mean; ***geometric mean; ****median

Table 5. Statistical characteristics of sorptivity estimates based upon land cover.

Land Cover[1]	Sorptivity (S)			
	number of measurements	mean values ($m\ s^{-1/2}$)	standard deviation ($m\ s^{-1/2}$)	maximum and minimum values ($m\ s^{-1/2}$)
A	51	0.6*	0.4	1.7
		0.9**		0.1
		0.8***		
		1.0****		
B	17	0.8	0.6	2.3
		0.6		0.1
		1.1		
		1.3		
C	42	1.0	0.5	2.2
		1.2		0.2
		1.1		
		1.2		
vegetated surfaces (B,C)	59	0.9	0.5	2.3
		1.3		0.1
		1.1		
		1.2		

[1] See Tables 1–3 and Figures 1 and 2.

* Harmonic mean; ** arithmetic mean; *** geometric mean; **** median

Table 6. Parameters identified for the best-fit generalized covariance models for near-surface soil hydraulic property data for Kaho'olawe.

Parameter	Number of estimates	Order	Nugget, C	b_0	b_1	b_2
Saturated hydraulic conductivity	110	0	3.17	0	0	0
Sorptivity	110	0	0.282	0	0	0

LIST OF FIGURES

Figure 1

FIGURE 2

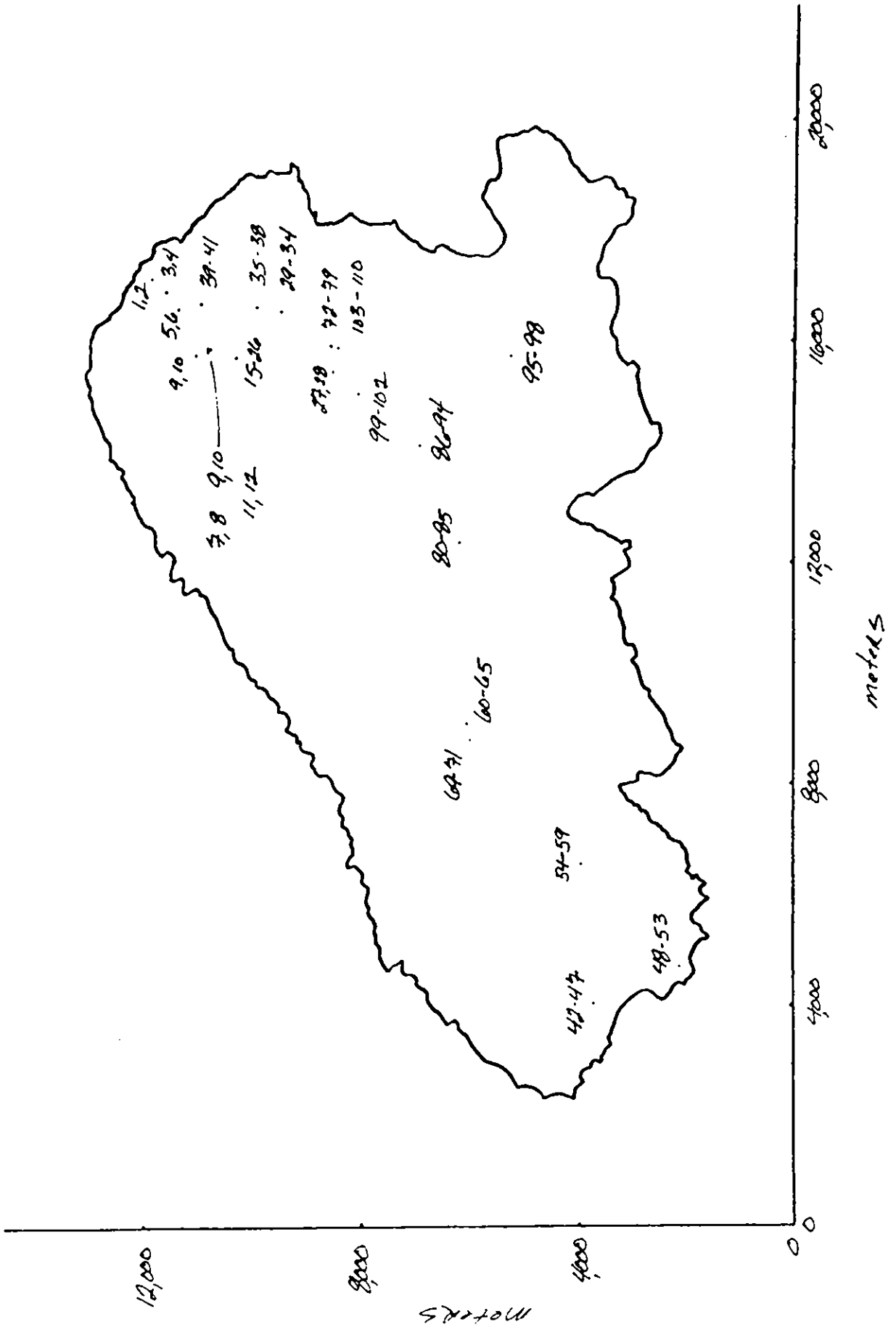
12,000
8000
4000
0
meters
0
4000
8000
12,000
16,000
20,000
meters
1,2
5,6
3,4
9,10
39-41
7,8
9,10
11,12
15-26
35-38
29-34
27-28
72-79
103-110
99-102
80-85
86-94
95-98
64-71
60-65
54-59
42-47
48-53

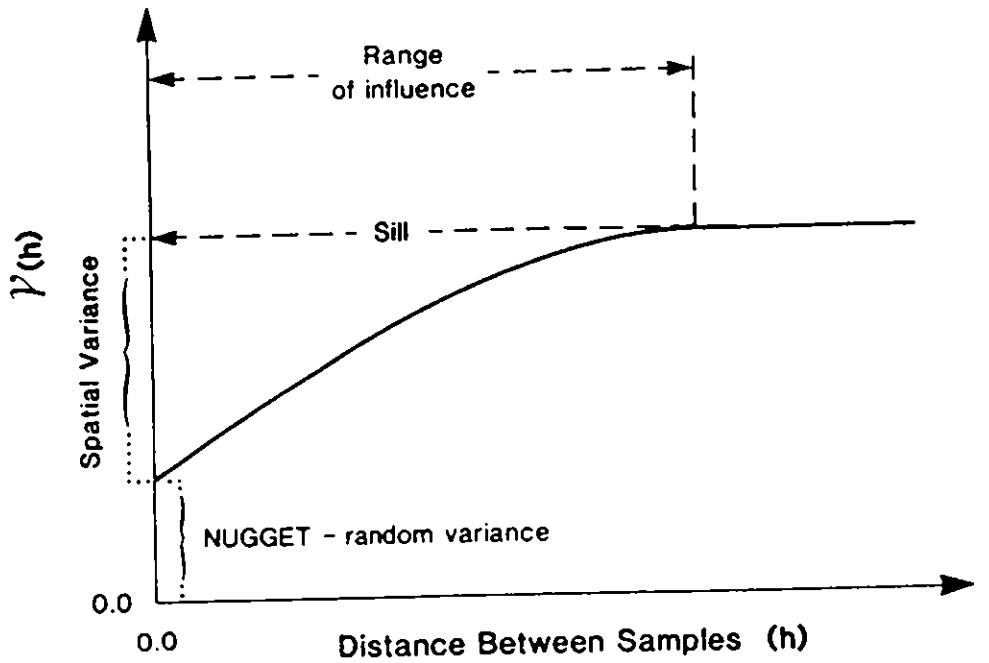
Range
of influence
Sill
γ(h)
Spatial Variance
NUGGET - random variance
0.0
0.0
Distance Between Samples (h)

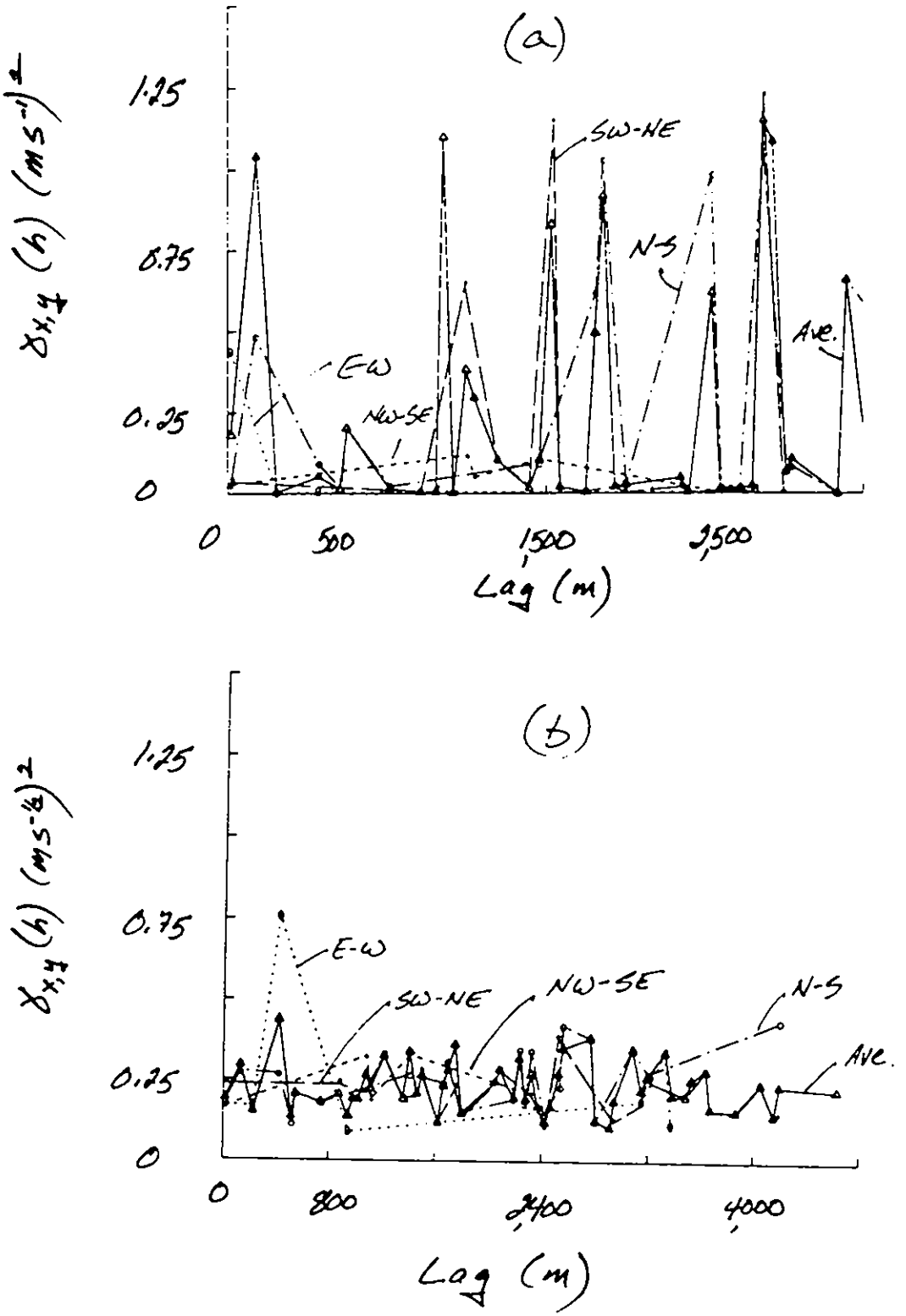
(a)
1.25
0.75
0.25
0
0
500
1,500
2,500
Lag (m)
E-W
NW-SE
SW-NE
N-S
Ave.
(b)
1.25
0.75
0.25
0
0
800
2,400
4000
Lag (m)
E-W
SW-NE
NW-SE
N-S
Ave.

APPENDICES

Electromagnetic Determination of Soil Water Content: Measurements in Coaxial Transmission Lines

G. C. Topp

Land Resource Research Institute, Agriculture Canada, Ottawa, Canada K1A 0C6

J. L. Davis[1] and A. P. Annan[2]

Geological Survey of Canada, Energy, Mines and Resources Canada, Ottawa, Canada K1A 0E8

The dependence of the dielectric constant, at frequencies between 1 MHz and 1 GHz, on the volumetric water content is determined empirically in the laboratory. The effect of varying the texture, bulk density, temperature, and soluble salt content on this relationship was also determined. Time-domain reflectometry (TDR) was used to measure the dielectric constant of a wide range of granular specimens placed in a coaxial transmission line. The water or salt solution was cycled continuously to or from the specimen, with minimal disturbance, through porous disks placed along the sides of the coaxial tube.

Four mineral soils with a range of texture from sandy loam to clay were tested. An empirical relationship between the apparent dielectric constant K_a and the volumetric water content θ_v, which is independent of soil type, soil density, soil temperature, and soluble salt content, can be used to determine θ_v from air dry to water saturated, with an error of estimate of 0.013. Precision of θ_v to within ±0.01 from K_a can be obtained with a calibration for the particular granular material of interest. An organic soil, vermiculite, and two sizes of glass beads were also tested successfully. The empirical relationship determined here agrees very well with other experimenters' results, which use a wide range of electrical techniques over the frequency range of 20 MHz and 1 GHz and widely varying soil types. The results of applying the TDR technique on parallel transmission lines in the field to measure θ_v versus depth are encouraging.

Introduction

Soil water content and the availability of water are fundamentally important to land activities, especially those involving agriculture, forestry, hydrology, and engineering. Knowledge of soil water contents over extensive areas is necessary for use in crop yield optimization and flood control. Currently available methods involve point measurements, which are too costly for extensive use, or remotely sensed techniques, which at best detect only surface conditions.

The neutron moderation technique has come into regular use for monitoring at established sites. The need for site calibration and the inherent radiation hazard make this technique less than ideal. Although the removal of samples and measuring their water content is both direct and reliable, the technique is destructive, time consuming, and thus impractical for large-scale determinations.

An ideal method would use a soil physical property, which is a function primarily of water content and which can be measured directly and reliably. In the frequency range of 1 MHz to 1 GHz, the real part of the complex dielectric constant (K') is not strongly frequency dependent, however, K' appears to be highly sensitive to the volumetric water content (θ_v) and weakly sensitive to soil type and density as discussed by *Nikodem* [1966], *Thomas* [1966], *Lundien* [1971], *Cihlar and Ulaby* [1974], *Hipp* [1974], *Hoekstra and Delaney* [1974], *Davis and Annan* [1977], and *Davis et al.* [1977]. Unfortunately, the reliability of published data that cover this frequency range is dubious, since the systems used for measuring the electrical properties were usually designed either for frequencies up to the MHz range or for frequencies in the microwave region (i.e., down to 1 GHz), and thus the 1-MHz to 1-GHz band was usually at the limit of the measuring systems.

The objective of the work reported here was to establish in the laboratory the dependence of K' on θ_v over this frequency range for a wide range of materials and in particular soils. The time-domain reflectometry technique used is reasonably simple to implement and is analogous to short-pulse radar systems [*Annan and Davis*, 1978], which may also prove to be practical for measuring soil water content rapidly and reliably.

Electrical Properties of Soils

A general discussion of the electrical properties of heterogeneous materials was given in *de Loor* [1956], *Chernyak* [1964], *van Beek* [1965], *Pearce et al.* [1973], *Selig* [1975], *Davis and Annan* [1977], *Wobschall* [1977], and *Wang and Schmugge* [1978]. These papers convinced us of the complexities of the electrical properties of wet soils and the need for reliable empirical data.

The electrical notation used in this paper is

$$K^* = K' + jK'' = K' + j(\sigma_{dc}/\omega\epsilon_0) \quad (1)$$

where K^* is the complex dielectric constant, K' is the real part of the dielectric constant, K'' is the imaginary part of the dielectric constant or the electric loss, σ_{dc} is the zero-frequency conductivity, ω is the angular frequency, ϵ_0 is the free-space permittivity, and j is $(-1)^{1/2}$. The magnetic properties of virtually all geologic materials do not vary significantly from the magnetic properties of free space. Therefore, the effect of variations in magnetic properties do not have to be considered when making electromagnetic measurements.

The variables which affect the electrical response in soils are texture, structure, soluble salts, water content, temperature, density, and measurement frequency. The most important variable is the excitation frequency. Over the frequency range of 1 MHz to 1 GHz, the real part of the dielectric constant does not appear to be strongly frequency dependent [*Davis and Annan*, 1977]. It is therefore unlikely that there ex-

[1] Now with Ensco Incorporated, Springfield, Virginia
[2] Now with Barringer Research, Toronto, Canada.

Paper number 9W1751.
0043-1397/80/009W-1751$01.00

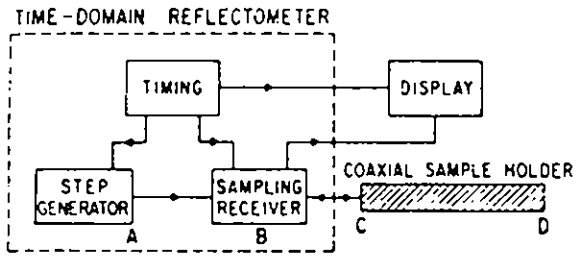

(a)

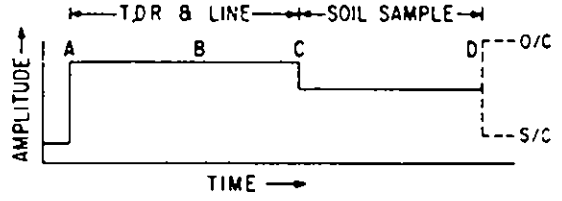

(b)

Fig. 1. (*a*) Block diagram of time-domain reflectometer (TDR) connected to soil sample holder. (*b*) An idealized representation of the TDR output from measurement on a soil sample; time interval C–D represents the travel time in the soil sample. O/C, S/C indicate open circuit and short circuit, respectively.

ist any relaxation mechanisms which impart strong temperature dependence to the real dielectric constant K'. *Davis and Annan* [1977] also indicated that the dielectric loss K'' was considerably less than K' in this frequency range.

Experimental Procedures

The experimental procedures are drawn from both electronics and soil science and have been separated into the following categories: (a) the TDR technique, (b) the coaxial transmission line soil column, (c) the soils and other porous media, and (d) the experimental variations applied to the soils.

The TDR Technique

The TDR technique as applied to the measurement of the electrical properties of materials was given in *Fellner-Feldegg* [1969]. A discussion of TDR applied to soils can be found in *Davis and Chudobiak* [1975] and Davis et al. (unpublished manuscript, 1980). Briefly, the propagation velocity (V) of an electromagnetic wave in a transmission line of a known length is determined.

$$V = c \left/ \left(K' \frac{1 + \{1 + \tan^2 \delta\}^{1/2}}{2} \right)^{1/2} \right. \tag{2}$$

where c is the velocity of an electromagnetic wave in free space (3×10^8 m/s) and

$$\tan \delta = \{K'' + (\sigma_{dc}/\omega\epsilon_0)\}/K' \tag{3}$$

If $\tan \delta$ is much less than 1 then

$$V \approx c/(K')^{1/2} \tag{4}$$

For all the soils studied by the authors, to date the electric loss has been small and has not significantly altered the measured propagation velocity. Even though not measurable, the effects of electrical loss did exist in our estimate of K', therefore we called our measured dielectric constant the apparent dielectric constant K_a. Thus for low-loss, nearly homogenous materials

$$K_a \approx K'$$

Figure 1(*a*) is a block diagram of the TDR system. The TDR source generated a fast rise time step function, as shown in Figure 1(*b*) at A. The step propagated down a standard transmission line through the receiver B to the transmission line under test C.

The receiver used an electronic sampling technique to put out a lower-frequency facsimile of the high-frequency input. The sampling principle is analogous to the principle of optical stroboscopes, which are used to make rapidly moving things appear to be at rest or moving very slowly. Many transmitted pulses were generated by the TDR in the time necessary to produce a scan, which was displayed on the record. The timing circuits of the sampling receiver were synchronized with the source. The TDR output consisted of a signal, which was displayed on a cathode ray tube and photographed, or plotted on an x-y plotter, and the data could also be recorded on analog or digital magnetic tape for future signal processing. A number of TDR systems are available. For the readers' benefit we include the name of the TDR system used in this study—Tektronix Model 7S12 TDR sampler with S-52 and S-6 pulse generator and sampling heads in a 7603 oscilloscope main frame.

The transmission line under test, C, usually had different electrical characteristics from the standard transmission line in the TDR, and thus part of the signal was reflected and part of the signal continued down the line to its end D, where all the signal was reflected from either an open or short circuit. Measuring the travel time of the step between C and D and knowing the transmission line length, we determined the propagation velocity V and thus derived K_a. Davis et al. (unpublished manuscript, 1980) discuss the practical details of the electrical responses observed and the interpretation technique used.

The Coaxial Transmission Line Soil Column

A coaxial soil container of 5-cm inside diameter was chosen as a minimum size that would give an adequate sampling of soil conditions when applied to transmission lines in the field. The necessary electrical response was verified by measuring K_a of water (81.5 at 20°C) and K_a of air (1) to better than 2% of reading. Since soil at all water contents measured somewhere between these limiting values, we assumed the trans-

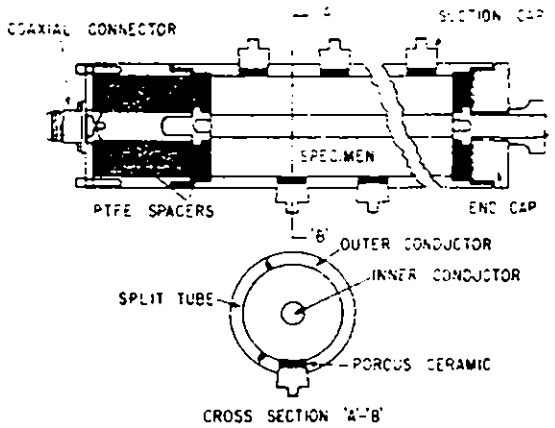

Fig. 2. Diagram of the coaxial transmission line soil column, showing the position relationship of the ceramic-capped cups.

mission line design was adequate for the intermediate values. This meant that these laboratory results could be applied directly to field measurements by using parallel transmission lines with 5-cm spacing [*Davis and Chudobiak*, 1975].

The lengths of the soil in the coaxial lines were either 1.0 m or 0.33 m, depending on the expected electrical loss in the soil under test. In a soil having high electrical attenuation (loss), the shorter transmission line length improved the precision of determining the electrical response from the end of the line.

Water was inserted into or removed from the soil, with minimal disturbance, through 1-cm-diameter porous ceramic disks spaced 5 cm apart on two sides of the coaxial sample holder as shown in Figures 2 and 3. PTFE (polytetrafluoroethylene, also known by the trade name Teflon) disks 1 cm thick were placed at the ends of the sample to hold in the soil and water and to support the center conductor. The water added or removed was measured in burettes with a precision better than 0.5% of the total sample volume (615 cm^3 or 1844 cm^3). The water content throughout the experiment was known to within 1%.

Usually water was added until it just began to flow out of the ends of the sample holder and then dried first under gravity and then suction. The wetting and drying cycles could be repeated as often as desired for any particular experiment. At the end of the final drying cycle the split coaxial soil sample holder was opened in half along its length, and the soil water content was measured, using regular gravimetric techniques. The air dry soil water content of the soil put into the holder was always determined before water was added. The soil density was measured before and after the wetting took place, and it was found that these density measurements agreed to better than 1%, in all cases.

Soils and Other Porous Media

In the initial evaluation of the TDR procedure, four mineral soil materials were chosen to give a wide range of textures (sandy loam to clay) and varying organic matter contents. The particle size distributions and percentages of organic material are listed in Table 1. As a further test of the applicability of these techniques, an organic soil, ground vermiculite mineral, and two sizes of glass beads were also studied. It was assumed that this range of materials, although chemically simpler, individually, than soil, would represent the chemical and physical extremes of pore sizes and surface properties encountered in soil and thus would represent the range of electrical properties given by soil materials. Using materials with well-defined physical properties, e.g., glass beads, allowed technique or equipment comparisons to be carried out.

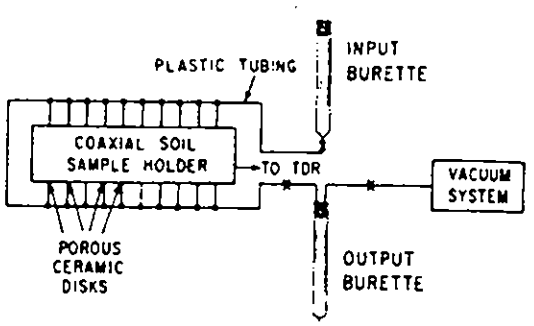

Fig. 3. Diagram of the water input and removal procedure.

The mineral soil materials were taken from the field, dried in air at room temperature, and passed through a 2-mm sieve. The vermiculite mineral was ground to pass through a 0.5-mm sieve. The organic soil was dried at room temperature in air, but was not sieved. All of these porous media, except the organic soil, were packed into the coaxial cylinders by using mechanical vibration of the cylinder, while a rotating funnel carefully deposited material around the center conductor of the coaxial cylinder. This method was a modification of that of *Jackson et al.* [1962] and was found to give very uniform lateral and longitudinal deposition of the materials. The organic soil was packed into the cylinder by manually adding increments of a few grams of soil to the cylinder and packing each one on the last one by using a disc which had clearance on the center conductor and walls of the coaxial cylinder.

Experimental Variations Applied

A series of 18 different experiments were carried out to ascertain the influence of selected parameters on the relationship between water content and apparent dielectric constant. A list of the experiments is presented as rows in Table 2, and variations on the parameters of each experiment are given in the columns.

In column B the size given for glass beads represents the median value, and the bracketed number gives the range of particle sizes. Column F gives the range and cyclic pattern of water content changes applied to each experiment in which the dielectric constant was measured. A sequence of numbers such as 0.018/0.431, 0.192, 0.415 means TDR measurements were made at θ_v = 0.018 (air dry) but not again until θ_v = 0.431, and then at θ_v increments of <0.02, during decreasing water content, to θ_v = 0.192, followed by increasing θ_v to 0.415, etc. Column H indicates the figure in which the data from each experiment have been presented.

The experiments were chosen to find out the effects of texture, bulk density, temperature, salinity, and hysteresis on the

TABLE 1. Soil Type, Particle Size Distribution, and Percentage of Organic Material of the Four Mineral Soils Tested

Soil Type, Depth in Centimeters	Percentage of Clay, <0.002 mm	Percentage of Silt, 0.002–0.05 mm	Percentage of Sand, 0.05–2.0 mm	Percentage of Organic Material	Textural Class
Rubicon (0–20 cm)	9	26	65	3	sandy loam
Bainsville (0–20 cm)	34	36	30	6	clay loam
Bainsville (40–50 cm)	36	42	22	1	clay loam
Bainsville (90–110 cm)	66	31	3	0	heavy clay

TABLE 2 Experiments Performed to Establish the Relationship Between Water Content and Apparent Dielectric Constant

Experiment	Medium	Size or Texture	Depth in Field	Dry Density During Study, gm cm^{-3}	Solution	Water Content, θ, Range, and Cycles	Date, Duration of Experiment, Days	Data Appear in Figure
1	Rubicon soil	sandy loam	0–20 cm	1.43	0.01 N $CaSO_4$	0.018/0.431, 0.192, 0.415, 0.223	6/16/1976 (11)	4, 5
2	Rubicon soil	sandy loam	0–20 cm	1.44	0.01 N $CaSO_4$	0.02, 0.431, 0.218	4/12/1977 (13)	4, 5, 8
3	Rubicon soil	sandy loam	0–20 cm	1.32	0.01 N $CaSO_4$	0.016, 0.455, 0.336, 0.403, 0 297, 0.407, 0.34	4/22/1977 (30)	4, 5
4	Rubicon soil	sandy loam	0–20 cm	1.38	2000 ppm NaCl	0 022, 0.449, 0.396	9/2/1977 (3)	8
5	Bainsville soil	clay loam	0–20 cm	1.23	0.01 N $CaSO_4$	0.072/0.458, 0.261, 0.439, 0 286	6/24/1976 (15)	4
6	Bainsville soil	clay loam	0–20 cm	1.23	0.01 N $CaSO_4$	0.324		7
7	Bainsville soil	clay loam	40–55 cm	1.04	0.01 N $CaSO_4$	0.069/0.532, 0.348, 0.501, 0.340	7/12/1976 (12)	4
8	Bainsville soil	clay loam	40–55 cm	1.04	0.01 N $CaSO_4$	0.073, 0.526, 0.337	7/23/1976 (8)	4
9	Bainsville soil	clay	90–110 cm	1.14	0.01 N $CaSO_4$	0.058, 0.454, 0.354	7/30/1976 (6)	4
10	Organic soil	n.d.	0–20 cm	0.422	0.01 N $CaSO_4$	0.033, 0.551	10/7/1977 (10)	6
11	Vermiculite	n.d.	n.a.	1.08	0.01 N $CaSO_4$	0.048, 0.539, 0.212	9/16/1977 (8)	6
12	Glass beads	30 μm (10–50)	n.a	1.51	water	0.35, 0.22	7/22/1977 (8)	6
13	Glass beads	30 μm (10–50)	n.a	1.51	water	0, 0.318, 0.039, 0.325, 0.124, 0.315, 0.113	5/3/1977 (26)	6
14	Glass beads	30 μm (10–50)	n.a	1.49	water	0, 0.338, 0.159	6/13/1977 (13)	6
15	Glass beads	30 μm (10–50)	n.a.	1.53	2000 ppm NaCl	0/0.348, 0.116, 0.307, 0.150	8/3/1977 (15)	6
16	Glass beads	450 μm (300–600)	n.a.	1.60	2000 ppm NaCl	0, 0.332, 0.06	7/12/1977 (9)	
17	Glass beads	450 μm (300–600)	n.a	1.60	water	0, 0.334, 0.046	6/27/1977 (11)	6
18	Glass beads	450 μm (300–600)	n.a	1.61	water	0, 0.327, 0.061, 0.299, 0.065	5/30/1977 (13)	6

Columns A–G give the value of particular parameters adjusted for each experiment listed in rows.
N d., not determined, n.a., not available.

relationship between water content θ_v and apparent dielectric constant K_a. In addition it was necessary to check the repeatability of the methods.

For a wide variation in soil materials, the texture and density were interrelated and could not be separated independently for this study. Those experiments whose results display the effect of texture were one from each material tested, e.g., 2, 5, 7, 9, 10, 11, 12, 18. In addition these materials had a wide range of specific surface area and still permitted the introduction and extraction of water. Although a range of density of 1 to 1.6 gm cm^{-3} was obtained for the inorganic materials, this range was not independent of the variation in texture. Experiments 2 and 3, for one soil type, show a 9% difference, which was the maximum range in density attainable while maintaining a uniform density in the sample during changes in water content.

The effect of temperature was studied in experiment 6, where the temperature of the room in which the experiments were carried out was varied from 10°C to 36°C. The water input and output connections to the coaxial cylinder were closed when the soil water content was 0.324. The apparent dielectric constant for this 1 m length of soil was measured at selected temperatures. The temperature of the soil was measured by using thermocouples placed inside the inner conductor and outside the outer conductor. The room, soil, and electronic equipment were allowed 24 hours to stabilize after each temperature change. All other experiments were conducted at a controlled temperature of 20.5°C.

In experiments 4, 15, and 16 the water (a 0.01 N $CaSO_4$ solution) was replaced by a solution containing approximately 2000 parts per million sodium chloride (2.112 gm l^{-1}). These experiments tested the influence of soluble salt on the apparent dielectric constant. Most of the experiments were cycled through changes in water content to determine if hysteretic effects existed in the θ_v versus K_a relationship. To determine the reproducibility of these procedures, duplicate experiments were carried out, e.g., 1 and 2, 7 and 8, 12 to 14, and 17 and 18.

RESULTS AND DISCUSSION

Dielectric Constant Versus Water Content

Figure 4 presents the relationship obtained between apparent dielectric constant K_a and soil water content θ_v for the four inorganic soil materials. Although these soils varied widely in both density and texture, there was little difference in the K_a versus θ_v relationship from one soil to another. Before discussing the relationship between K_a and θ_v in detail, we shall determine first what effects texture, density, temperature, and soluble salts had on the relationship. We shall also discuss our experimental reproducibility to give evidence of the significance of the data.

Effects of Texture and Density

A comparison of the results of experiment 2 (•), which used a sandy loam soil, with those of experiment 9 (○), which used a clay soil, indicated differences that texture or specific surface area had on the relationship. The clay soil showed a lower K_a at $\theta_v = 0.1$ but a higher K_a when θ_v was increased to 0.40 than was observed for the sandy loam soil. Therefore, for the fine-grained material the K_a versus θ_v relationship showed greater curvature above $\theta_v = 0.1$. A similar effect was observed for vermiculite and the organic soil. A possible cause for this is

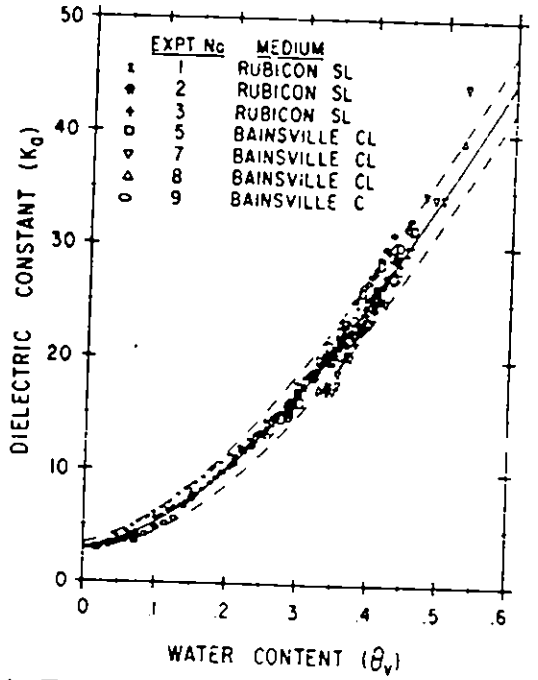

Fig. 4. The measured relationship between K_a and θ_v for the four mineral soils. The solid line is the empirical best-fit equation and the dashed lines are shifted ±0.025 in θ_v. The experiment numbers refer to those used in Table 2.

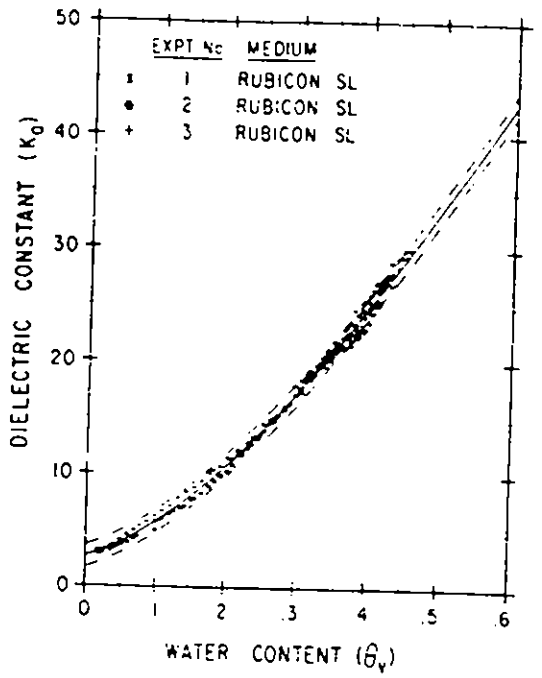

Fig. 5. The measured relationship between K_a and θ_v for the Rubicon soil; the measurements were made at different times and on different subsamples. The solid line is the best-fit equation (see Table 3) and the dashed lines are shifted ±1 in K_a.

discussed in the section below, entitled Relationship Between K_a and θ_v in Different Materials.

In Figure 5, the data from experiments 1, 2, and 3 show that the 9% change in bulk density of the Rubicon sandy loam soil had no measurable effect on K_a. The error of estimate of K_a for these three experiments combined is 0.56 as shown in Table 3, which is of the same order as the measurement accuracy. Similarly, the data in Figure 4 resulted from soil with density ranging from 1.14 to 1.44 gm cm^{-3}, and it is impossible to identify any effect resulting from density alone.

Experimental Reproducibility

Table 4 lists the third-order polynomial equations derived and the error of estimates of K_a and θ_v for each experiment. The numbers in brackets are the standard deviations of each coefficient. The error of estimate is the square root of the residual variance or the standard deviation of K_a when θ_v is known and vice versa for the error of estimate of θ_v. Table 3 lists the derived equation and error of estimates for a number of combinations of the experiments.

The major source of uncertainty was from the measurement of the travel time on the photograph records, resulting in an error of estimate of ±1 in K_a. The uncertainty of the volumetric water content, owing to evaporation and other water losses during the experiment, was less than ±0.008 in all cases. In an attempt to show the magnitude of the data scatter in relation to these measurement uncertainties, we show in Figure 5 a band whose vertical height is 2 in K_a. This band encompassed most of the data points of the three experiments. When we doubled the error of estimate (the 95% confidence limits) of K_a for the combination of experiments 1, 2, and 3 shown on Table 3, we noted that it was ±1.1, which was similar to the results of our first estimate. Experiments 1 and 2 were carried out 7 months apart in different designs of sample holder and by different experimenters. Tables 3 and 4 show a number of other examples of the excellent experimental reproducibility.

Relationship Between K_a and θ_v in Different Materials

The use of glass beads as a study medium provided, first, the opportunity to study the K_a versus θ_v relationship over a wide range of θ_v, where θ_v could be changed relatively easily; second, a means to measure hysteresis, if any, in the K_a versus θ_v relationship; and third, a relatively easy means to introduce saline solution without the associated problem of changing the physical structure of the study medium, as happened with soil.

The experiments that used the glass beads again demon-

TABLE 3 Equation and Error of Estimate for Combinations of Experiments to Determine the Relationship of K_a versus θ_v

Experiment	Medium	Coefficients of $K_a = A + B\theta_v + C\theta_v^2 - D\theta_v^3$, ± Standard Deviation				Error of Estimate of K_a and $\theta_v \times 10$
		A	B	C	D	
1, 2, 3	Rubicon SL	2.59 (±0.16)	21.9 (±1.9)	102 (± 5.6)	44.8 (±3.9)	0.56 0.89
2, 4	Rubicon H_2O and Rubicon NaCl	2.65 (±0.09)	16.5 (±1.1)	123 (± 3.2)	61.0 (±2.3)	0.26 0.83
1, 2, 3, 5, 7, 8, 9	all mineral soils	3.03 (±0.25)	9.3 (±2.8)	146 (± 8.2)	76.7 (±5.7)	1.07 1.3
12, 13, 14	glass, 30 μm	3.79 (±0.25)	41.3 (±3.2)	63.4 (±10.8)	27.0 (±8.0)	0.71 1.07
17, 18	glass, 450 μm	3.57 (±0.21)	31.7 (±2.9)	114 (±10.7)	68.2 (±8.0)	0.71 1.14
12, 13, 14, 17, 18	glass, 30 μm and 450 μm	3.55 (±0.17)	38.0 (±2.2)	84.1 (± 7.9)	44.1 (±5.9)	0.75 1.16

TABLE 4. Equation and Error of Estimate for Each of the Experiments

Experiment	Medium	Coefficients $K_a = A + B\theta_v + C\theta_v^2 - D\theta_v^3$				Error of Estimate of K_a and $\theta_v \times 10^{-2}$
		A	B	C	D	
1	Rubicon SL + H_2O	2.74 (±0.32)	18.2 (± 3.2)	113 (± 9.6)	52.5 (± 6.8)	0.42 0.73
2	Rubicon SL + H_2O	2.56 (±0.14)	16.1 (± 1.7)	127 (± 5.1)	64.4 (± 3.6)	0.32 0.77
3	Rubicon SL + H_2O	2.65 (±0.28)	27.6 (± 3.4)	80.3 (± 9.9)	29.0 (± 7.0)	0.65 0.79
4	Rubicon SL + NaCl	2.87 (±0.15)	15.4 (± 1.8)	125 (± 5.3)	61.8 (± 3.7)	0.28 0.83
5	Bainsville CL + H_2O	2.76 (±0.54)	−1.9 (± 5.4)	196 (±16.0)	115 (±11.3)	0.62 1.2
6	Bainsville CL + H_2O	4.23 (±1.22)	−56.6 (±12.9)	350 (±37.1)	216 (±25.5)	1.43 1.2
8	Bainsville CL + H_2O	2.86 (±1.13)	−2.26 (±11.8)	192 (±33.7)	111 (±23.3)	1.31 1.6
9	Bainsville C + H_2O	3.34 (±0.53)	−7.7 (± 6.4)	222 (±18.6)	136 (±18.8)	0.69 1.1
10	organic soil	1.74 (±0.22)	−0.34 (± 2.3)	135 (± 6.2)	55.3 (± 4.2)	0.38 1.8
11	vermiculite	2.45 (±0.35)	1.8 (± 3.5)	83.1 (± 9.5)	22.2 (± 6.5)	0.63 1.4
12	glass, 30 μm + H_2O	3.62 (±0.26)	41.3 (± 2.9)	59.2 (±10.2)	22.6 (± 7.5)	0.26 0.33
13	glass, 30 μm + H_2O	3.88 (±0.13)	41.3 (± 1.9)	74.5 (± 6.7)	38.1 (± 5.0)	0.35 0.53
14	glass, 30 μm + H_2O	3.03 (±0.17)	43.5 (± 2.1)	49.6 (± 7.0)	14.6 (± 5.1)	0.28 0.46
15	glass, 30 μm + NaCl	3.89 (±0.74)	39.6 (± 8.2)	69.3 (±25.7)	31.3 (±18.4)	0.85 1.3
16	glass, 450 μm + NaCl	3.30 (±0.34)	31.0 (± 5.0)	110 (±18.3)	63.1 (±13.8)	0.84 1.4
17	glass, 450 μm + H_2O	3.33 (±0.25)	32.8 (± 3.7)	116 (±14.7)	70.9 (±10.3)	0.61 1.0
18	glass, 450 μm + H_2O	3.76 (±0.31)	30.5 (± 4.3)	115 (±15.6)	67.8 (±11.7)	0.75 1.2

strated the excellent reproducibility, as shown in Tables 3 and 4 and Figure 6. A possible reason for the slightly greater scatter of data in the 450-μm glass beads was because the water was not distributed as uniformly in the coarse material in the large sample holder. The measured relationship between K_a and θ_v for glass beads was observed to be less curved, especially for the 30-μm beads, than that for the soil material (see the second- and third-order coefficients in Table 4). In addition, there was a vertical displacement of the curve for glass beads, which resulted from a higher K_a (≈3.5) for dry glass beads as opposed to ≈3 for dry soil. The vermiculite and organic soil showed relationships with greater curvature at θ_v up to 0.2 than either glass beads or the other soils. Both the vermiculite and the organic soil showed little measurable change in K_a until θ_v was greater than 0.10. The remainder of these curves was similar to that of the soil material. The dashed lines in Figure 6 enclosed 93% of the data given in Figure 4. These curve shapes gave qualitative confirmation of the hypothesis that the active surface area of the soil controls the dielectric properties of the first few molecular layers of water added to the soil. The first layers, being constrained by the electric field of the soil particles, showed a dielectric constant nearer to that of water constrained in ice structures (i.e., $K' = 3$). Subsequent molecular layers had dielectric constants somewhere between 3 and 81 for liquid water. *Wang and Schmugge* [1978] discuss this further. Inconsistencies in standard laboratory measurements of the surface of the soil materials frustrated attempts to quantify the relationships governing surface area, added water, and measured dielectric constant.

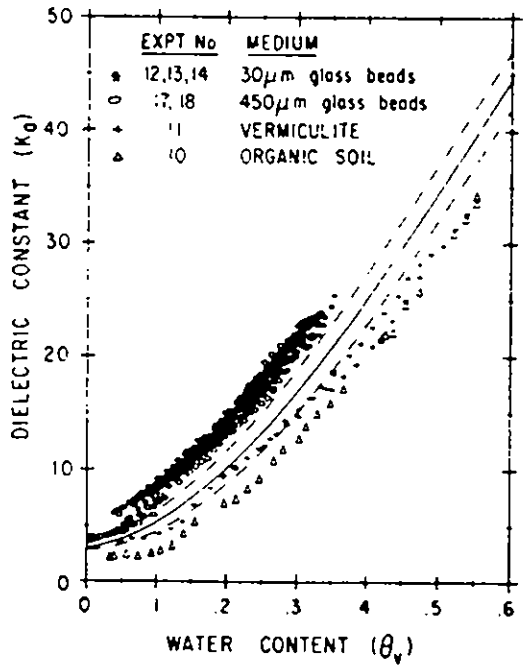

Fig. 6. The measured relationship between K_a and θ_v for the mineral soils, 30 μm glass beads, ground vermiculite, and an organic soil. The area between the dashed lines is the same region as between the dashed lines in Figure 4.

Hysteresis of the K_a vs θ_v Relationship

Although there was little reason to expect hysteresis in the K_a versus θ_v relationship, we did observe some. The separation between wetting and drying branches of a cycle were seldom greater than 2 in K_a and are therefore within the limits of experimental error. An apparent hysteresis was observed with both sizes of glass beads at low water contents. We now believe this was an experimental artifact that resulted from the nonuniformly distributed water during the initial wetting from the porous cups positioned on the outer conductor of the coaxial cylinder. *Annan*'s [1977] calculations indicated that for cases of nonuniform distribution the measured K_a was biased toward the K_a of the material surrounding the inner conductor. Our observations were in accord with those calculations. This factor should be present in all experiments but was only observable with the glass beads that could be dried easily to $\theta_v = 0.05$ or less. The distribution problem of the water occurred mainly on the initial wetting. After an increase of about 0.05 in θ_v, there was no longer any significant effect of unequal water distribution on the measured K_a versus θ_v relationship.

Variations Due to Temperature

The results of experiment 6, to ascertain the influence of temperature, are given in Figure 7. The overall variation of K_a from 10°C to 36°C is less than the experimental error of ±1 shown by the vertical bar at $T = 20.5$°C. *Davis and Annan* [1977] and *Wobschall* [1978] reported that K_a in wet soils did not vary significantly as the temperature was varied from 0° to 30°C.

Variations Due to Change of Soluble Salt Content

A comparison of K_a versus θ_v from experiments 2 and 4 (Figure 8), shows that the presence of salt in the liquid phase of the soil-water system caused no measurable effect on the apparent dielectric constant. The results for the glass bead experiments were similar. In other words, the dissolved salt did not alter the speed of travel of the voltage step in the medium. However salt did increase the attenuation of the voltage step as it traveled in the soil medium.

Usually more scatter was found in the relationship between K_a and θ_v where salt solution replaced the water. This increasing attenuation effect was not only observed when salt was added to solution, but it was also noted as the soil temperature was increased or as the soil grain size decreased and as the soil water content was increased. A quantitative analysis of the shape of the reflected signal from a known length of soil has the potential of showing the attenuation of the various frequency components of the step pulse.

The TDR technique, being wide band, had the advantage of preferentially using the optimum frequencies in the soil under test, which were a compromise of minimum attenuation and maximum resolution. The attenuation of electromagnetic signals in the wetter soil increased with frequency, and the resolution decreased with decreasing frequency. It is hoped that the data from these experiments can be used to identify the best compromise of frequency for particular soil types. Using a narrower bandwidth system over the optimum frequency range will enable us to increase the signal power into the soil and thus maintain resolution and possibly increase penetration range.

Empirical Relationship Between K_a and θ_v

This study showed that the TDR approach has a great deal of potential, both for further use in the laboratory and in the field. A third-degree polynominal equation was fit to the data from the four mineral soils in Figure 4. The equation for this

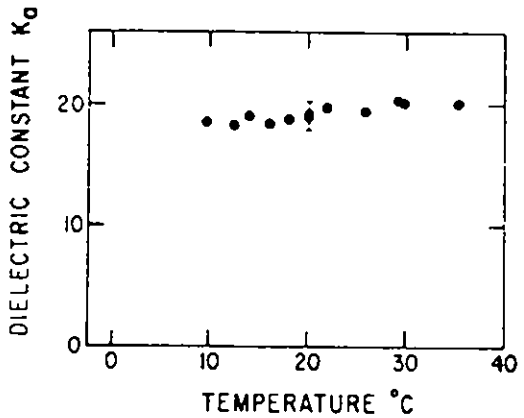

Fig. 7. K_a versus temperature from experiment 6 with Bainsville clay loam surface soil at $\theta_v = 0.324$. The vertical bar at $T = 20$ is ±1 in K_a and represents the measurement precision.

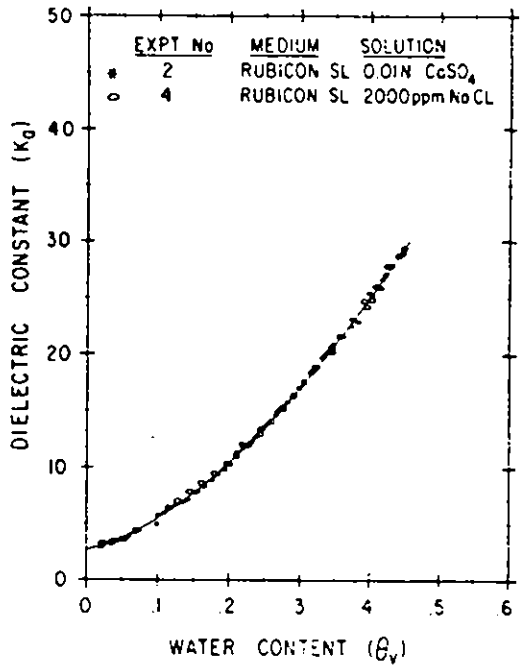

Fig. 8. The measured relationship between K_a and θ_v for the Rubicon soil, where the water solution (0.01 N $CaSO_4$) for experiment 2 was replaced by 2000 ppm NaCl in experiment 4.

line is

$$K_a = 3.03 + 9.3\,\theta_v + 146.0\,\theta_v^2 - 76.7\,\theta_v^3 \qquad (6)$$

This equation was constrained to pass through (81.5, 1) the data point for pure water at 20°C. Measurements of K_a versus θ_v for clays at water contents between 0.6 and 0.95 have also been carried out. The data points lie along the empirical curve (6) satisfactorily.

The lines on either side of the data were shifted from the above equation by 0.025 in θ_v, and the band so formed was found to enclose more than 93% of the measured data. Many of the data points falling outside this band occurred at low or high water content extremes, which are less often encountered in the field. Note that the usual statistical methods for determining the confidence limits were not strictly appropriate here because the scatter was due not only to measurement noise, but, more significantly, to variations from soil type, soil density, soil temperature, and soluble salts in the water, and therefore, the data were not necessarily normally distributed. If statistical methods were employed as shown in Table 4 for experiments 1, 2, 3, 5, 7, 8, and 9, then doubling the error of estimate gave the 95% confidence limit of 0.026 in θ_v. This result was similar to the nonstatistical technique we first employed because there are a large number of data points. For general application to mineral soil, this curve can be used as an empirical calibration for determination of water content with a standard error of estimate of 0.013 (i.e., 1.3%) over the complete range of water contents (Table 4). Specialized applications requiring greater precision, to the instrumental limit ±0.01, or using unusual soils require calibration for the particular soil understudy.

In practice we usually measure K_a and want to determine θ_v. The following equation, which uses the same data as (6) assumed K_a was known. To find θ_v, we use

$$\theta_v = -5.3 \times 10^{-2} + 2.92 \times 10^{-2} K_a - 5.5 \times 10^{-4} K_a^2 + 4.3 \times 10^{-6} K_a^3 \qquad (7)$$

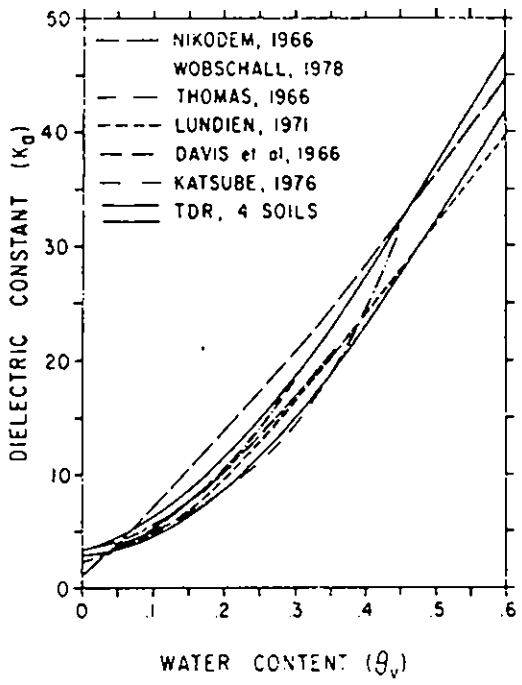

Fig. 9. A comparison of results of the TDR experiments on four different soils possessing a wide range of textures with the results of other experiments which use a variety of techniques and soils.

Comparisons With Other Electrical Measurements

The strong relationship between K_a and θ_v found in these experiments has been observed by other experimenters, using different electrical techniques within the same frequency range. Figure 9 shows a comparison of our TDR experiments on four mineral soils with six other reported experiments that use many different mineral soils and range in frequency from 30 MHz to 1.8 GHz. The data of *Hoekstra and Delaney* [1974] and *Hipp* [1974] were not shown because their data at the lowest experimental frequencies used, 500 MHz and 30 MHz, respectively, gave much higher dielectric constants (up to 12 in dielectric constant at water contents around 0.15 and 0.20) than those shown in Figure 9. Hoekstra and Delaney's data diverged from ours significantly at water contents above 0.1. Both Hoekstra and Delaney's, and Hipp's data points at 4 GHz and 1 GHz, respectively, agreed to within $K_a = \pm 3$ of the empirical curve obtained by using the TDR reported here. It was difficult to explain why the Hoekstra and Delaney data at water contents greater than 0.1 and at 500 MHz, using the TDR technique, did not agree with our data nor with other experimenters' results at 300 MHz and 1 GHz. *Wobschall's* [1978] theoretical curve was lower than any of the other data reported, though his 1977 curve [*Wobschall*, 1977] appeared to fit *Thomas'* [1966] curve at water contents below 0.3. It was clear though that Wobschall's theoretical curve did run low compared to all the experimental data reported. *Selig* [1975] showed many data points of K_a versus θ_v obtained at 20 MHz by three different experimenters, and these fell satisfactorily around our empirical equation over the 0.30 to 0.60 water content range.

It was interesting to note that measurements made at 6 GHz on wet snow samples over a water content range of 0.05 to 0.20 agreed well with the curve given here [*Sweeny and Colbeck*, 1974]. This was not too surprising, since the dielectric constant of ice was 3.15, which was very similar to the dielectric constant of dry soil, 3.0, and the other components of the mixture were the same. At higher water contents Sweeney and Colbeck's curve diverged from ours, which was probably due to the increasing effects of the relaxation mechanisms of the water molecules. It was further evidence that there is a fundamental relationship between the apparent dielectric constant and volumetric water content in wet granular mixtures.

Conclusions

The results of this study have shown that the apparent dielectric constant is strongly dependent on the volumetric water content of the soil. In addition, the dielectric constant was almost independent of soil density, texture, and salt content. There was no significant temperature dependence. The apparent dielectric constant varied over a range of 3 to 40 for a change in the volumetric water content of 0 to 0.55 in mineral soils. The simplicity of measurement, using time-domain reflectometry, and the empirical equation derived here provide a powerful tool for measuring soil water content rapidly and reliably.

The fact that the results of more than 10 different experimenters, who used widely differing soils, electrical measuring techniques, and frequencies, agreed closely with the empirical curve reported here is further evidence that K_a was strongly dependent on θ_v and only weakly on soil type, density, temperature, and frequency between 20 MHz and 1 GHz. The excellent agreement with other experimenters also showed that TDR is a useful technique for measuring at high frequencies the electrical properties of materials.

Although coaxial transmission lines are inappropriate for field use, the installation of parallel transmission lines are being evaluated as a tool to determine soil water content versus depth. The preliminary results of these experiments are very encouraging as indicated by *Davis et al.* [1975]. Two practical problems require resolution: first, the design of transmission line components for optimum resolution of the dielectric constant with depth in the soil, and second, the development of procedures for installation of the transmission lines so that the lines do not influence the wetting and drying processes in the soil. Both laboratory and field experiments are underway to develop further the application of this technique to obtain rapid reliable measurements of volumetric water content in the field.

Acknowledgements. The authors are grateful to Denis Brûle, Walter Zebchuk, and Janet Otoroski for their assistance with experiment procedures and data analyses.

References

Annan, A. P., Time-domain reflectometry air-gap problem for a coaxial line, Report of Activities, Part B, *Pap. 77-1B*, 55–58, Geol. Surv. Can., Ottawa, 1977.

Annan, A. P., and J. L. Davis, High-frequency electrical methods for the detection of freeze-thaw interfaces, *Proc. Third Int. Conf. Permafrost, 1*, 496–500, 1978.

Chernyak, G. Ya., and N. A. Ogilvy (Ed.), *Dielectric Methods for Investigating Moist Soils* (in Russian), Izdatel'stvo 'Nerdra,' Moskva, 1964 (English translation, 106 pp., Israel Program for Scientific Translations, Jerusalem, 1967).

Cihlar, J., and F. T. Ulaby, Dielectric properties of soils as a function of moisture content, *RSL Tech. Rep. 177-47*, Univ. Kans. Center Res., Inc., Lawrence, Kansas, 1974.

Davis, D. R., J. L. Lundien, and A. N. Williamson, Feasibility study of the use of radar to detect surface and ground water, *Tech. Rep. 3-727*, U.S. Army Corps of Eng., Vicksburg, Miss., 1966.

Davis, J. L., and W. J. Chudobiak, In-situ meter for measuring relative permittivity of soils, *Pap. 75-1A*, pp. 75–79, Geol. Surv. Can., Ottawa, 1975.

Davis, J. L., and A. P. Annan, Electromagnetic detection of soil moisture: Progress report I, *Can J Remote Sensing*, *3*, 1, 76–86, 1977.
Davis, J. L., G. C. Topp, and A. P. Annan, Electromagnetic detection of soil water content, Proceedings of the Workshop on Remote Sensing of Soil Moisture and Groundwater, Toronto, Ontario, Canada, November 1976, *Progr. Rep 3*, pp. 96–109, Can. Aeronaut. Space Inst., Ottawa, Canada, 1977.
de Loor, G. P., Dielectric properties of heterogeneous mixtures, Ph D. thesis, Univ. of Leiden, 94 pp., Leiden, Holland, 1956.
Fellner-Feldegg, J., The measurement of dielectrics in the time domain, *J. Phys. Chem.*, *73*, 616–623, 1969.
Hipp, J. E., Soil electromagnetic parameters as a function of frequency, soil density, and soil moisture, *Proc. IEEE*, *62*, 98–103, 1974.
Hoekstra, P., and A. Delaney, Dielectric properties of soils at UHF and microwave frequencies, *J Geophys. Res.*, *79*, 1699–1708, 1974.
Jackson, R. D., R. J. Reginato, and W. E. Reeves, A mechanical device for packing soil columns, *Publ 41-52*, Agr. Res. Serv., U.S Dep. Agr., Washington, D. C., 1962.
Katsube, T. J., Electrical properties of water in rocks and soils, Proceedings of the Workshop on Remote Sensing of Soil Moisture and Groundwater, Toronto, Ontario, Canada, November 1976, report, pp. 110–121, Can. Aeronaut and Space Inst., Ottawa, Canada, 1977.
Lundien, J. R., Terrain analysis by electromagnetic means, *Tech. Rep. 3-693*, U.S. Army Corps of Eng., Vicksburg, Miss., 1971.
Nikodem, H. J., Effects of soil layering on the use of VHF radio waves for remote terrain analysis, Proceedings of the 4th Symposium on Remote Sensing of Environment, report, pp. 691–703, Univ. Mich., Ann Arbor, 1966.
Pearce, D. C., W. H. Hulse, and J. W. Walker, The applications of the theory of heterogeneous dielectrics to low surface area soil systems, *IEEE Trans. Geosci. Electron.*, *11*, 167–170, 1973.
Selig, E. T., and S. Mansukhani, Relationship of soil moisture to the dielectric property, *J Geotech Eng Div., Amer. Soc. Civil Eng.*, *101*(GT8), 755–769, 1975.
Sweeny, B. D., and S. C. Colbeck, Measurements of the dielectric properties of wet snow using a microwave technique, *Res. Rep. 325*, 31 pp., U.S. Army Cold Reg. Res. and Eng. Lab., Hanover, N. H., 1974.
Thomas, A. M., In situ measurement of moisture in soil and similar substances by fringe capacitance, *J. Sci. Instr.*, *43*, 21–27, 1966.
van Beek, L. K. H., Dielectric behaviour of heterogeneous systems, in *Progress in Dielectrics*, vol. 7, edited by J. B. Birks, pp. 69–114, C.R.C. Press, Boca Raton, Fla., 1965.
Wang, J. R., and T. J. Schmugge, An empirical model for the complex dielectric permittivity of soils as a function of water content, *NASA Tech Memo. 79659*, 35 pp., Goddard Space Flight Center, Greenbelt, Md., 1978.
Wobschall, D., A theory of the complex dielectric permittivity of soil containing water: The semi-disperse model, *IEEE Trans. Geosci. Electron.*, *15*, 49–58, 1977.
Wobschall, D., A frequency shift dielectric soil moisture sensor, *IEEE Trans. Geosci. Electron.*, *GE-16*, 2, 112–118, 1978

(Received July 18, 1979;
revised November 29, 1979,
accepted December 13, 1979.)

ILLEGIBLE COPY

The documents appearing on the following page is the complete reproduction of the original document and was created during the normal course of business and, as delivered and in my legal custody at the time of filming. The following document is a true copy of the original document.

WATER RESOURCES RESEARCH, VOL. 26, NO. 5, PAGES 973-987, MAY 1990

R-5 Revisited
2. Reevaluation of a Quasi-Physically Based Rainfall-Runoff Model With Supplemental Information

KEITH LOAGUE

Department of Soil Science, University of California, Berkeley

In this paper a new set of infiltration data for a small rangeland catchment, described in the companion paper (Loague and Gander, this issue), is used to reexcite and reevaluate a quasi-physically based rainfall-runoff model that was previously tested by Loague and Freeze (1985). The rainfall-runoff model is an event-based simulator of the Horton overland flow mechanism. The performance of the model is shown to be somewhat improved in this study with the supplemental information over the original study. However, the model does not fully approximate the rainfall-runoff processes for the catchment, a combination of Horton and Dunne overland flow, and therefore the new data do not lead to an overwhelming improvement in the model performance.

> Can it be that the vast labor of characterizing these systems, combined with the vast labor of analyzing them, once they are adequately characterized, is wholly disproportionate to the benefits that could conceivably follow?
>
> J. R. Philip, 1980

INTRODUCTION

In an earlier part of this study the efficiencies of three underlying event-based rainfall-runoff modeling techniques were compared using data from three small upland catchments [*Loague and Freeze*, 1985]. We reported, somewhat surprisingly at the time, that a quasi-physically based rainfall-runoff model (QPBRRM) did not perform well for a rangeland catchment (R-5) whose characteristics were believed, from some distance, to be well represented by the model. This paper is an extension of the work reported by Loague and Freeze.

The primary barrier to successful application of deterministic-conceptual rainfall-runoff models, depending upon the scale of interest, is the spatial and temporal variability of rainfall rates and near-surface soil hydraulic properties. To improve the spatial characterization of runoff response across R-5, a large new set of steady state infiltration measurements were made. The results from this field study are reported in the companion paper [*Loague and Gander*, this issue]. The supplemental infiltration information for R-5 is used here to reexcite and reevaluate QPBRRM to test, in general, whether the performance of catchment-scale models of the same spirit as QPBRRM can be expected to improve, as is often anticipated, given additional data.

Streamflow Generation

The mechanisms of streamflow generation [*Freeze*, 1974; *Dunne*, 1978; *Pearce et al.*, 1986] have been studied in some detail for at least 50 years. There is now considerable knowledge regarding rainfall-runoff processes and their controls. This understanding is the result of both careful observations from field experiments [e.g., *Dunne and Black*, 1970*a*, *b*] and the heuristic simulations of hypothetical realities with rigorous mathematical models [e.g., *Freeze*, 1972*a*, *b*].

The discharge that is measured at the downstream end of a channel reach is supplied by channel inflow at the upstream end of the reach and by the lateral inflows that enter the channel from the hillslope along the reach. These lateral inflows arrive at the channel in the form of groundwater, subsurface storm flow, and/or overland flow. Groundwater provides a base flow component to streamflow while the flashy response in streamflow to individual precipitation events is usually ascribed to either subsurface storm flow or overland flow. Subsurface storm flow can be a dominant streamflow generation mechanism only when the impeding subsoil horizon laterally diverts infiltrating water downslope. Under intense rainfall events, where the surface soil layer becomes saturated to some depth, water is able to migrate through preferred pathways rapidly enough to deliver contributions to the stream during the peak runoff period. The conditions for subsurface storm flow are quite restrictive. The mechanism is most likely to be operative on steep, humid, forested hillslopes with very permeable surface soils. *Beven and Germann* [1982] review the importance of large continuous openings for water flow in soils.

Overland flow is generated on a hillslope only after surface saturation and ponding take place. It is now widely accepted that surface saturation can occur because of two quite distinct mechanisms, Horton overland flow and Dunne overland flow [*Freeze*, 1980]. The classic mechanism of Horton overland flow is for a precipitation rate that exceeds the saturated hydraulic conductivity of the surface soil. The necessary conditions for the generation of overland flow by the Horton mechanism are a rainfall rate greater than the saturated hydraulic conductivity of the soil and a rainfall duration longer than the required ponding time for a given initial moisture profile.

As a parallel to naming Horton overland flow after its discoverer, *Freeze* [1980] referred to the second mechanism as Dunne overland flow. In this case, the precipitation rate is less than the saturated hydraulic conductivity, and the initial water table is shallow or there is a shallow impeding layer. Surface saturation occurs because of a rising water table.

Paper number 89WR03132.
0043-1397/90/89WR-03132$05.00

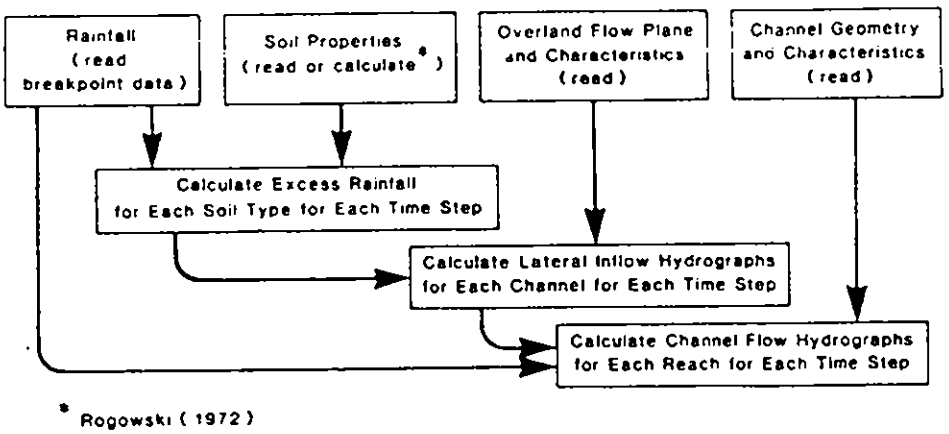

Fig. 1. Flow chart of the operational structure of QPBRRM (adapted from *Engman* [1974]).

Ponding and overland flow occur at a time when no further soil moisture storage is available.

Horton overland flow is generated from partial areas of the hillslope where surface hydraulic conductivities are lowest. Dunne overland flow is generated from partial areas of the hillslope where water tables are shallowest. Both the Horton and Dunne mechanisms lead to variable source areas that expand and contract through wet and dry periods.

Modeling Hydrologic Response

Twenty years ago, *Freeze and Harlan* [1969] proposed a blueprint for a deterministic-conceptual hydrologic response model based upon coupling the partial differential equations which describe water movement. In general, the rainfall-runoff process can be divided into three water transport phases describing (1) flow into, through, and out of saturated-unsaturated porous media, (2) overland flow, and (3) open channel flow.

On a three-dimensional hillslope the processes of infiltration, subsurface flow, and exfiltration are generally described by the equations of saturated and unsaturated porous media flow. These equations result from combining a continuity relationship with Darcy's law. The groundwater flow equation and Richards' equation describe saturated and unsaturated flow, respectively.

On a recharging and discharging sheet flow plane, overland flow is described by the simultaneous solution of the hydrodynamic equations of continuity and motion. Collectively, these relationships are known as the St. Venant or shallow water equations. The shallow water equations also describe the flow in a recharging and discharging channel.

A model that rigorously couples the three water transport phases as described here, once seemingly well within reach but as of yet undeveloped, is probably best suited as a research tool for the formulation of concepts based upon generic simulations at the hillslope scale. This type of model is, however, of little use as far as the operational hydrologist is concerned due to staggering data requirements.

TABLE 1. Characteristics of QPBRRM

Characteristic	QPBRRM
Streamflow Generation Mechanisms	
Horton overland flow	yes
Dunne overland flow	no
Subsurface storm flow	no
Groundwater flow	no
Hydrologic Response Processes	
Infiltration	yes
Reinfiltration	yes
Exfiltration	no
Spatially Variable Input	
Soil properties	yes
Overland and channel flow characteristic parameters	yes
Rainfall	no

Model Efficiency

League and Freeze [1985] discuss calibration, verification, and model efficiency as each relates to simulating rainfall-runoff processes with mathematical models. The same ideas are carried over to this paper except the term validation is substituted for verification based upon the definitions recommended by the American Society for Testing and Materials [1984].

The *Nash and Sutcliffe* [1970] coefficient of efficiency criterion, employed by *League and Freeze* [1985], is again used here. The coefficient of efficiency is calculated as

$$E = \frac{\sum_{i=1}^{n} (Q_i - \hat{Q}_i)^2 - \sum_{i=1}^{n} (\hat{Q}_i - \bar{Q})^2}{\sum_{i=1}^{n} (Q_i - \bar{Q})^2} \qquad (1)$$

TABLE 2. Saturated Hydraulic Conductivity Values for R-5 Used to Excite QPBRRM

Soil Name	Saturated Hydraulic Conductivity, m/s	
	League and Freeze [1985]	This Study
Kingfisher	7.6E−6*	9.5E−6
Grant	7.6E−6	19.9E−6
Renfrow	7.6E−6	13.4E−6

*7.6×10^{-6}.

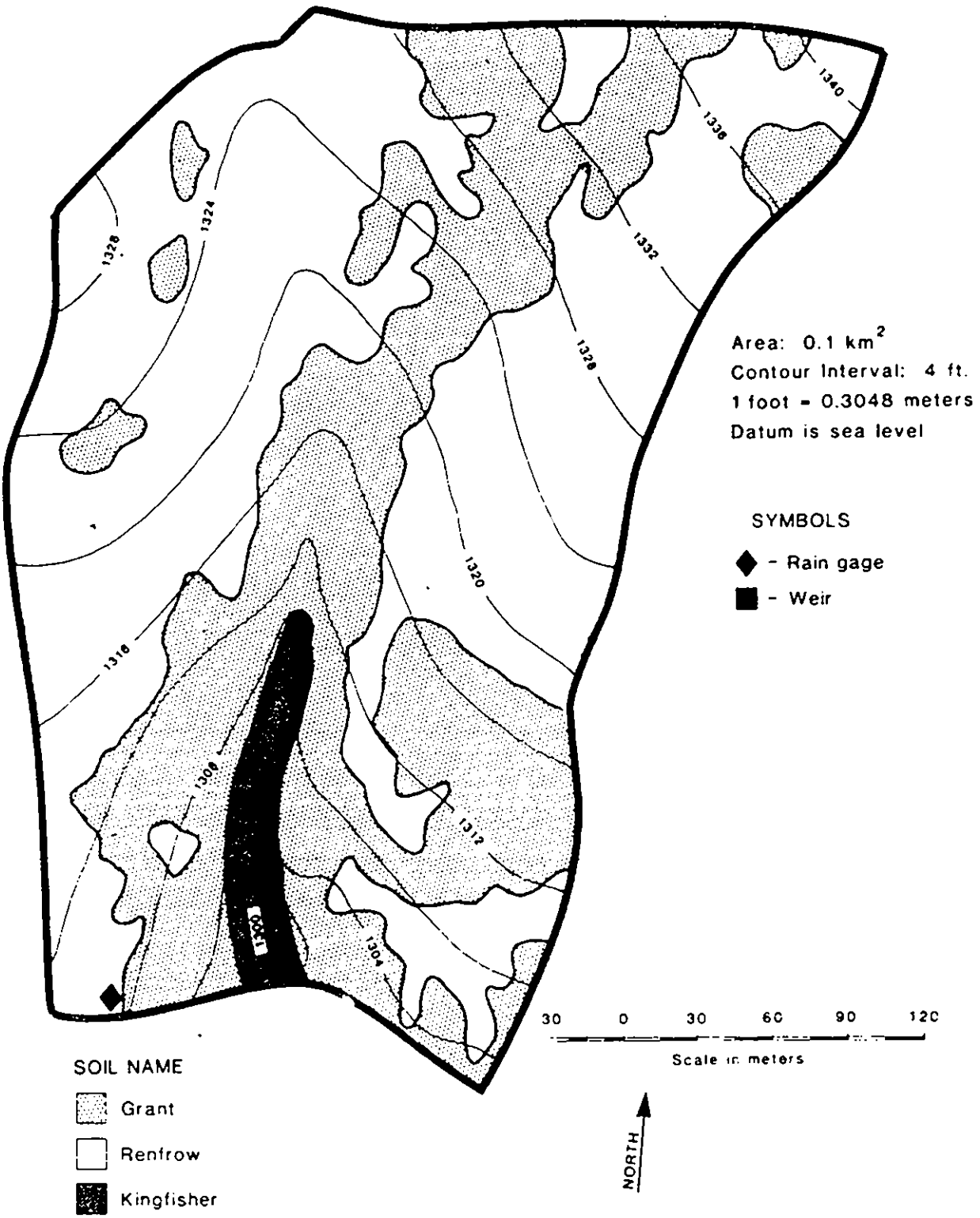

Fig. 2. Distribution of soils across the R-5 catchment (G. Gander, personal communication, 1981). The three soil types identified for the R-5 catchment are principally defined by vegetation: buffalo and blue grama grasses with the Renfrow soils; bluestem grass with the Grant and Kingfisher soils.

where $\hat{Q}_i$ is a predicted runoff summary variable for event i, Q_i is the observed runoff summary value for event i, and $\bar{Q}$ is the mean of Q_i for all the events $i = 1$ to m. When calibration and validation periods are considered, the m rainfall-runoff events are divided such that events $i = 1$ to n are used for calibration and events $i = n+1$ to m are used for validation. With a split sample, E is based only on the events bounded by the sample delimiters. Efficiency values calculated for calibration and validation periods are denoted as E^c and E^v, respectively. The event summary variables referred

TABLE 3. Characteristics for R-5 Rainfall-Runoff Events

Event Number	Observed Event Summary Variables							
	Date	P_D, mm	P_{MX}, mm/h	t_{MX}, hours	Q_D, mm	Q_{PK}, L/s	t_{PK}, hours	θ_θ^* (dimensionless)
				1966				
1	July 24	51	145	0.23	3.53	187.66	0.71	35
				1967				
2	April 9	27	97	0.70	0.15	0.73	2.41	78
3	April 10	29	127	0.10	4.47	108.37	0.52	78
4	April 12	63	77	1.03	20.39	584.75	1.60	80
5	April 20	14	49	0.47	0.18	1.12	2.34	78
6	May 5	28	84	3.47	0.60	12.53	4.28	70
7	May 20	35	51	3.30	0.48	8.19	4.10	67
				1968				
8	March 18	24	62	6.00	3.02	51.51	6.93	85
9	May 25	27	58	0.03	0.85	14.59	5.12	70
10	June 1	23	13	10.10	0.52	3.42	4.18	78
11	June 7	13	76	0.37	0.62	7.45	1.37	78
12	July 1	50	54	0.77	0.13	0.91	4.88	52
13	July 13	30	119	0.23	0.21	2.25	1.42	46
14	July 14	11	36	0.03	0.03	0.15	5.57	57
15	Sept. 4	30	77	0.27	0.30	4.38	1.33	30
16	Nov. 26	32	12	0.03	0.28	2.25	10.85	78
17	Nov. 27	19	8	0.03	0.25	0.44	6.15	78
				1969				
18	Feb. 20	15	12	0.80	0.94	3.42	7.89	87
19	Feb. 21	5	6	0.03	0.68	4.38	3.32	87
20	May 3	37	83	1.30	0.37	4.38	5.86	74
21	May 4	14	18	1.33	0.09	0.57	5.30	74
22	May 6	43	91	4.90	14.24	477.71	5.18	76
23	May 11	19	9	3.90	0.18	1.65	6.62	80
24	June 13	87	194	8.93	10.44	262.19	9.26	78
25	July 20	81	87	1.07	4.24	167.72	1.54	37
				1970				
26	April 30	24	24	0.40	0.04	0.44	5.40	67
27	May 14	43	72	0.47	0.46	10.66	1.23	39
28	May 29	35	61	0.03	0.48	9.79	2.24	55
29	Oct. 7	18	26	0.13	0.11	1.63	1.78	75
30	Oct. 8	15	30	2.27	0.28	3.00	3.82	75
				1971				
31	June 2	19	120	0.60	0.29	5.49	1.38	48
32	June 3	19	55	0.33	3.21	136.06	0.74	48
33	June 12	78	85	0.57	4.22	115.87	1.00	65
34	Sept. 24	42	58	0.20	2.94	40.63	1.20	67
35	Oct. 2	90	107	0.63	25.30	281.61	2.35	53
36	Dec. 14	26	56	0.83	6.29	75.27	1.52	89
				1972				
37	April 20	15	30	0.67	0.04	0.23	2.95	59
38	May 12	45	52	0.93	1.27	15.70	4.33	65
39	Oct. 30	67	94	2.13	5.91	97.62	2.66	80
40	Oct. 31	68	86	20.23	27.36	131.87	5.55	80
				1973				
41	Jan. 2	29	20	3.87	1.44	10.66	7.62	91
42	Jan. 21	20	47	0.13	2.20	31.55	5.88	98
43	Jan. 25	17	12	9.37	1.63	10.66	11.94	96
44	March 6	27	56	0.97	3.10	51.51	2.03	87
45	March 9	25	31	3.13	7.86	69.49	0.70	89
46	March 23	45	30	6.80	11.42	153.65	9.55	100
47	March 24	31	70	0.53	25.59	268.59	1.09	100
48	April 15	15	6	2.33	0.23	3.00	3.69	85
49	April 15	7	32	0.03	0.68	6.11	0.94	85
50	April 19	15	83	0.83	1.54	23.39	1.85	83
51	May 22	32	116	0.80	0.16	2.25	1.72	87
52	May 24	91	248	0.33	45.60	1785.95	0.51	87
53	May 30	53	152	0.07	5.07	97.64	6.22	93
54	June 2	44	104	1.63	22.43	375.77	2.26	96
55	June 4	33	214	1.67	16.68	505.74	2.03	98
56	June 19	15	70	0.43	0.36	5.49	1.00	83
57	Aug. 9	33	122	0.50	0.22	4.38	0.99	28
58	Sept. 12	22	164	0.10	0.02	0.15	1.52	61

TABLE 3 (continued)

Event Number	Observed Event Summary Variables							
	Date	P_D, mm	P_{MX}, mm/h	t_{MX}, hours	Q_D, mm	Q_{PK}, L/s	t_{PK}, hours	θ_e^* (dimensionless)
59	Sept. 26	55	65	0.03	0.70	4.92	3.62	80
60	Oct. 11	24	86	0.03	0.37	2.61	3.24	80
61	Oct. 12	11	18	0.70	0.11	0.73	5.20	80
62	Oct. 27	12	65	0.33	0.49	7.45	1.05	78
63	Nov. 19	57	169	1.03	15.11	564.36	1.27	70
64	Nov. 24	30	16	6.93	5.44	64.02	8.09	74
				1974				
65	Feb. 20	33	46	0.13	0.27	3.89	3.86	80
66	March 10	20	64	0.60	1.59	27.96	1.16	93
67	April 11	33	56	0.37	0.003	0.03	6.78	74
68	April 29	50	72	1.93	10.15	220.16	2.97	67
69	May 1	29	43	10.00	6.52	87.61	10.41	67
70	Nov. 3	5	35	0.20	0.003	0.01	1.17	67
71	Nov. 3	8	31	0.20	0.22	2.61	1.29	67
72	Nov. 3	8	51	0.13	0.10	0.91	0.67	67

The complete hydrograph and hyetograph for each R-5 event can be obtained in breakpoint form from the USDA ARS Hydrology Laboratory in Beltsville Maryland.

*Antecedent soil-water contents; expressed as percent saturation; values are estimated for the surface layer at the start of each event; see *Loague* [1986] for description of estimates.

to in describing (1), abstracted from complete hydrographs, are total stormflow depth (Q_D), peak storm flow (Q_{PK}), and time to Q_{PK} from the start of the event (t_{PK}).

Loague and Freeze [1985] differentiate between forecasting and prediction efficiencies calculated with (1). For forecasting, the more rigorous of the two tests, the Q_i and $\dot{Q}_i$ in (1) are defined for summary variables from sequential events, which are used to compute forecasting efficiencies E_f. For prediction, the Q_i and $\dot{Q}_i$ in (1) are defined for summary variables from ranked events, which are used to compute prediction efficiencies E_p. Also calculated for this study are null case efficiencies E_n, where the Q_i and $\dot{Q}_i$ in (1) are defined such that the observed and predicted summary variables are ranked in reverse order. For any set of observed and predicted values, $E_p \geq E_f \geq E_n$. If all $Q_i = \dot{Q}_i$, then E_p, E_f, and E_n all equal 1. For any realistic case, E_p, E_f, and E_n will all be <1. It is possible for the Nash and Sutcliffe criterion to become negative, which simply infers that the model's predicted values are worse than using the observed mean. Large summary variables are weighted more heavily in (1); therefore a calculated efficiency can be biased when a model is evaluated for a large range of events.

The coefficient of efficiency given in (1) is certainly not the only procedure for evaluating model performance. For example, *Loague and Green* [1990] discuss various statistical and graphical criteria which can be used for evaluation of solute transport models. In addition, the papers by *James and Burges* [1982], *Wilmott et al.* [1985], and *Green and Stephenson* [1986] all offer excellent reviews of model assessment procedures.

Quasi-Physically Based Rainfall-Runoff Model

The quasi-physically based rainfall-runoff model (QPBRRM) employed by *Loague and Freeze* [1985] was developed by *Engman* [1974]. The structure and attributes of this model are reviewed by several authors [*Engman and Rogowski*, 1974; *Gburek*, 1978; *Dunne*, 1982; *Betson and Ardis*, 1978]. The model is somewhat similar to the U.S. Geological Survey distributed routing rainfall-runoff model [*Dawdy et al.*, 1978; *Alley and Smith*, 1982] and many others. The data requirements and limitations of QPBRRM, relative to the application described herein, are discussed by *Loague and Freeze* [1985]. The remainder of this section is a brief overview of QPBRRM. The reader interested in more detail is referred to the references given here.

The operating algorithms for QPBRRM are based on solutions and or simplifications to the full set of coupled partial differential equations which describe hydrologic response. The model has three major components: (1) an infiltration algorithm that allows calculation of the rainfall excess by difference, (2) a routing algorithm that translates rainfall excess, generated on the overland flow planes, into lateral inflow hydrographs at the stream channel, and (3) a routing algorithm for tracking the streamflow hydrograph through the channel system.

The three major components of QPBRRM each rest upon one-dimensional equations that, when linked together, result in a quasi-three-dimensional representation of rainfall-runoff via the Horton mechanism. The infiltration equation is similar to Philip's two-parameter equation, which is a particular solution to Richards' equation for vertical flow in an unsaturated-saturated soil profile. Estimates of antecedent soil-water contents are required for the event-based infiltration calculations. The equations for overland and channel flow routing are each based upon numerical solution to kinematic forms of the shallow water equations. The model allows partial source areas to expand and contract during a storm. Implementation of QPBRRM for a given catchment is accomplished using a set of overland flow planes that divide the areas of interest into segments. Figure 1 schematically illustrates the operational sequence for a QPBRRM simulation. The characteristics of QPBRRM are summarized in Table 1.

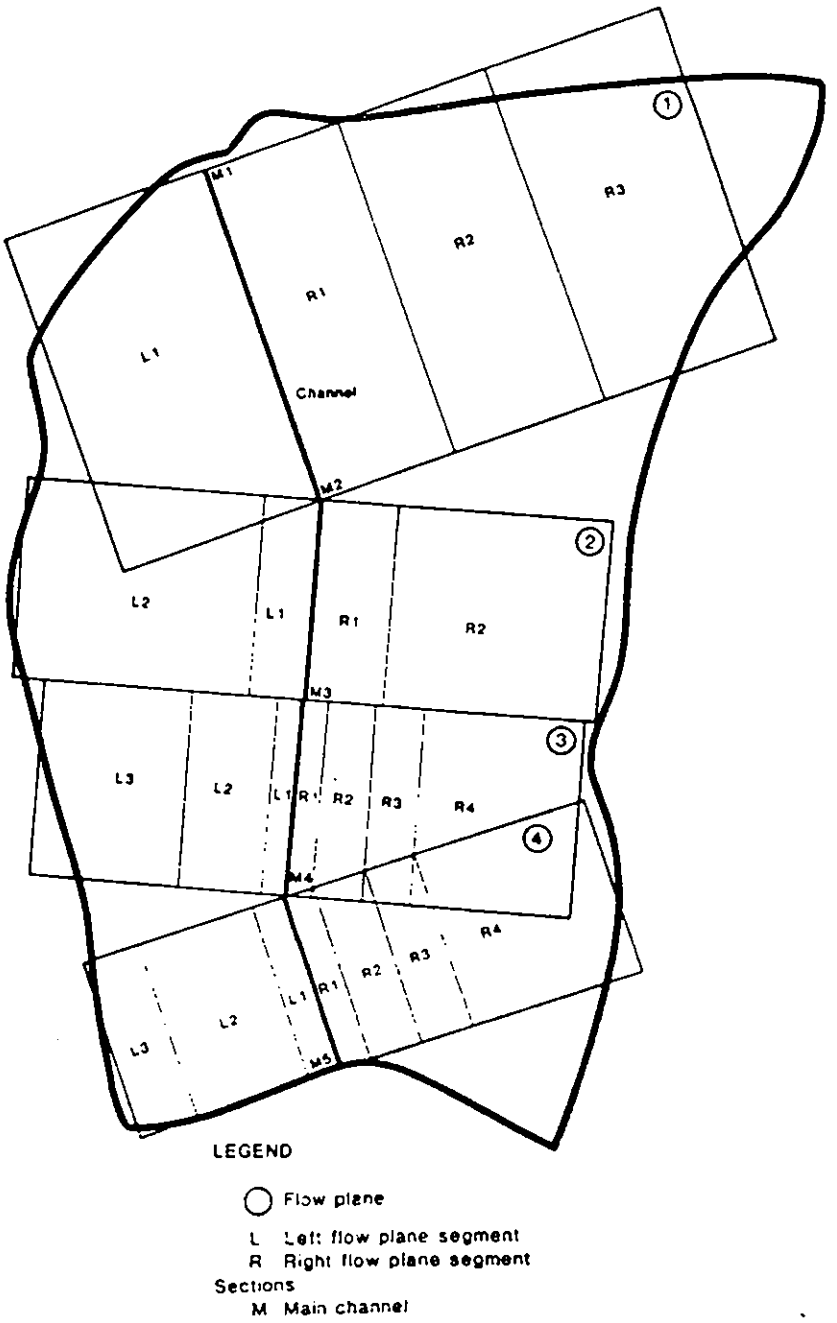

Fig. 3. Segments used to transform the R-5 catchment into overland flow planes [*Loague and Freeze*, 1985].

R-5 CATCHMENT

Data Base

The various streamflow generation mechanisms and their environmental controls have been generalized by *Dunne* [1978]. Based upon that classification it is quite reasonable to characterize Horton overland flow as the dominant streamflow generation mechanism for R-5. It seems likely, therefore, that R-5 and QPBRRM are candidates for a good marriage. The R-5 catchment has been described at length elsewhere [*Sharma et al.*, 1980; *Loague and Freeze*, 1985; *Loague and Gander*, this issue]. *Loague* [1986] summarizes research studies that have utilized data from R-5.

The distribution of soil types across the catchment are shown in Figure 2. The water table at R-5, usually visible in a well near the weir at the head of the channel, has a very slight slope and is therefore several meters below the surface in the upper parts of the catchment (J. Naney, personal communication, 1984).

Except for the saturated hydraulic conductivity values, all the characteristic parameters for R-5 used to reexcite QPBRRM are the same as given by *Loague and Freeze* [1985, pp. 235–236]. Undoubtedly, there is substantial uncertainty for many of the parameter values used here (e.g., Manning's roughness coefficient for overland flow) even though they were each selected carefully.

The near-surface saturated hydraulic conductivity values used by Loague and Freeze and those employed here are

TABLE 4. Forecasting Efficiencies E_f for the Three Summary Output Variables for QPBRRM for R-5

Data Set	Events	E_f Q_D	Q_{PK}	t_{PK}
Loague and Freeze [1985]*	1–36	−0.31	−0.79	−0.19
This study	1–36	0.06	0.03	−0.26
Loague and Freeze [1985]	37–72	0.26	0.44	−0.20
This study	37–72	0.28	0.80	−0.25
Loague and Freeze [1985]*	1–72	0.15	0.26	−0.20
This study	1–72	0.26	0.68	−0.25

*Not previously reported.

TABLE 6. Null Case Efficiencies E_n for the Three Summary Output Variables for QPBRRM for R-5

Data Set	Events	E_n Q_D	Q_{PK}	t_{PK}
Loague and Freeze [1985]*	1–36	−2.44	−3.60	−2.10
This study	1–36	−0.68	−0.87	−2.28
Loague and Freeze [1985]*	37–72	−1.83	−3.07	−3.52
This study	37–72	−0.99	−1.63	−3.55
Loague and Freeze [1985]*	1–72	−1.88	−3.10	−2.92
This study	1–72	−0.85	−1.47	−3.01

*Not previously reported.

given in Table 2. The revised conductivity estimates are based upon the infiltration experiments reported in paper 1 [*Loague and Gander*, this issue].

The individual rainfall-runoff events from R-5 used by *Loague and Freeze* [1985] are again used here. Rainfall-runoff summary variables, as well as initial soil-water contents, for each of the 72 events are given in Table 3. The overland flow planes used here for R-5 (Figure 3) are the same as in the original study. The configuration in Figure 3 could have been improved for this study, but it was maintained to facilitate direct comparisons with the original study.

RESULTS

Tables 4–6 summarize the forecasting, prediction, and null efficiencies for QPBRRM for the three summary output variables (Q_D, Q_{PK}, t_{PK}) for the R-5 data set for this study and for the results of *Loague and Freeze* [1985]. Table 7 summarizes the means and standard deviations for the summary output variables for the observed and the predicted R-5 events. Figure 4 presents observed versus predicted scattergrams for each of the three output summary variables for all 72 R-5 events for this study and for Loague and Freeze. The results in Tables 4–7 are divided into three groups: (1) events 1–36, (2) events 37–72, and (3) events 1–72. Loague and Freeze earmarked the first 36 events for calibration and the last 36 events for verification. The split sample has been carried over to this study even though there was no attempt to calibrate QPBRRM.

TABLE 5. Prediction Efficiencies E_p for the Three Summary Output Variables for QPBRRM for R-5

Data Set	Events	E_p Q_D	Q_{PK}	t_{PK}
Loague and Freeze [1985]*	1–36	0.81	0.43	0.50
This study	1–36	0.57	0.71	0.40
Loague and Freeze [1985]	37–72	0.48	0.47	0.66
This study	37–72	0.35	0.80	0.62
Loague and Freeze [1985]*	1–72	0.72	0.51	0.63
This study	1–72	0.47	0.80	0.57

*Not previously reported.

DISCUSSION

Event Selection

The saturated hydraulic conductivity value, K_0, used by *Loague and Freeze* [1985], for the entire R-5 catchment, is 7.6×10^{-6}. It turns out that 11 of the 72 R-5 events (15%) have maximum 2-min rainfall intensities, P_{MX}, less than this value (27.4 mm/h) and therefore could not lead to Horton type runoff on the hillslopes. In this study, K_0 is different for each of the three R-5 soil types (see Table 2). Each of the conductivity values used here is greater than the value used by Loague and Freeze. It turns out therefore that 24, 32, and 42% of the R-5 events would not lead to Horton type runoff on the Kingfisher, Renfrow, and Grant soils, respectively, because the P_{MX} values are less than the K_0 values. The distribution of R-5 events with P_{MX} less than the various K_0 values is shown in Table 8.

The summary in Table 8 helps to conceptualize how the partial area aspect of QPBRRM can lead to distributed areas of runoff generation. Based on the number of events that can be expected not to generate infiltration excess, it appears that QPBRRM is ill suited for many of the R-5 events used by *Loague and Freeze* [1985]. Many of the smaller runoff events at R-5 probably resulted from rainfall directly to the channel area which is simulated by QPBRRM. The reader is also reminded that the efficiency criterion used here is most sensitive to the larger events.

Table 9 summarizes the means and standard deviations for the observed rainfall summary variables and the antecedent soil-water contents, θ_0, for the R-5 catchment. The rainfall depth, P_D, averages are very similar for the first and last half of the R-5 events. The maximum 2-min rainfall intensity, P_{MX}, and the time to the end of P_{MX} from the beginning of the event, t_{MX}, are slightly larger and longer, respectively, for the second half of the R-5 events. The average antecedent soil-water content, θ_0, is significantly higher for the second half of the R-5 events.

The summary in Table 7 shows that both the observed storm flow depth, Q_D, and observed peak storm flow rate, Q_{PK}, are higher in the second half of the R-5 events. These higher runoff values, with essentially the same rainfall, are clearly due to the higher θ_0 values. Of course, the higher the θ_0 value is, the more likely it is that excess infiltration will occur with high rainfall intensities. The θ_0 values used in this study [*Loague and Freeze*, 1985] are based upon thousands of soil-water measurements made across R-5 (G. Gander, personal communication, 1981) within the same time frame that the 72 R-5 rainfall-runoff events took place.

TABLE 7. Statistics for Observed and Predicted Summary Output Variables for the R-5 Events

	Summary Variables					
	Q_D, mm		Q_{PK}, L/s		t_{PK}, hours	
	Mean	Standard Deviation	Mean	Standard Deviation	Mean	Standard Deviation
Events 1–36						
Observed*	3	6	72	136	3.7	2.6
Simulated, *Loague and Freeze* [1985]†	3	8	94	229	2.1	2.0
Simulated, this study	1	3	32	99	1.8	2.1
Events 37–72						
Observed*	6	10	128	317	3.6	3.0
Simulated, *Loague and Freeze* [1985]†	3	12	132	523	3.1	4.2
Simulated, this study	2	8	78	374	2.9	4.2
Events 1–72						
Observed*	5	8	100	244	3.6	2.8
Simulated, *Loague and Freeze* [1985]†	3	10	113	402	2.6	3.3
Simulated, this study	1	6	55	273	2.4	3.4

Note: The coefficient of variation (CV) referred to in the text is equal to the standard deviation divided by the mean.
*See Table 3 for individual event values.
†Not previously reported.

There are, of course, problems associated with extrapolating information such as θ_0 values. For example, in this study, events which occur on the same day (see Table 3) are assigned the same estimated θ_0 value due to the daily disaggregation scheme used to glean daily values from sparse information.

An assessment of performance for a physically or quasi-physically based rainfall-runoff model should take place first on an event basis. When acceptable (or identifiable) levels of performance are established, then the assessment can proceed to continuous simulation. This rationale is based upon the fact that soil-water accounting between events is laced with tremendous uncertainty. In general, the event selection for this study is felt to be quite satisfactory.

Scattergrams and Statistics

The scattergrams in Figure 4 illustrate that there are fewer large events in the R-5 data set than smaller events. With close inspection of Figure 4 one can see that QPBRRM underestimates the three summary output variables for the majority of the R-5 events. This observation is true for both our original results (Figure 4*a*) and the results presented here (Figure 4*b*). The previously described saturated hydraulic conductivity estimates used to excite QPBRRM are the only differences in model input for the two sets of R-5 event simulations summarized in Figure 4. As one would expect, and is shown in Table 10, the larger conductivity values used in this study resulted in an increased number of events which are underpredicted by QPBRRM. For the largest event the predictions of Q_D and Q_{PK} are improved with the new simulations.

A perusal of the statistics displayed in Table 7 leads to the following generalized comments:

1. The predicted means and standard deviations for the three summary output variables from our previous simulations [*Loague and Freeze*, 1985] are closer to the observed statistics than the predicted means and standard deviations for the revised simulations reported here. It would appear, therefore, that based solely on these statistics, the original simulations are superior.

2. The predicted means for the summary output variables are all reduced for the simulations in this study as compared to those of *Loague and Freeze* [1985].

3. The coefficient of variation (CV) for the observed and predicted summary output variables is smallest for t_{PK}, larger for Q_D, and largest for Q_{PK}; the CV values for each of the predicted summary output variables is larger than for the same observed summary output variables; the CV values are larger for the revised simulations than for those of *Loague and Freeze* [1985].

Forecasting, Prediction, and Null Case Efficiencies

A perusal of the forecasting efficiencies E_f in Table 4 leads to the following generalized comments:

1. The E_f values are low. Model performance is better for Q_D and Q_p than for t_{PK}.

2. Model performance is better in this study than in the previous effort. The exception here is for t_{PK}, which is predicted poorly in both efforts. The improved model performance here is due to the supplemental saturated hydraulic conductivity estimates [*Loague and Gander*, this issue] used to excite QPBRRM. The results here are the opposite of those reported in the previous section, which helps to illustrate how different model evaluation criteria can result in different model performance interpretations.

3. The E_f values are higher for the second half of the R-5 events. These events are more likely to be of the Horton type because of the higher antecedent soil-water contents.

4. Model performance is best for Q_{PK}, which is in many instances the most important of the three summary output variables. The $0.80E_f$ value for the second half of the events approaches a level that might be considered acceptable depending upon the intended model application. The reader is reminded that all QPBRRM results presented here are for an uncalibrated model using best parameter estimates.

5. The E_f values for t_{PK} are all quite poor. This will be addressed in a later section.

A perusal of the prediction efficiencies E_p in Table 5 and the null case efficiencies E_n in Table 6 leads to the following generalized comments:

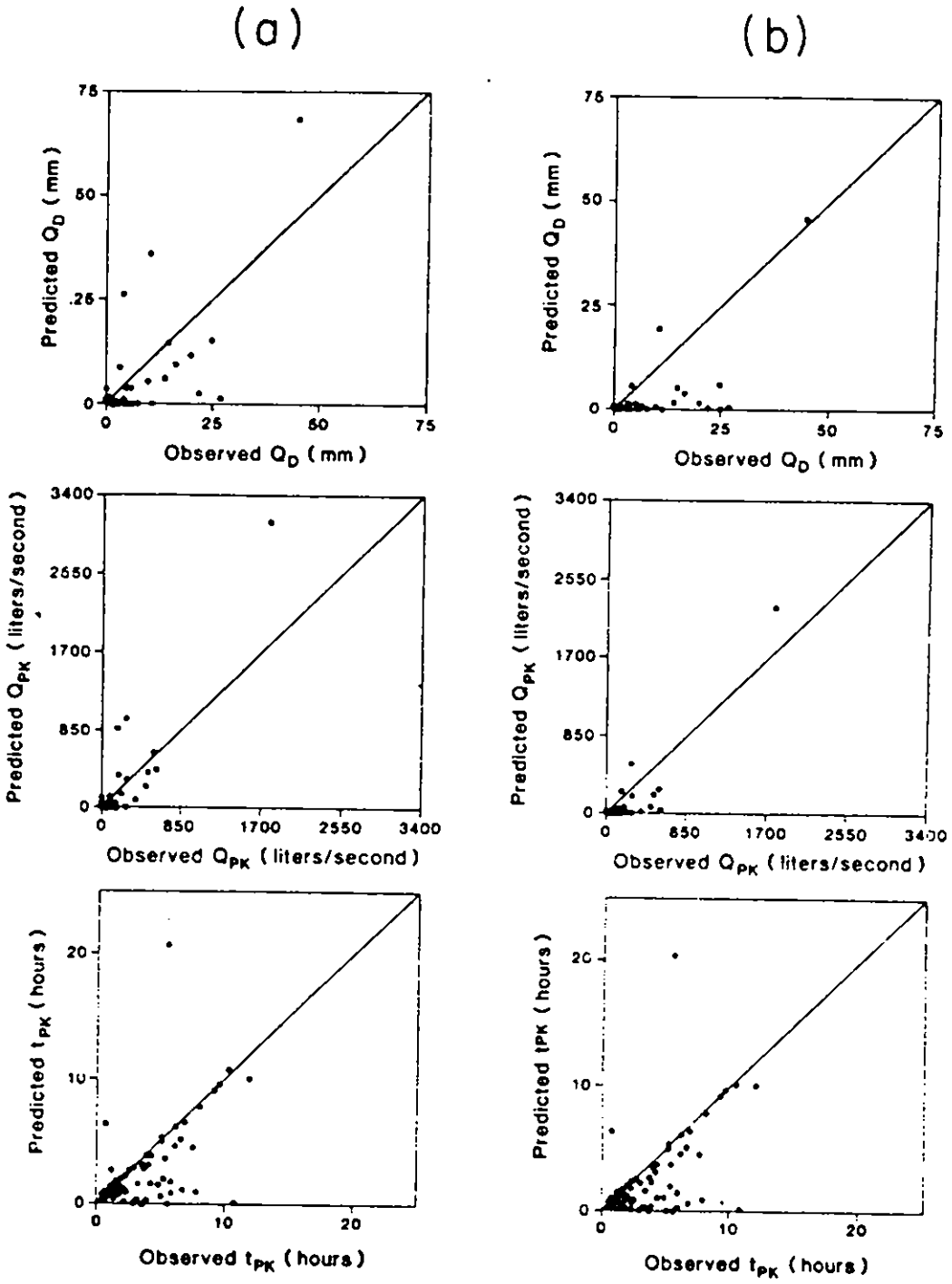

Fig. 4. Scattergrams of observed and predicted summary output variables for the 72 R-5 events. (*a*) *Loague and Freeze* [1985]. (*b*) This study.

1. An item-by-item comparison of the prediction and null case efficiencies (Tables 5 and 6) with the forecasting efficiencies (Table 4) shows that $E_p \geq E_f \geq E_n$, as it must be by definition.

2. The minimum E_p value for the 72 events is 0.47, for Q_D, for the simulations in this study. The maximum E_n value for the 72 events is −0.85, also for the Q_D for the simulations in this study. The E_f values are closer to the E_p values than the E_n values for both the simulations in this study and those reported earlier [*Loague and Freeze*, 1985].

3. The E_p and E_n values are superior for Q_D and t_{PK} for the original simulations [*Loague and Freeze*, 1985] and better for Q_{PK} in this study.

R-5 Is Not a Sand Box

Many of the hydrologic nuances of R-5 do not lend themselves easily to physically based modeling. A somewhat ideal or naive picture of the catchment has been painted here and elsewhere. Several of the snags associated with simulating rainfall-runoff events at R-5 are described below.

TABLE 8. Number of Events With Maximum 2-min Rainfall Intensity Less Than the Saturated Hydraulic Conductivity Value

Saturated Hydraulic Conductivity, m/s	Events	*Loague and Freeze* [1985]	This Study
7.6E−6*	1–36	7	NA
(entire catchment)	37–72	4	NA
9.5E−6	1–36	NA	8
(Kingfisher)†	37–72	NA	9
13.4E−6	1–36	NA	9
(Renfrow)	37–72	NA	14
19.9E−6	1–36	NA	18
(Grant)	37–72	NA	24

See Table 3 for 2-min rainfall intensity values. NA is not applicable.

*7.6 × 10^{-6}.

†See Figure 3 for distribution of soils across R-5.

It is generally well established that biological factors have significant impacts on the dynamics of microscale hydrology. Vegetation states and burrowing activities at R-5 are important, yet poorly understood, variables which have not been considered in this or other rainfall-runoff modeling exercises for the catchment. R-5 is normally used as a low-intensity cattle nursery by the landowner. It is important to recognize, however, that even for a well-managed pasture the impact of grazing unquestionably influences streamflow generation processes.

The extent of a semidefined R-5 channel is portrayed in Figure 5. The channel area is the most active geomorphologic part of the catchment with slumping and erosion features prevalent along the entire length. These dynamics [illegible] simulated. The locations of other major features that influence runoff at R-5, which are not typically included in modeling exercises or even reported, are also illustrated in Figure 5. Not shown in Figure 5 are the many [illegible] across R-5 which are also usually ignored.

Surface runoff at R-5, via the Horton mechanism, was [illegible] during the field component of this study [*Loague*, 1988a]. However, in the upper parts of the catchment much of this overland flow is subject to run-on and therefore does not contribute to lateral inflow to the channel. The rainfall rates of these events suggest that extensive sheet flow is not very common at R-5. In general, runoff from R-5 measured at the weir is generated primarily near the channel.

With this closer look at R-5 it should be obvious, and not surprising as reported by *Loague and Freeze* [1985], that a simple model like QPBRRM may not perform uniformly well in an uncalibrated mode for a suite of quite different rainfall-runoff events.

TABLE 10. Performance Summary for the Three Summary Output Variables for the 72 R-5 Events

Summary Output Variable	*Loague and Freeze* [1985]		This Study	
	Over Prediction	Under Prediction	Over Prediction	Under Prediction
Q_D	13	59	7	65
Q_{PK}	21	51	8	64
t_{PK}	15	57	6	66

Appropriateness of QPBRRM for R-5

Both the Horton and Dunne overland flow mechanisms are operative at R-5. The small catchment is, however, not easily understood or modeled. Small differences in near-surface characteristics account for large differences in the catchment's response for a given rainfall event. Further field study is needed to determine the quantitative importance of each runoff process under various rainfall scenarios. In that QPBRRM does not account for the Dunne mechanism, it is only partially suited to R-5.

Infiltration rates across R-5 are strongly influenced by vegetation and climate as shown in paper 1 [*Loague and Gander*, this issue]. Several other factors, however, also influence streamflow generation:

1. The transient nature of the water table controls streamflow generation at R-5. For different antecedent conditions, different streamflow generation mechanisms will dominate. Early on during the infiltration experiments, reported by Loague and Gander, when the catchment was relatively dry, approximately 2 m^3 of water was hosed into a single gopher hole located near the dry channel. This water was not discharged to the channel because the water table was too deep and became of regional importance. There was no evidence to suggest, based on this simple experiment, that subsurface storm flow is a dominant streamflow generation mechanism at R-5 as has been proposed by *Sloan and Leaman* [1979]. When the water table is at depth, runoff only results from large intense rainfall events due to the Horton mechanism. When the water table is near the surface, smaller less intense rainfall events can produce runoff by the Dunne mechanism.

TABLE 9. Statistics for Rainfall and Soil-Water Content Characteristics for the R-5 Catchment

	Rainfall Summary Variables*							
	P_D, mm		P_{XX}, mm/h		t_{XX}, hours		$\theta_{0.5}$† (dimensionless)	
Events	Mean	Standard Deviation	Mean	Standard Deviation	Mean	Standard Deviation	Mean	Standard Deviation
1–36	34	22	67	41	1.6	2.4	67	17
37–72	31	20	73	50	2.3	4.1	80	15
1–72	32	21	70	45	2.0	3.3	74	17

*See Table 3 for individual event values.

†Antecedent soil-water content, expressed as percent saturation, estimated for the surface layer only; see Table 3 for individual event values.

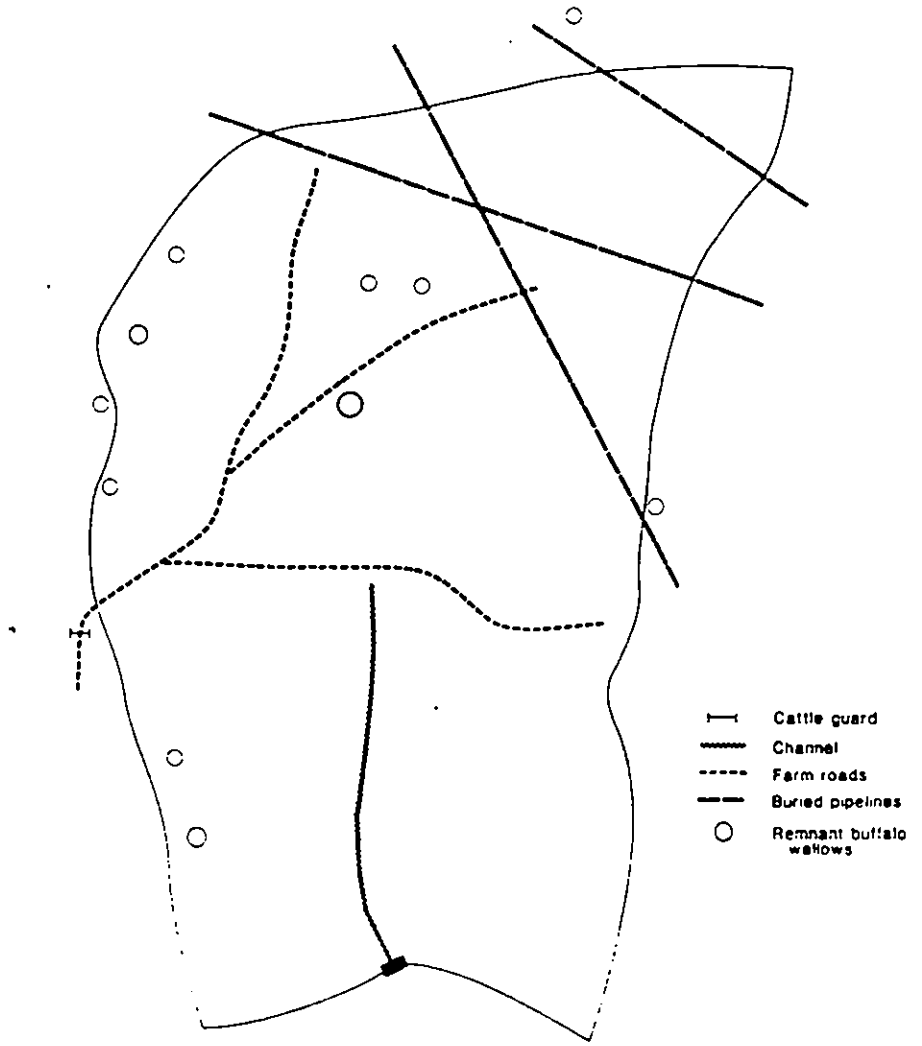

Fig. [illegible] Previously unreported characteristics of the R-5 catchment.

2. During prolonged rainfall events at R-5 it is typical for the remnant buffalo wallows across the catchment (Figure 5) to fill up like small ponds. This type of depression storage is on a much larger scale than is usually considered. These wallows are essentially sinks in the overland flow plane concept.

3. The roads and trails that cut across R-5 have tremendous impact on the routing and short-circuiting of runoff. Figure 6 illustrates the occurrence of Horton overland flow on an R-5 road.

4. Fertilizers, and other agricultural chemicals, have been used on R-5 at various times in the past, resulting in grasses several feet high (G. A. Gander, personal communication, 1985). The impact of such drastic changes in vegetation cover has not been considered but obviously is important to infiltration, surface roughness, detention storage, and overland flow paths.

It is widely held that the use of average soil hydraulic properties, determined from soil texture, can be used to effectively excite conceptual rainfall-runoff models like QPBRRM. It is the opinion of this writer, however, that the performance of physics-based models excited with average values based upon soil texture data gleaned from soil survey maps will be quite tenuous if the uncertainty in these data is not considered. The field observations at R-5, reported in paper 1 [*Loague and Gander*, this issue], support this conclusion.

Large Events

Admittedly, many of the runoff events from the R-5 catchment used in our original analysis [*Loague and Freeze*, 1985] are quite small, perhaps even smaller than the accuracy of the rainfall data. These events were considered in the earlier study to aid in the development of the regression and unit hydrograph models which were included in our comparative evaluation of underlying event-based rainfall-runoff modeling techniques. All 72 of the original R-5 runoff events are again included in the results discussed here. The reason for this is that the primary objective of this effort was to reevaluate QPBRRM based solely upon new information gleaned from the infiltration experiments reported in the companion paper [*Loague and Gander*, this issue]. In this section, however, the performance of the uncalibrated QPBRRM is also described for a subset of the largest R-5 events where runoff is not a small fraction of rainfall.

Table 11 summarizes the forecasting, prediction, and null case efficiencies for QPBRRM for the three summary output

ILLEGIBLE COPY

The documents appearing on the following page is the complete reproduction of the original document and was created during the normal course of business and, as delivered and in my legal custody at the time of filming. The following document is a true copy of the original document.

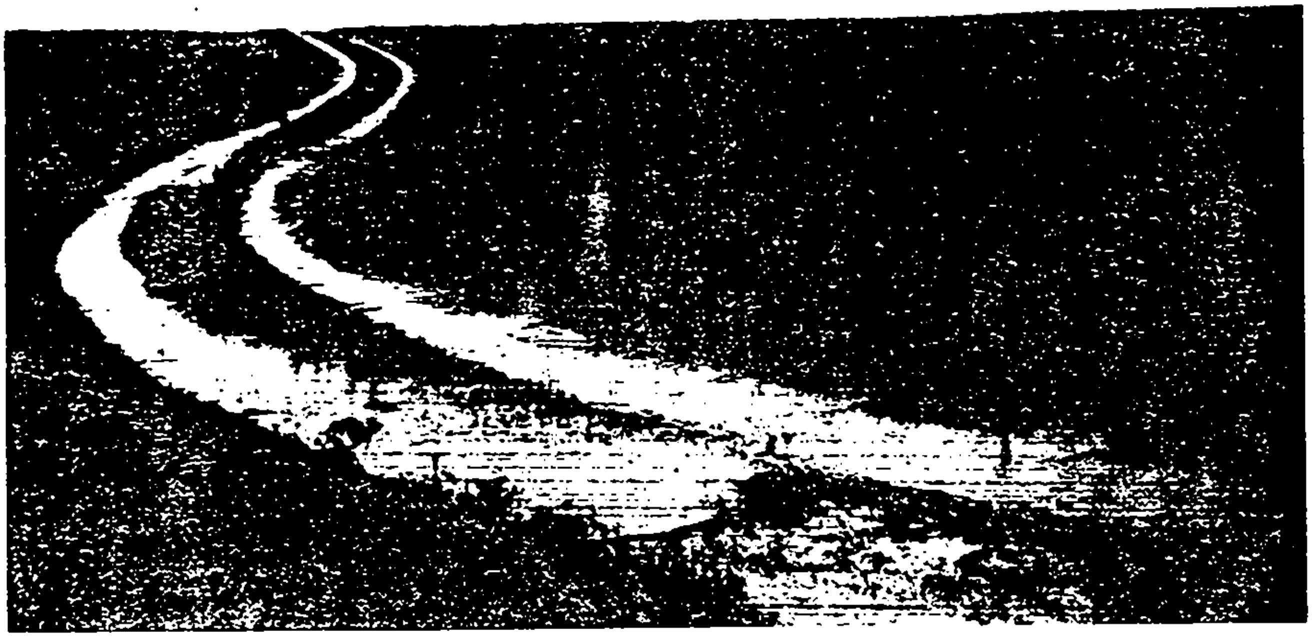

Fig. [illegible] A runoff event on the R-5 catchment resulting from a [illegible] rainfall event (November [illegible], 1984).

variables for nine selected R-5 events. Table 12 summarizes [illegible] deviations for the predicted and observed summary output variables for the selected R-5 events. Each of the selected events has the following observed characteristics: [illegible] [illegible] [illegible] for each of the nine selected [illegible] generalized remarks.

1. [illegible] values in Table [illegible] are poorer than those in Tables [illegible]. The efficiency values are higher for Q_{PK} than Q_D or t_{PK}; the performance of QPBRRM is improved with supplemental data.

2. The predicted means and standard deviations for Q_D and Q_{PK} in Table 12 are closer to the observed statistics for the simulations which do not incorporate the supplemental data. [illegible] predicted summary output variables.

3. The event summary [illegible] presented in Table 13 show both overestimates and underestimates in each set of results. In the [illegible] were [illegible] events. In the new simulations Q_D, Q_{PK}, and t_{PK} are overestimated for 2, 2, and 4 [illegible] events.

The E_2 values for [illegible] in Table [illegible] are [illegible]. Close inspection of the observed and predicted t_{PK} values in Table 13, however, reveals that only event 40 is poorly predicted. When the event 40 summary variables are omitted from the model evaluation calculations, the E_2 values for Q_D, Q_{PK}, and t_{PK} are changed to [illegible], [illegible], and 0.99, respectively, for the simulations with supplemental data. Obviously, the E_2 value of 0.99 for t_{PK} is very good for the eight events. This

TABLE 11. Forecasting, Prediction, and Null Case Efficiencies for the Three Summary Output Variables for QPBRRM for Nine Large R-5 Events

	E_1			E_2			E_3		
Data Set	Q_D	Q_{PK}	t_{PK}	Q_D	Q_{PK}	t_{PK}	Q_D	Q_{PK}	t_{PK}
Loague and Freeze [1985]*	−1.64	0.22	−2.77	−0.20	0.03	−1.34	−6.67	−5.55	−8.71
This study	−1.45	0.48	−2.64	−0.70	0.67	−1.26	−4.88	−3.33	−8.49

*Not previously reported.

TABLE 12. Statistics for Observed and Predicted Summary Output Variables for Nine Selected R-5 Events

	Summary Variables					
	Q_D, mm		Q_{PK}, L/s		t_{PK}, hours	
	Mean	Standard Deviation	Mean	Standard Deviation	Mean	Standard Deviation
Observed*	21	11	520	499	3.4	2.8
Simulated, *Loague and Freeze* [1985]†	18	22	658	963	5.0	6.5
Simulated, this study	9	15	372	721	5.0	6.4

Note: The coefficient of variation (CV) referred to in the text is equal to the standard deviation divided by the mean.
*See Table 13 for individual event values.
†Not previously reported.

example helps to illustrate the sensitivity of the evaluation criteria (E_f changes from −2.64 to 0.99). One should also note that E_f for Q_{PK} goes down (0.48 to 0.43) when event 40 is removed from the evaluation using the large events and that the E_f for Q_D is still very poor.

The criteria used to select individual rainfall-runoff events from the R-5 data base are presented with our original evaluations [*Loague and Freeze*, 1985, p. 235]. The duration of on-again, off-again rainfall for event 40 is more than 21 hours with multiple periods of high intensity. The antecedent soil-water content for this event is given in Table 3. The observed hydrograph shows more than one response. Simulations with QPBRRM do show a response at the time of the observed peak flow but predict the t_{PK} much later. Events with less than simple form, over longer periods of time where soil-water contents can vary substantially, are not well predicted with QPBRRM.

The QPBRRM predictions for the subset of large R-5 events presented here probably could be improved upon with calibration through parameter adjustments. In our original evaluation [*Loague and Freeze*, 1985] we reported a limited calibration of QPBRRM for a broad range of R-5 events. As the events become more alike, the calibration becomes easier. In our earlier evaluation we demonstrated that it was relatively easy to fit QPBRRM to a single event by adjusting the saturated hydraulic conductivity. The challenge is to simulate a broad range of events equally well.

CONCLUSIONS

Analyses of rainfall-runoff processes with physics-based mathematical models requires considerable information. The heterogeneity of near-surface hydrogeologic regimes and the irregularities of precipitation in both time and space, even at the catchment scale, weave a complex web of information that can never be fully obtained or transmitted to a deterministic-conceptual rainfall-runoff model. The best that can be hoped for is that a realistic sample of information will be sufficient to produce acceptable model results. However, the number of samples and the configuration of the sampling networks required to determine this representative level of information are never known a priori. It is, therefore, necessary to characterize the spatial distributions of soil hydraulic properties and precipitation to define sampling schemes that will give the best estimate of distributed hydrologic parameters.

In the first part of this study it was possible to address the spatial variability of infiltration across a small rangeland catchment at an admittedly impractical intensity. Even this effort failed to provide enough information to excite a distributed rainfall-runoff model with other than averaged values. The obvious question is whether it is worthwhile, or in fact even possible, to collect sufficient information to warrant the kind of grid-based data collection exercise described by *Loague and Gander* [this issue].

TABLE 13. Runoff Characteristics for Nine Large R-5 Rainfall-Runoff Events

Event Number	Q_D, mm			Q_{PK}, L/s			t_{PK}, hours		
	Observed*	Simulated, *Loague and Freeze* [1985]†	Simulated, This Study	Observed*	Simulated, *Loague and Freeze* [1985]†	Simulated, This Study	Observed*	Simulated, *Loague and Freeze* [1985]†	Simulated, This Study
4	20.39	11.88	1.25	584.75	422.21	32.80	1.60	1.63	1.50
22	14.24	6.28	1.59	477.71	228.51	68.34	5.18	5.23	5.20
24	10.44	36.45	19.52	262.19	978.28	531.47	9.26	9.10	9.13
35	25.30	15.38	5.96	281.61	300.61	184.57	2.35	0.93	2.30
40	27.36	1.29	0.34	131.87	41.85	11.51	5.55	20.63	20.40
52	45.60	69.32	46.15	1785.95	3103.64	2239.64	0.51	0.67	0.63
54	22.43	2.50	0.37	375.77	86.65	10.99	2.26	2.17	1.80
63	15.11	14.72	5.44	564.36	606.98	256.77	1.27	1.43	1.37
68	10.15	5.44	0.38	220.16	149.00	9.6	2.97	2.87	2.27

*Abstracted from Table 3.
†Not previously reported

The question of appropriate simulation scale is also obviously fundamental to physically based modeling. The established concept of a representative elementary volume [*Bear*, 1979] and the more recent idea of a representative elementary area [*Wood et al.*, 1988] are important considerations in rainfall-runoff modeling and data collection strategies. It is of course not possible to dig up the surface of the Earth just to identify the spatial variability of near-surface soil hydraulic properties so that we can effectively characterize, and then simulate, rainfall-runoff relationships.

Since our earlier paper [*Loague and Freeze*, 1985] several researchers [e.g., *Abbott et al.*, 1986; *DeCoursey*, 1988; D. Dawdy, personal communication, 1985] have felt that we had unilaterally endorsed simpler methods of rainfall-runoff modeling. This is not true. There is, however, considerable emotional baggage associated with parameter estimation for physically based rainfall-runoff models when the simulation scale and the parameter measurement scales are different. When parameter values are adjusted to calibrate a model, one must question if there is still a physical significance attached to the parameter estimates or if the physically based model has reverted to little more than an elegant black box. In this paper there was no calibration of the model.

The results presented here illustrate that the performance of QPBRRM is improved, in some instances, with supplemental information. However, the reported efficiencies also clearly show that the performance of physically based rainfall-runoff models can indeed be quite poor under "seemingly" appropriate conditions. Obviously, more information does not necessarily always lead to improved model performance when there is error inherent to the makeup of the model relative to the application, as in this study.

Storm Hydrograph Peak

The QPBRRM simulations and most of the model performance evaluations reported here were conducted in 1985. Recently I have learned that the runoff data for R-5 were not corrected for the rate of change of stage in the weir pond as is usually done for runoff data for U.S. Department of Agriculture (USDA) Agricultural Research Service (ARS) watersheds. At notch elevation the R-5 weir pond stores approximately 0.8 mm of water over the catchment. For this study, no information was provided on the stage of the pond when runoff began during the rainfall-runoff events before water crossed the weir. For these reasons the storm flow depths reported in Table 3 are biased low. Because the weir pond was not simulated with QPBRRM, the model would tend to overpredict the peak storm flow and underpredict the time to peak storm flow for the R-5 events. The storm flow depths were underestimated with QPBRRM for the smaller R-5 events so the pond probably had a comparatively small impact on the model efficiencies determined for Q_p. The impact may have been more significant for the model efficiencies determined for Q_{pK} and t_{pK}. An effort is currently under way (D. A. Woolhiser, personal communication, 1989) to examine the effects of the pond on the R-5 runoff data. If significant effects are found, then the model evaluations reported both here and in the work by *Loague and Freeze* [1985] will of course be revised.

Acknowledgments. The work reported here was initiated while the author was a student at the University of British Columbia. Partial support for this research, in the early stages, was by way of a grant to Al Freeze from the National Science and Engineering Research Council of Canada. The cooperation of Gene Gander and Ted Engman is gratefully acknowledged. Anh Nguyen and Fred Cheng helped with some of the final efficiency computations. The presentation benefited from comments by Steve Burges, Al Freeze, Gary Sposito, David Woolhiser and the WRR reviewers. The manuscript was typed by Terri DeLuca. The figures were drafted by Gord Hodge.

REFERENCES

Abbott, M. B., J. C. Bathurst, J. A. Cunge, P. E. O'Connell, and J. Rasmussen, An introduction to the European hydrological system–systeme hydrologique, "SHE," 1. History and philosophy of a physically based distributed modelling system, *J. Hydrol.*, *87*, 45–59, 1986.

Alley, W. M., and P. E. Smith, User's manual: Distributed routing rainfall-runoff model—Version 11, *U.S. Geol. Surv. Open File Rep.*, *82-344*, 1982.

American Society for Testing and Materials, Standard practice for evaluating environmental fate models of chemicals, *Rep. E978-84*, ASTM, Philadelphia, PA., 1984.

Bear, J., *Hydraulics of Groundwater*, McGraw-Hill, New York, 1979.

Betson, R. P., and C. V. Ardis, Implications for modeling surface-water hydrology, in *Hillslope Hydrology*, edited by M. J. Kirkby, pp. 295–323, Wiley Interscience, New York, 1978.

Beven, K., and P. Germann, Macropores and water flow in soils, *Water Resour. Res.*, *18*, 1311–1325, 1982.

Dawdy, D. R., J. C. Schaake, and W. M. Alley, User's guide: Distributed routing rainfall-runoff model, *U. S. Geol. Surv. Water Resour. Invest. Rep.*, *78-90*, 1978.

DeCoursey, D. G., A critical assessment of hydrologic modeling, in *Proceedings of International Symposium on Modeling Agricultural, Forest and Rangeland Hydrology*, pp. 478–493, American Society of Agricultural Engineers, St. Joseph, Mich., 1988.

Dunne, T., Field studies of hillslope flow processes, in *Hillslope Hydrology*, edited by M. J. Kirkby, pp. 227–293, Wiley Interscience, New York, 1978.

Dunne, T., Models of runoff processes and their significance, in *Scientific Bases of Water-Resource Management*, pp. 17–30, National Academy Press, Washington, D. C., 1982.

Dunne, T., and R. D. Black, An experimental investigation of runoff production in permeable soils, *Water Resour. Res.*, *6*, 478–490, 1970*a*.

Dunne, T., and R. D. Black, Partial area contributions to storm runoff in a small New England watershed, *Water Resour. Res.*, *6*, 1296–1311, 1970*b*.

Engman, E. T., A partial area model for simulating surface runoff from small watersheds, Ph.D. thesis, Pa. State Univ., University Park, 1974.

Engman, E. T., and A. S. Rogowski, A partial area model for storm flow synthesis, *Water Resour. Res.*, *10*, 464–472, 1974.

Freeze, R. A., Role of subsurface flow in generating surface runoff, 1. Base flow contributions to channel flow, *Water Resour. Res.*, *8*, 609–623, 1972*a*.

Freeze, R. A., Role of subsurface flow in generating surface runoff, 2. Upstream source areas, *Water Resour. Res.*, *8*, 1272–1283, 1972*b*.

Freeze, R. A., Streamflow generation, *Rev. Geophys.*, *12*, 627–647, 1974.

Freeze, R. A., A stochastic-conceptual analysis of rainfall-runoff processes on a hillslope, *Water Resour. Res.*, *16*, 391–408, 1980.

Freeze, R. A., and R. L. Harlan, Blueprint for a physically-based, digitally simulated, hydrologic response model, *J. Hydrol.*, *9*, 237–258, 1969.

Ghurek, W. J., Modeling storm hydrograph water quality—A partial area approach, Ph.D. thesis, Pa. State Univ., University Park, 1978.

Green, I. R. A., and D. Stephenson, Criteria for comparison of single event models, *Hydrol. Sci. J.*, *31*, 395–411, 1986.

James, L. D., and S. J. Burges, Selection, calibration, and testing of hydrologic models, in *Hydrologic Modeling of Small Watersheds*, edited by C. T. Haan, H. P. Johnson, and D. L. Brakensick, pp. 437–472, American Society of Agricultural Engineers, St. Joseph, Mich., 1982.

Loague, K. M., An assessment of rainfall-runoff modeling methodology, Ph.D. thesis, Univ. of B. C., Vancouver, 1986.

Loague, K. M., and R. A. Freeze, A comparison of rainfall-runoff modeling techniques on small upland catchments, *Water Resour. Res.*, *21*, 229–248, 1985.

Loague, K., and G. A. Gander, R-5 revisited, 1, Spatial variability of infiltration on a small rangeland catchment, *Water Resour. Res.*, this issue.

Loague, K., and R. E. Green, Statistical and graphical methods for evaluating solute transport models: Overview and application, *J. Contam. Hydrol.*, in press, 1990.

Nash, J. E., and J. V. Sutcliffe, River flow forecasting through conceptual models, 1, A discussion of principles, *J. Hydrol.*, *10*, 282–290, 1970.

Pearce, A. J., M. K. Stewart, and M. G. Sklash, Storm runoff generation in humid headwater catchments, 1, Where does the water come from?, *Water Resour. Res.*, *22*, 1263–1272, 1986.

Philip, J. R., Field heterogeneity: Some basic issues, *Water Resour. Res.*, *16*, 443–448, 1980.

Rogowski, A. S., Two- and three-point models of the soil moisture characteristics and hydraulic conductivity for field use, in *Joint IAHR and ISSS Symposium on Fundamentals of Transport Phenomena in Porous Media*, vol. 1, pp. 124–136, Huddleston and Barney, Woodstock, Ont., 1972.

Sharma, M. L., and P. J. Luxmoore, Soil spatial variability and its consequences on simulated water balance, *Water Resour. Res.*, *15*, 1567–1573, 1979.

Sharma, M. L., G. A. Gander, and G. C. Hunt, Spatial variability of infiltration in a watershed, *J. Hydrol.*, *45*, 101–122, 1980.

Wilmott, C. J., S. G. Ackleson, R. E. Davis, J. J. Feddema, K. M. Klink, D. R. Legates, J. O'Donnell, and C. M. Rowe, Statistics for the evaluation and comparison of models, *J. Geophys. Res.*, *90*(C5), 8995–9005, 1985.

Wood, E. F., M. Sivapalan, K. Beven, and L. Band, Effects of spatial variability and scale with implication to hydrologic modeling, *J. Hydrol.*, *102*, 29–47, 1988.

K. Loague, Department of Soil Science, University of California, 108 Hilgard Hall, Berkeley, CA 94720.

(Received March 13, 1989;
revised October 4, 1989;
accepted October 6, 1989.)

SOIL SCIENCE SOCIETY OF AMERICA
JOURNAL

VOL. 52 SEPTEMBER-OCTOBER 1988 NO. 5

DIVISION S-1—SOIL PHYSICS

Designs for Disc Permeameters[1]

K. M. PERROUX AND I. WHITE*

ABSTRACT

Disc permeameters are designed to measure hydraulic properties of field soils containing macropores and preferential flow paths and are particularly useful in soil management studies. We present here designs for disc permeameters for both positive and negative water supply heads. The effects of the water supply membrane and soil contact material on permeameter performance are examined using approximate quasi-analytic solutions to the flow equation. This analysis provides approximate criteria for the selection of membrane and soil contact materials. Limitations to performance caused by restricted air entry are considered and design criteria are given also. We present in situ tests of the disc permeameter for the early stages of one-dimensional infiltration and an example of the deterministic variation of sorptivity of a field soil with supply potential. Finally, we use ponded and unsaturated sorptivities measured in situ with disc permeameters to find the saturated hydraulic conductivity and the area-weighted mean characteristic pore dimension of a field soil.

Recognition of the importance of biologically generated macropores and preferential flow paths to field infiltration and plant water uptake (e.g., Bouwer, 1964; Dixon, 1972; Clothier and White, 1981; Beven and Germann, 1982; Watson and Luxmoore, 1986; Passioura, 1985) has led to a renewed interest in measurement techniques in which preferential water flow through macropores and soil cracks is selectively controlled. Since soil management practices and/or environmental factors can dramatically change macroporosity, such techniques are valuable in quantifying alterations in soil properties, particularly those leading to changes in infiltration, time-to-ponding, runoff, and erosion.

A convenient means of controlling macropore flow is to apply water to soil at water potentials, Ψ_0, less than zero. The maximum diameter of vertical pores, connected to the soil surface, through which water can enter is given by simple capillarity theory and is proportional to $(-\Psi_0)^{-1}$. The more negative Ψ_0, the smaller the maximum diameter of pores that can participate in flow from the soil surface. We note, though, that such simple arguments do not hold for nonvertical pores or those buried below the surface (Philip et al., 1987, personal communication).

In this work we describe our designs for disc permeameters in which water can be supplied to in situ soils at readily selectable, positive and negative pressures. These permeameters have evolved from our previous sorptivity tube design (Clothier and White, 1981). In addition, we estimate the effects of the permeameter's supply membrane, soil contact material and air delivery system on flow measurement, and develop criteria for their selection. Finally, we give comparative tests and examples of the performance of the permeameters in the field, showing the contribution of supply potential to perceived variability, and demonstrate their use in measuring sorptivity, hydraulic conductivity, and in estimating in situ characteristic mean pore size.

PREVIOUS TECHNIQUES

Talsma's (1969) technique for the in situ determination of sorptivity is restricted to water supply pressures greater than zero. It suffers from the disadvantage that Ψ_0 decreases during measurement, a disadvantage that we rectify here. Dixon (1975) designed a closed-top, single-ring infiltrometer to study flow in macropores. With this device, Ψ_0 in the range $-0.03 \leq \Psi_0 \leq -0.01$ m H_2O were achievable. This closed-top system appears somewhat cumbersome, however, for routine field use.

CSIRO Division of Environmental Mechanics, GPO Box 821, Canberra ACT 2601, Australia. Contribution from CSIRO, Australia. Received 30 Nov. 1987. *Corresponding author

Published in Soil Sci. Soc. Am. J. 52:1205-1215 (1988).

[1] Comment from the Editor-in-Chief—The first disc permeameter was built in 1982 by Mr. K. M. Perroux by modification of the sorptivity tube design reported by Clothier and White (1981). Since then, the instrument has been generously made available to other scientists and some publications have preceded the present paper reporting the design and performance of disc permeameters by the instrument developers. The authors of two papers published in the *SSSA Journal* reporting the use of the disc permeameter (Watson and Luxmoore, 1986; Wilson and Luxmoore, 1988), request that Perroux and White receive full credit in any research with their instrument design by citation of their paper published here.

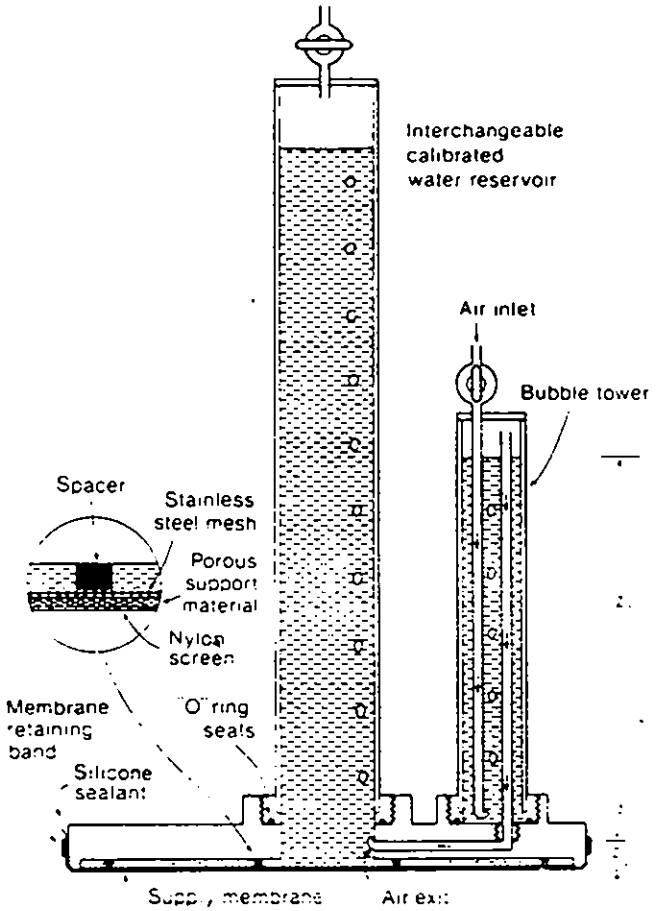

Fig. 1. Disc permeameter for supplying water at pressures less than or equal to zero. Reservoirs of varying diameters may be interchanged. Arrows show direction of air flow.

Dirksen (1975), following Smiles and Harvey (1973), employed measurements of sorptivity at a range of negative Ψ_0 to estimate soil-water diffusivity using a specially designed permeameter. His permeameter was not intended specifically to study preferential flow and appears not to have been used much in the field. Its simplicity, with a membrane to supply water, makes it attractive for such studies.

Clothier and White (1981) retained features of Dirksen's design but produced a simpler and more convenient permeameter for field use. Their sorptivity tube is essentially a Mariotte bottle in which Ψ_0 was determined by the bubbling pressure of a capillary or hypodermic needle through which air entered a water reservoir. Water was supplied to the soil via a sintered glass plate of appropriate bubbling pressure. The practical range of supply potentials was $-0.1 \leq \Psi_0 \leq 0$ m H_2O. A modified water supply plate design was published by Chong and Green (1983). This modification seems restricted to an even narrower range of Ψ_0, because of its smaller bubbling pressure.

Clothier and White's (1981) sorptivity tube has been used in a variety of hydrological and soil management studies (Clothier et al., 1981; Clothier and White, 1982; White et al., 1982; Hamilton et al., 1983; Packer et al., 1984; Walker and Chong, 1986).

In the course of our work several limitations of the original design became apparent. Firstly, the size of sintered glass plates available restricted the permeameter to diameters < 0.1 m. Secondly, direct measurement of Ψ_0 at the soil surface during the initial stages of infiltration showed, for soils with high sorptivity, that air entry through the capillary was insufficient to maintain Ψ_0 constant. Larger diameter devices exacerbate this problem. Also, in the rigors

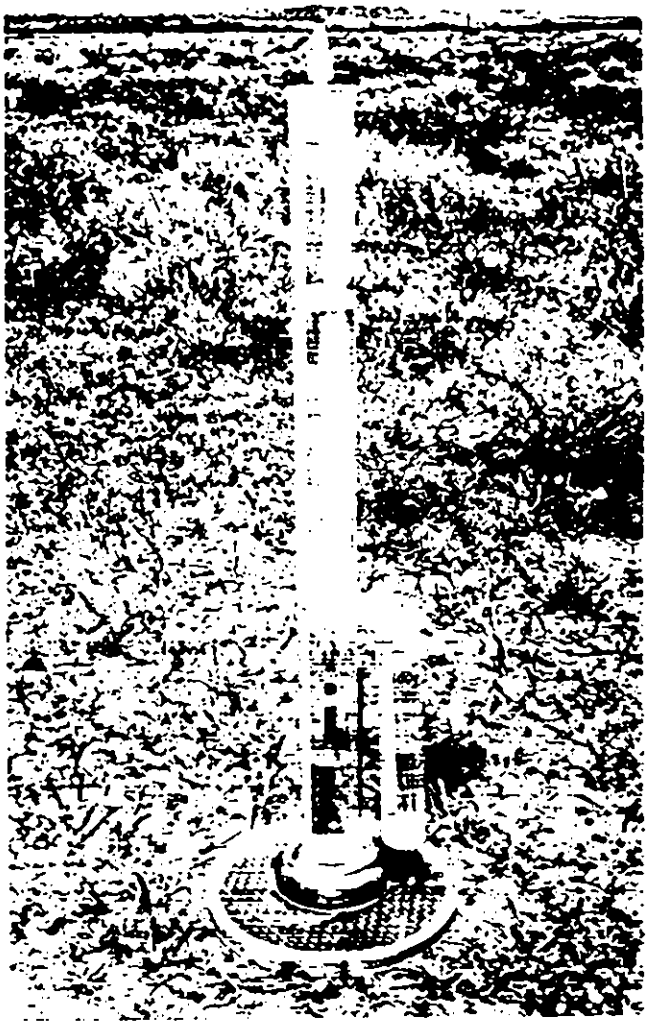

Fig. 2. Disc permeameter at use in an arid saline and stoney environment, Finke's Gap, far western New South Wales, Australia.

of field use, the hypodermic needles employed as the capillary tubes may prove unsuitable due to complete blockage. Finally, situations arise that required wider ranges of Ψ_0.

We describe here improvements to the sorptivity tube that [illegible] its versatility.

DISC PERMEAMETER DESIGNS

Supply Pressures Less Than or Equal to Zero

In our improved design, shown in Fig. 1, the original hypodermic needle is replaced by a bubbling tower. The water height in it is used to select and control Ψ_0. Here Ψ_0 is simply the difference between the distance from the air exit tube to the membrane (z_1) and the height of water in the bubble tower above the bubble entry point (z_2, see Fig. 1), so that

$$\Psi_0 = z_1 - z_2 \qquad [1]$$

We have independently measured Ψ_0 by contacting a fast-response tensiometer against the supply membrane during rapid absorptive flows and find that Eq. [1] is an adequate description.

The new water supply membrane is a composite material whose principal component is a nylon screen material with known and uniform mesh size (we have used Nytal 25 nylon screen material). The other two layers, a porous 1.5-mm thick material ("Vylene" shirt collar stiffener) and a coarse

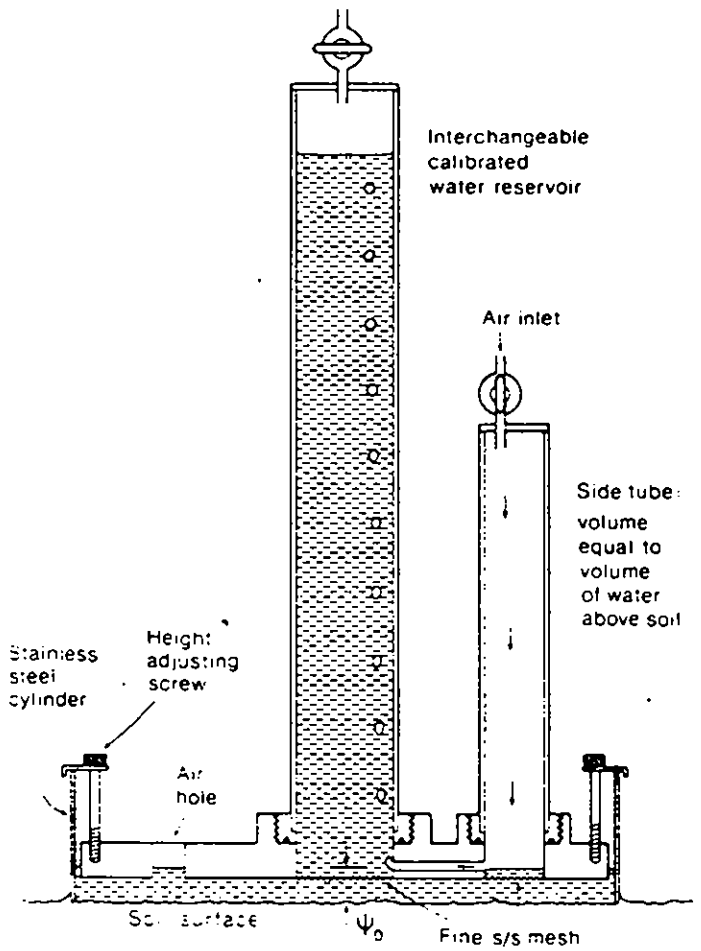

Fig. 3. Disc permeameter for supplying water at positive pressures. Volume of side-tube is equal to volume of water between the soil surface and the permeameter and is supplied to surface at commencement of infiltration

stainless steel mesh (4.80-mm aperture) stiffener, support the nylon membrane and are shown in detail in Fig. 1. This composite membrane can be cut to any diameter up to 1 m.

The nylon material is available in a variety of pore sizes that enable Ψ_0 to be selected in the range $-1 \leq \Psi_0 \leq 0$ m H_2O. We have limited our attention here to 63-μm mesh size with an air entry pressure of 0.2 m H_2O. The membrane is stretched and attached to the outer body of the permeameter head with Silicone rubber sealant and held in place with a retaining "O" ring or band. Membranes may be readily changed in the field.

The permeameter is fabricated from either clear acrylic or polycarbonate plastic. It is essential that the supply membrane be visible during infiltration to permit examination for air leaks. Both the water reservoir tubes and bubbling tower have metal distance scales attached. To increase accuracy, transportability and versatility, the reservoir and bubbling tube may be unscrewed from the permeameter head. This permits the use of reservoirs of various diameters (we are grateful to Dr. M.D. Melville, University of New South Wales, for this suggestion). A permeameter in operation on a difficult soil is shown in Fig. 2.

Supply Pressures Greater Than Zero

To assess all macropore contributions to flow, supply pressures greater than zero must be used also. The disc permeameter design for $\Psi_0 > 0$ is shown in Fig. 3. Its superficial resemblance to that in Fig. 1 is apparent. The permeameters were designed deliberately so that reservoirs and air entry tubes are interchangeable.

The supply pressure here is the distance between the air bubble exit point and the soil surface, and is selected by adjusting the three level-adjustment screws. The egress of water from the reservoir and air-entry side-tube before the initiation of flow is prevented by fine stainless steel meshes at the bottom of the reservoir and side tube.

The air-entry side-tube initially contains water whose volume is adjusted approximately equal to the volume between the permeameter head and the soil surface. This water is rapidly deposited on the soil surface by opening the side-tube stopcock to commence infiltration. The soil surface may be protected by a permeable membrane (such as paper toweling) if desired.

OPERATION OF PERMEAMETERS

Negative or Zero Supply Pressures

The reservoir for the negative head permeameter (Fig. 1) is filled by placing the head of the permeameter in water, closing the air-inlet stopcock, opening the reservoir stopcock, and evacuating air from the reservoir. The level of water in the bubbling tower is adjusted to give the desired Ψ_0.

In the one-dimensional mode of operation a thin-walled stainless steel cyclinder is driven carefully into the soil to ensure one-dimensional flow. Its top is flush with the soil surface. Any disturbed soil around the perimeter of the cylinder is tamped down with a thin tamping rod. A 30-mm wide annulus of soil is removed from the outside of the cylinder to a depth of 20 mm to prevent any interference with the permeameter head.

Good contact between the disc and the soil is *absolutely essential*. Any vegetation within the sample is trimmed to ground level. For uneven soil surfaces a 3-mm high extension ring is fitted over the cylinder and packed with contact material. After smoothing and leveling the contact material, the extension ring is removed leaving the soil sample capped with contact material.

Infiltration is commenced by opening the air-inlet stopcock and placing the permeameter firmly on the sample. Volumes of water infiltrated are then recorded from the fall of the water level in the reservoir at known times.

Positive Supply Pressures

In the one-dimensional mode (Fig. 3), a thin-walled cylinder is driven part way into the soil and any disturbed soil around the perimeter is tamped down. The distance from the top of the cylinder to the soil is adjusted to contain the selected head of water and the permeameter. No contact material is necessary here. The empty permeameter is placed on the cylinder and the adjustment screws are altered to give the required Ψ_0. The permeameter is then removed and filling is as above except here the air-entry side-tube is filled as well and its stopcock closed. The permeameter is repositioned on the cylinder, and infiltration commences after the side-tube stopcock is opened allowing the side-tube water volume to be rapidly deposited onto the soil. Infiltrated volumes are recorded as a function of time.

Sorptivity

The sorptivity, $S_0 = S(\Psi_i, \Psi_0)$, is found at any supply potential from the time dependence of cumulative infiltration, i, at early times (Philip, 1957) using:

$$\lim_{t \to 0} \frac{di}{dt^{1/2}} \to S_0 . \qquad [2]$$

For one-dimensional infiltration Philip (1969) argued that

capillarity should dominate one-dimensional flow for infiltration times, $t < t_{grav}$, with

$$t_{grav} = S_i^2/(K_0 - K_n)^2 . \quad [3]$$

Here $K_0 = K(\Psi_0)$ and $K_n = K(\Psi_n)$ are hydraulic conductivities at the supply and antecedent potentials, respectively. Talsma (1969) found that the influence of gravity on one-dimensional infiltration was negligible for $t \leq 0.02\ t_{grav}$.

In the field we have found t_{grav} varying between 0.08 and 34 h (White and Sully, 1987) so we expect the linearity of $i(t^{1/2})$ implied by Eq. [2] to hold for as little as 6 s to as long as at least 2450 s. Commonly we find linearity for at least 60 s. We note that sorptivity and hence t_{grav} are dependent on antecedent soil-water potential.

Hydraulic Conductivity

If the sample-containing cylinder is sufficiently long, hydraulic conductivity at the supply potential Ψ_0, $K_0 = K(\Psi_0)$, may be found from the long-time infiltration rate for $t \gg t_{grav}$:

$$\lim_{t \to \infty} \frac{di}{dt} = K_0 . \quad [4]$$

With some soils this may involve impractically long measurement times. We also note that $K_0(\Psi)$ may be determined over a range of Ψ_0 by measuring S_0 over the same range of Ψ_0 (White and Perroux, 1987).

When information is required on thinner soil samples, the soil core contained in the cylinder may be carefully removed from the profile and its conductivity determined as in Clothier and White (1981).

ANALYSIS OF DISC PERMEAMETER PERFORMANCE

In the negative head version of the permeameter, water is supplied to the soil through a membrane and, usually, through a thin layer of contact material. In this section we give the results of an approximate analysis of the effect of these and air entry into the permeameter on the permeameter's performance. The influence of these factors will be most apparent during the early stages of flow. We thus concentrate on absorption.

Effect of Supply Membrane on Water Absorption

The conductance, α, of the permeameter membrane is taken to be time-independent and the sorptivity of the soil at the supply potential is S_0. We take the soil initially to be dry, with antecedent potential $\Psi_n \to -\infty$. For simplicity we assume the exponential or quasi-linear model for soil hydraulic conductivity (Philip, 1966):

$$K(\Psi) = K_0 \exp(\Psi/\lambda) . \quad [5]$$

Here λ is the macroscopic capillary length (Philip, 1983; White and Sully, 1987) and $K_0 = K(\Psi = 0)$. Note that Eq. [5] may be fitted to any $K(\Psi)$ by taking (Philip, 1985)

$$\lambda = [K_0 - K_n]^{-1} \int_{\Psi_n}^{\Psi_0} K(\Psi)\, d\Psi . \quad [6]$$

We shall take K_n as zero here. The length scale in Eq. [6] may be used as a scaling length in this problem.

The early stages of flow into soil through a membrane have been treated in convenient quasi-analytic fashion by Smiles et al. (1982). In the Appendix we develop an approximate solution based on their integral expressions.

The approximate analytic solution for cumulative absorption into dry soil through a membrane in terms of the dimensionless variables defined in the Appendix is ([A13] to [A15])

$$(S_i/S_0)^2 \alpha_*^2 t_* = \tfrac{1}{2}\{(S_i/S_0)^2 \alpha_* i_* [1 + \alpha_*/(di_*/dt_*)] - E_1[(di_*/dt_*)/\alpha_*]\} \quad [7]$$

with

$$di_*/dt_* = \alpha_* \Delta\Psi_* \quad [8]$$

and

$$(S_i/S_0)^2 \alpha_* i_* = \frac{\exp(-\Delta\Psi_*)}{\Delta\Psi_*} \quad [9]$$

with $\Delta\Psi_* = \Psi_{*0} - \Psi_{*1}(t)$, $\Psi_{*1}(t)$ is the dimensionless soil-water matrix potential just below the membrane, and $E_1(x)$ is the exponential integral (Gautschi and Cahill, 1972).

We note here that use of the dimensionless similarity variables $\alpha_* i_*$, $\alpha_*^{-1} di_*/dt_*$, $\alpha_*^2 t_*$ (Ahuja and Swartzendruber, 1973) together with $\Delta\Psi_*$ gives a solution which, for dry soils, is independent of membrane conductance, soil hydraulic properties, and supply potential.

For small times where $\Psi_{*1} \to \Psi_{*n}$ and $E_1(\Delta\Psi_*) \to [\exp(-\Delta\Psi_*)]/(1 + \Delta\Psi_*)$, we find from Eq. [7] through [9] that

$$\lim_{t \to 0} i_* \to \alpha_*(\Psi_{*0} - \Psi_{*n}) t_* \quad [10]$$

while for large absorption times where $\Delta\Psi_* \to 0$

$$\lim_{t \to \infty} \frac{1}{2}\, di_*^2/dt_* \to (S_0/S_i)^2 . \quad [11]$$

That is, in the small time limit, the membrane conductance and initial potential difference across the membrane dominate flow, as they must, while in the "long time" limit, in the absence of gravity, only soil sorptivity is important. For infiltration flows this "long

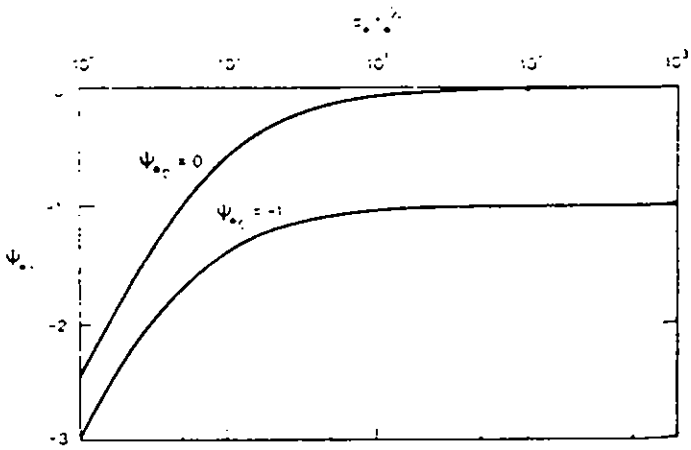

Fig. 4. Effect of supply membrane on flow. Dimensionless surface potential at soil/membrane interface as a function of dimensionless time for two supply potentials. The α_* is the dimensionless membrane conductance.

time" limit has to be clearly less than t_{gra}, of Philip (1969).

To illustrate these solutions, we select two values of Ψ_{*0}, 0 and -1. For many field soils $\lambda \approx 0.1$ m (White and Sully, 1987) so these dimensionless potentials correspond approximately to $\Psi_0 = 0$ and -0.1 m.

The dimensionless time-dependence of potential at the membrane/soil surface, Ψ_{*1}, for these two potentials is given in Fig. 4. The asymptotic approach to Ψ_{*0} is obvious.

In Fig. 5 we show the dimensionless cumulative infiltration as a function of dimensionless square root of time. For both supply potentials the departure of $\alpha_* i_*$ from linearity in $\alpha_* t_*^{1/2}$ is most noticeable for $\alpha_* t_*^{1/2} < 1$. At the smaller supply potential, $\Psi_{*0} = -1$, the approach to linearity is faster than at $\Psi_{*0} = 0$.

This approach to linearity in $\alpha_* t_*^{1/2}$ is best seen in Fig. 6, where we plot $\frac{1}{2} di_*^2/dt_*$ as a function of $\alpha_* t_*^{1/2}$. We recall that in the absence of a membrane $\frac{1}{2} di_*^2/dt_* = (S_0/S_1)^2$, which, for $\Psi_{*0} = 0$, is 1 and for $\Psi_{*0} = -1$ is 0.3679. The asymptotic approach to these values is apparent. We may use the results in Fig. 6 as a method of establishing criteria for the membrane conductance and determining the time at which the influence of the membrane becomes negligible.

Criterion for Membrane Conductance

Absorption

We fix the criterion for absorption by requiring a membrane conductance such that $\frac{1}{2} di_*^2/dt_*$ attains 95% of its long-term absorption limit in a time, t_{95}. To be of practical use, t_{95} must be a sufficiently short time. The dimensionless times at which this occurs are shown in Fig. 5 and 6 for both supply potentials. This 95% criterion can be seen from Fig. 5 to be adequate for field use.

It follows from Eq. [7] to [9] that we require the membrane conductance to be

$$\alpha_* t_{95}^{1/2} \geq 14\ (S_0/S_1) \qquad [12]$$

This inequality becomes, in dimensional terms, for *any* supply potential, Ψ_0:

$$\alpha \geq 10\ S_0/[\lambda t_{95}^{1/2}]\ . \qquad [13]$$

The inequality Eq. [13] is one of the criteria we seek. If we now specify $t_{95} = 10$ s, as seems reasonable, and accept $\lambda \approx 0.1$ m, then $\alpha \geq 30\ S_0$. Under negative supply heads, which are close to zero, S_0 seldom exceeds 10^{-3} m s$^{-1/2}$. If follows that we require, approximately, $\alpha \geq 0.03$ s^{-1} for Ψ_0 close to zero.

Infiltration

When gravity starts to dominate flow, it is essential that the membrane conductance not impede flow. If it does, flow instabilities may develop (Raats, 1973; Philip, 1975). The criterion for this is merely that the membrane conductance be equal to or greater than the soil conductance. It follows from identifying λ as the appropriate macroscopic soil-based length scale and the definition of the dimensionless membrane conductance, [A4], that this is so when

$$\alpha \gg K_{\psi}/\lambda\ . \qquad [14]$$

To estimate the magnitude of α, we take $\lambda \approx 0.1$ m again. Except for rock heaps, values of K_{ψ} seldom exceed 10^{-3} m s^{-1} so that the condition Eq. [14] corresponds to $\alpha \gg 10^{-2}$ s^{-1}. The gravity criterion Eq. [14] is thus less stringent than that for absorption, Eq. [13], as is expected.

Criteria for Capping Material

It is obvious that the depth, L_c, of capping material must be as small as possible to minimize its effect on flow. This depth will depend on surface roughness. Usually L_c varies between 3 and 5 mm. Because of the small depth involved, we can approximate the behavior of the capping material as a Green-Ampt material and treat the thin cap as a membrane or surface crust. We designate properties of the cap with sub-

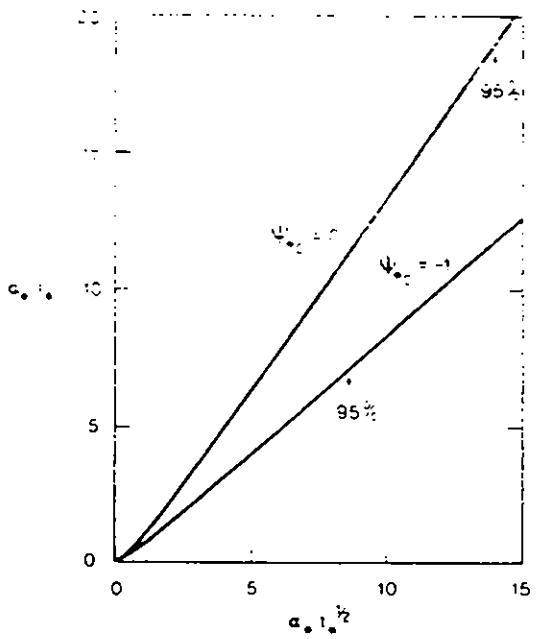

Fig. 5. Effect of supply membrane on flow. Dimensionless cumulative infiltration as a function of dimensionless time for two supply potentials. The arrows mark the times when $1/2\ di_*^2/dt_*$ is 95% of the longtime absorption limit.

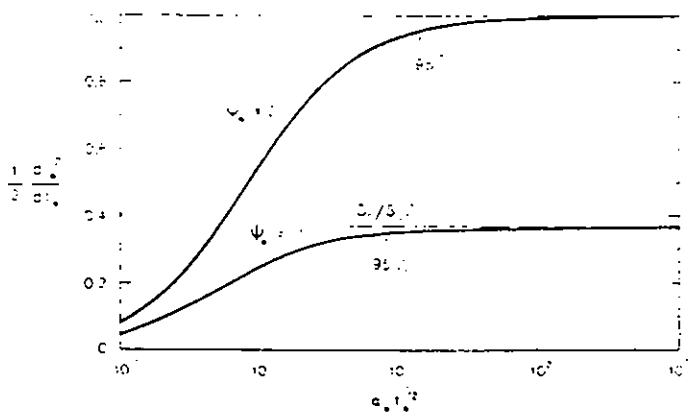

Fig. 6. Effect of supply membrane on flow. Slope of cumulative infiltration as a function of dimensionless time for two supply potentials. The arrows mark the times when $1/2\ di_*^2/dt_*$ is 95% of the longtime absorption limit.

script c. Some time obviously is required for water to move through the thickness, L_c, of the cap.

For Green-Ampt materials of small L_c the initial water flow will be governed entirely by capillarity. We may, therefore, write the cumulative infiltration into the capping as:

$$i_c = \Delta\theta_c L_c = S_c t_c^{1/2}.$$

Here S_c is the sorptivity of the capping at the supply potential Ψ_0. The time for water to move through the cap, t_c, is then

$$t_c = [\Delta\theta_c L_c / S_c]^2. \quad [15]$$

Taking $\Delta\theta_c = 0.3$, $L_c = 5$ mm, $S_c \approx 5 \times 10^{-4}$ m s^{-1} we have typically $t_c \approx 10$ s. Clearly in the initial stages of flow capping materials will need to have appreciable sorptivities over a range of supply potentials. Materials with uniform pore sizes will be inappropriate unless their "tension saturated" zone covers the required supply potential range.

Absorption

The cap conductance, α_c, will be strictly time-dependent with

$$\alpha_c(t) \approx [\{\Psi_0 - \Psi_c(t)\} \cdot L_c]^{-1} \int_{\Psi_c(t)}^{\Psi_0} K(\Psi) d\Psi. \quad [16]$$

where Ψ_0 is the supply potential at the cap surface, and $\Psi_c(t)$ the potential at the cap/soil interface (White et al., unpublished data). Invoking the Green-Ampt assumption, we approximate this with a time independent α_c.

$$\alpha_c \approx K(\Psi_0)/L_c \quad [17]$$

If we specify infiltration time as the time after the wetting front has moved through the cap, then we may use the preceding analysis for flow through a membrane. It follows from Eq. [17] and [13] that we require

$$K_c(\Psi_0) \gg 10 S_c^2 L_c / [\lambda t_{ss}^{1/2}] \quad [18]$$

With the above estimates of S_c, λ, t_{ss}, θ_s, and $L_c = 5$ mm, we find from Eq. [18] that $K_c(\Psi_0) \gg 1.6 \times 10^{-6}$ m s^{-1}, which is a large conductivity. We emphasize that this is expected to be a maximum value applicable to Ψ_0 close to zero. With high subsoil sorptivities, the effect of the cap material may persist for times as long as 60 s. The rapid decrease of S_c with Ψ_0 in the field (White and Perroux, 1987) means that we can expect Eq. [18] to be less restrictive at more negative Ψ_0.

Infiltration

During the later stages of infiltration the assumption of constant cap conductance is appropriate and the arguments leading to Eq. [14] apply. With this and Eq. [17] we have

$$K_c(\Psi_0) \gg K_c L_c / \lambda. \quad [19]$$

To a first-order approximation the maximum required K_c for $L_c = 5$ mm is $K_c \approx 5 \times 10^{-6}$ m s^{-1}, again less stringent than the absorption criterion.

The above estimates of the effect of the contact material on flow are admittedly crude but suffice for order-of-magnitude estimates of the maximum required cap properties. Clearly, the best capping material would be one whose hydraulic properties were identical to those of the underlying soil. This is, of course, not always practical. When one contact material is used for a wide range of soils, the above estimates indicate that the material should have both high sorptivity and conductivity for Ψ_0 close to zero but have a weakly Ψ-dependent $K_c(\Psi)$. The material should have a broad particle size distribution or have a "tension saturated zone" that covers the desired Ψ_0 range. We have found that the aeolian deposit, Bungendore fine sand, is very suitable with $S_0 \approx 2 \times 10^{-3}$ m s$^{-1/2}$ and $K_0 \approx 3 \times 10^{-5}$ m s^{-1}.

Air Entry into the Permeameter

We now examine how air entry into the disc permeameter may affect measurements, and seek to find acceptable air-entry tube radii. We ignore air compression, as seems appropriate for the small pressure changes involved.

The volumetric air flow rate, q_a, through the air-entry tube in Fig. 1 of radius r and length l is assumed to be described by Poiseuille's law:

$$q_a = (\pi r^4 / 8\eta_a) \Delta P / l \quad [20]$$

with η_a the viscosity of air and ΔP the pressure difference across the air-entry tube.

In order to keep Ψ_0 constant, we require $\Delta P \approx (z_2 - \Psi_0)\rho_w g$ with ρ_w the density of water, z_2 given in Fig. 1, and g acceleration due to gravity. The volumetric flow rate of air must also equal the volumetric flow rate of water, q_w, from the device. In the initial stages of infiltration

$$q_w = (\pi R^2/2) S_0 t^{-1/2} \quad [21]$$

While in the later stages of infiltration

$$q_w = \pi R^2 K_0 \quad [22]$$

with R the radius of the disc.

Equating Eq. [20] with Eq. [21] and [22] for short infiltration times gives

$$t = 64\eta_a^2 R^4 S_0^2 / [(z_2 - \Psi_0)^2 \rho_w^2 g^2 r^8] \quad [23]$$

and for long infiltration times,

$$t = 8\eta_a R^2 K_0 l / [(z_2 - \Psi_0)\rho_w g] r^4. \quad [24]$$

We see in Eq. [23] that for $t \to 0$ there will be a small period where air-entry tubes of any reasonable dimensions must impede flow. It is sensible, however, to ask whether this is also the case at times of, say, $t = 1$ s. Using this time and typical values of $l = 0.2$ m, $z_2 = 0.01$ m, $\Psi_0 = 0$, Eq. [23] becomes

$$r \approx 2 \times 10^{-2} (R^2 S_0)^{1/4}. \quad [25]$$

For $R = 0.1$ m and $S_0 \approx 10^{-3}$ m s$^{-1/2}$ we find from Eq. [25] that the air-entry tube radius necessary to permit constant Ψ_0 at $t \gg 1$ s is 1.1 mm. The 3- to 4-mm diam. tubes we have used for $R \approx 0.1$ m are therefore adequate.

As steady state is approached, for typical values given above, Eq. [24] reduces to

$$r \approx 2 \times 10^{-2}(R^2K_0)^{1/4} \quad [26]$$

With the maximum $K_0 \approx 10^{-4}$ m s^{-1} and $R = 0.1$ m, Eq. [26] gives $r \approx 0.6$ mm, which is naturally less stringent than that for flow governed by capillarity. Note that Eq. [23] may also be used to find the time t_r given r, at which air entry no longer influences Ψ_0.

We now illustrate the performance of disc permeameters in the field in the one-dimensional mode.

FIELD PERFORMANCE OF THE DISC PERMEAMETERS

Membrane Conductance

In order to measure the membrane conductance, disc permeameters (Fig. 1) were set up as falling head permeameters by opening the reservoir stopcock. The conductance of several composite membranes using the 63-μm nylon mesh was found to be 0.066 ± 0.005 s^{-1}. This is nearly twice the conductance of the porous glass plates, 0.034 ± 0004 s^{-1}, used by Clothier and White (1981) in the sorptivity tube. We note that both measured conductances satisfy our approximate criterion Eq. [13] that $\alpha \geq 0.03$ s^{-1}.

Comparison of Disc Permeameter and Sorptivity Tube in the Field

Eight one-dimensional side-by-side comparison tests between the disc permeameter with a diameter of 200 mm and an 85.5-mm diam. sorptivity tube of Clothier and White (1981) were performed on a 2-m^2 site. Tests were conducted at the Bungendore fine sand field site described by Clothier and White (1981), where sorptivities are known to be high. We expect here to test the adequacy of the conductance of the supply membrane. The supply potential was −35 mm H_2O. No contact material was necessary. Typical results for the initial stages of infiltration for both devices are shown in Fig. 7.

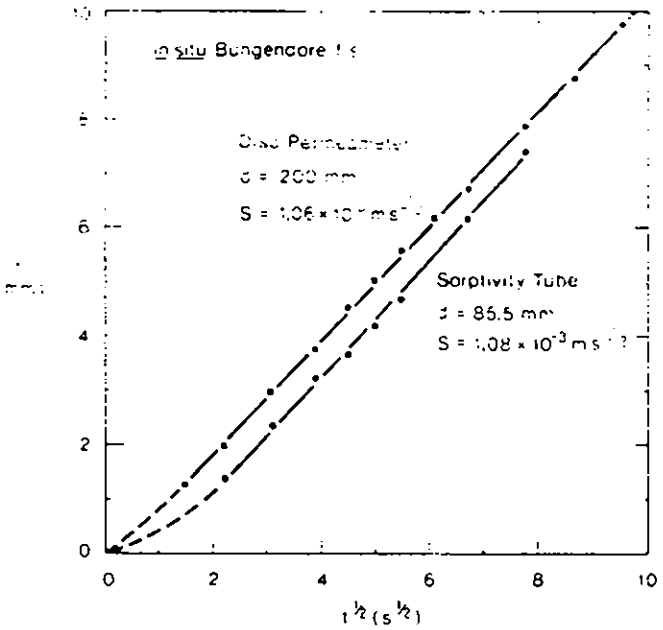

Fig. 7. Comparison of disc permeameter and sorptivity tube. Cumulative infiltration as a function of square root of time for early stages of infiltration.

Table 1. Comparison of mean sorptivities from disc permeameter and sorptivity tube. In situ Bungendore fine sand, $\theta_n = 0.020$ ± 0.002, $\Psi_0 = -0.035$ m.

	d	$10^3 S_0$	$10^3 \sigma$	CV	n
	m	m s$^{-1/2}$		%	
Disc	0.200	9.56	1.32	13.8	8
Tube	0.0855	10.1	3.7	36.6	8

Nonlinear $i(t^{1/2})$ behavior in Fig. 7 similar to that predicted in Fig. 5 is discernible in the early time portion of the results of both devices. It is more pronounced for the sorptivity tube. Using Eq. [13], the measured values of S_0, $\lambda = 0.1$ m and values of $t_{0.5}^{1/2}$ of 1.5 s$^{1/2}$ and 2.24 s$^{1/2}$ for the disc and the tube, respectively, we find estimates of conductance for the two membranes to be 0.071 and 0.045 s^{-1}, reasonably close to the directly measured values above. We note, however, that for the hypodermic needles used in the tube, Eq. [23] predicts that air flow should be limiting for the sorptivity tube for $t^{1/2} \approx 4$ s$^{1/2}$.

The arithmetic mean sorptivities found for both devices at this site are given in Table 1 together with their standard deviations and coefficients of variation. There is no significant difference (99% level) between the means irrespective of whether the distribution function is normal or lognormal. The 2.7 times reduction in coefficient of variation with the 2.3 times increase in sample diameter for the disc permeameter is not unexpected.

Despite the difference in membrane conductance of the two devices coupled with air-entry limitations in

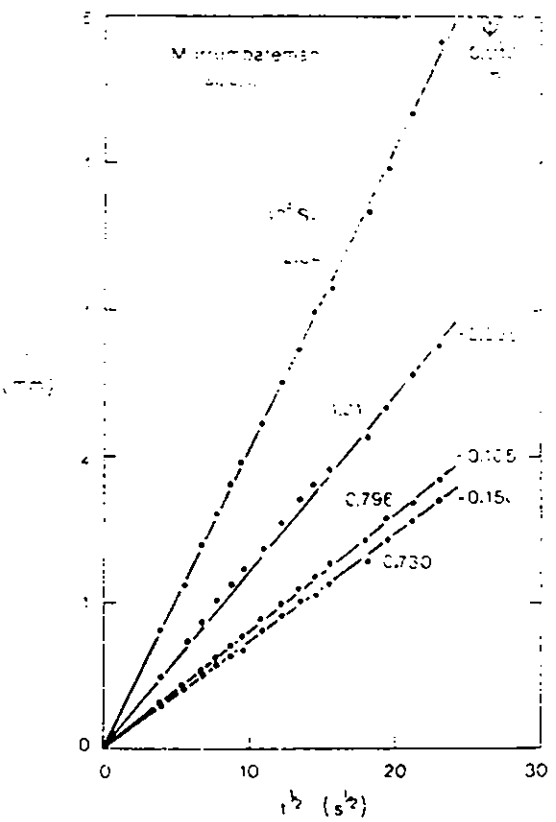

Fig. 8. Effect of supply potential on early stages of infiltration into an intact field soil sample, Murrumbateman silty clay loam. Measurements performed on the same air-dried sample.

Table 2. Effect of water supply potential on coefficient of variation of sorptivity.†

Ψ_0‡	$10^3 S$‡	$10^3 \sigma$‡	CV
m	m s$^{-1/2}$		%
−0.01	2.37	0.692	29.2
−0.035	1.35	0.235	17.5
−0.105	1.04	0.186	17.8
−0.150	1.01	0.179	17.7

† Intact samples. Murrumbateman silty clay loam, θ_n = 0.03, n = 20.
‡ Data from White and Perroux (1987).

the sorptivity tube, which, in Fig. 7, influence the very early stages of absorption, the mean sorptivities in Table 1 are identical. The larger disc permeameter does, however, give a lower coefficient of variation.

Supply Potential and Unsaturated Sorptivity

The effect of supply potential on the early stages of field infiltration is illustrated in Fig. 8 for four Ψ_0 in the range $-0.15 \leq \Psi_0 \leq -0.01$ m. Measurements were taken on the *same* undisturbed sample, which was air-dried back to the original $\theta_n = 0.03$ before each measurement. The soil is a pasture site, Murrumbatemen silty clay loam (Haplustalf). We discuss the use of such measurements to determine field hydraulic properties elsewhere (White and Perroux, 1987). Bungendore fine sand was used as the contact material.

The dramatic increase in sorptivity as Ψ_0 approaches zero is evident in Fig. 8. For the two lower supply potentials, −0.105 and −0.15 m, the difference is much less dramatic. This indicates the absence of significant numbers of macropores capable of filling at these potentials.

Note here that time zero was taken as the time when water passed through the contact material. The 5-mm

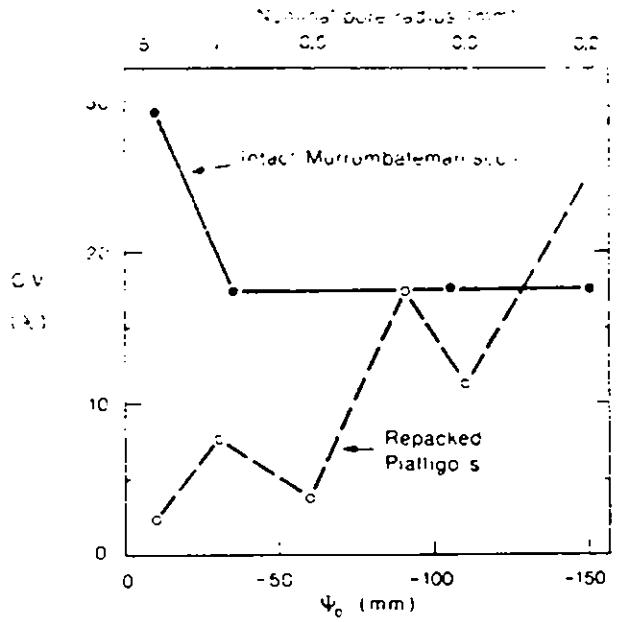

Fig. 9. Effect of supply potential on coefficient of variation (CV) of sorptivity for intact samples of Murrumbateman silty clay loam. Also shown for comparison are the CVs for vertical columns of repacked Pialligo sand and nominal radii for soil pores that fill with water at the supply potential. Data from White and Perroux (1987).

contact layer does not seem to have influenced the flows in Fig. 8 appreciably. Had it done so, these plots would not be linear with $t^{1/2}$.

Supply Potential and Coefficient of Variation of Sorptivity

White and Perroux (1987) have tabulated the influence of Ψ_0 on mean sorptivities for 20 intact samples of Murrumbateman silty clay loam. Measurements at four supply potentials were carried out on each sample. The mean values reflect the trends evident in Fig. 8. It is of interest to examine how their coefficients of variation (CVs) change with supply potential. We list these in Table 2 and plot them in Fig. 9 as a function of Ψ_0. Also shown in Fig. 9 is the nominal pore radius that just fills with water at the Ψ_0 in question.

It must be recalled that the CVs in Fig. 9 and Table 2 for each Ψ_0 come from a single set of soil samples, not four replicates. The stabilization of CV evident for $\Psi_0 \leq -40$ mm suggests that below this pressure variation in sorptivity is either due to the inherent soil variability or to measurement error. Above −40 mm a considerable portion of the variation seems due to macropores or preferential flow paths.

Clothier et al. (1981) assumed a "Swiss'cheese" type model of the soil in which the soil was viewed as being composed of a relatively uniform soil matrix interspersed with macropores of radius $\geq$ 0.75 mm (ant holes), equivalent to $\Psi_0 \approx -40$ mm. At the time we recognized the gross simplification of this model but it fitted our measurements of rainfall infiltration surprisingly well. The data in Fig. 9 may support this "Swiss-cheese" model, at least for the Murrumbateman site.

In order to put these results in some perspective, we show a comparison, in Fig. 9, with CV data for sorptivity of repacked vertical columns of Pialligo sand (Ustochrept), White and Perroux, 1987. Measurement procedures for these were identical to those for intact soil. We note that for $\Psi_0 \geq -60$ mm the repacked samples have CVs of order 5%, typical of laboratory results. At lower supply potentials, however, the CVs bracket those of the field soil. Thus, the experimental uncertainty in the repacked soil in the laboratory matches that for the intact field soil for measurements made under identical conditions for $\Psi_0 \geq -60$ mm. This seems to imply that topsoil matrix of the Murrumbateman site is indeed pedologically uniform, as soil survey suggests (J. Loveday, 1985, personal communication), and that observed variations in flow at Ψ_0 close to zero are due mostly to preferential flow paths in the soil matrix.

Ponded vs. Unsaturated Measurements

In order to assess the complete influence of macropores and preferential channels on flow as well as alterations brought about by management practices, it is necessary to compare ponded with unsaturated measurements.

We list in Table 3 such a comparison for 40 side-by-side pairs of in situ ponded and unsaturated sorptivity measurements made using devices shown in Fig. 1 and 3. These measurements were taken along a 72-m transect at a pasture site on Raintree silty loam

Table 3. Comparison of ponded and unsaturated sorptivities.†

	Ponded	Unsaturated
Ψ_0 (m)	+0.008	−0.02
$10^4 S_+$ (m s$^{-1/2}$)	4.47	1.45
$10^4 \sigma$ (m s$^{-1/2}$)	2.79	0.472
CV (%)	62.4	32.5
n	40	40

† In situ Raintree silty loam. θ_n = 0.110 ± 0.008, θ_s = 0.524 ± 0.040. d = 0.200 m.

(Ustifluvent) near Cowra, New South Wales. Ponded and unsaturated measurements were performed with Ψ_0 of +0.008 and −0.02 m using 0.2-m diam. samples. The measurements were spatially uncorrelated.

The arithmetic mean sorptivity for the ponded condition is three times that of the unsaturated value in Table 3 and the difference is highly significant (99% level). This significant difference also applies if we assume that the data are lognormally distributed. This threefold change brought about by a 28-mm change in supply head is obviously due to macropores whose nominal diameters are >1.5 mm (equivalent to Ψ_0 = −0.02 m).

Table 3 also shows a marked increase in coefficient of variation in going from negative to positive Ψ_0, which is commonly observed (Clothier and White, 1981).

Saturated Hydraulic Conductivity and Mean Pore Size from Sorptivity Measurements

The mean sorptivities in Table 3 can be used to estimate the saturated hydraulic conductivity, K_s, and the macroscopic capillary length, λ. Following White and Perroux (1987), K_s is given, to a good approximation, by

$$K_s = (S_+ - S_-)^2/[2\Delta\theta_s\Delta\Psi]\,. \qquad [27]$$

where the subscripts + and − refer to positive and negative supply heads, $\Delta\Psi$ is the difference in heads and $\Delta\theta_s = \theta_s - \theta_n$, with $\theta_s = \theta(\Psi \geq 0)$. Using Eq. [27] and the values in Table 3, we find $K_s = 3.9\ \mu m\ s^{-1}$. The capillary length follows from White and Sully (1987):

$$\lambda \approx 1.1(\Delta\Psi)/[(S_+/S_-)^2 - 1]\,. \qquad [28]$$

Philip (1987) has shown that λ is related to a flow-weighted characteristic pore size, λ_m, of the soil with

$$\lambda_m = 7.4/\lambda\,, \qquad [29]$$

where λ_m and λ are in millimeters. We have demonstrated that λ_m calculated from Eq. [28] and [29] give physically realistic estimates of mean pore sized (White and Sully, 1987).

The mean sorptivities in Table 2 together with Eq. [28] and [29] give λ = 3.6 mm and λ_m = 2.0 mm for this site. This λ_m is large and reflects the dramatic effect of macropores on flow under ponded conditions.

CONCLUDING COMMENTS

We have presented here designs for positive and negative supply-head disc permeameters. The effects of the water supply membrane, the soil capping material, and the air-entry delivery system have been estimated for the negative head permeameter, and criteria for their selection and control have been given. In addition, they can be used to delineate situations for which the device is limiting.

In demonstrating the field use of disc permeameters, we have concentrated on one-dimensional sorptivity measurements. While regarded by some as a largely unimportant hydraulic property, we have been able to demonstrate the use of sorptivity in estimating field hydraulic properties such as saturated hydraulic conductivity, as shown in this work and elsewhere (White and Perroux, 1987), and in estimating characteristic mean pore sizes of field soils (White and Sully, 1987). In addition, we have demonstrated a "deterministic" contribution to perceived variability brought about by small changes in supply potential.

These permeameters are particularly useful in following management or natural changes in soil properties. We and our colleagues have used them extensively since 1982 to assess the alteration of soil by management and tillage practices.

The use of disc permeameters in three-dimensional flow measurements that involve minimal soil disturbance will be reported elsewhere.

ACKNOWLEDGMENT

We gratefully acknowledge the assistance and advice of many colleagues, particularly M.J. Sully of the CSIRO Division of Environmental Mechanics, G.J. Hamilton of the Western Australia Department of Agriculture, I.J. Packer and B. Murphy of the New South Wales Soil Conservation Service, and M.D. Melville of the University of New South Wales, in the field testing of these permeameters. We thank B.E. Clothier, Department of Scientific and Industrial Research, Plant Physiology Division, New Zealand, for helpful discussion, and J.R. Philip for his interest in this work. The work was supported by Australian Water Research Council under Grant 84/157.

APPENDIX

Effect of Supply Membrane on Water Absorption

For a membrane of constant conductance, α, and supply potential, Ψ_m, the time-dependent surface flux through the membrane, $v_0(t)$, follows from Smiles et al. (1982):

$$v_0(t) = \alpha[\Psi_m - \Psi_1(t)]\,. \qquad [A1]$$

with $\Psi_1(t)$ the time dependent water-potential at the membrane/soil interface. For simplicity we write $v_0 = v_0(t)$ and $\Psi_1 = \Psi_1(t)$. The solution of Smiles et al. (1982) may be rewritten in terms of potential to give:

$$v_0 = \int_{\Psi_n}^{\Psi_1} [(\theta - \theta_n)K(\Psi)/F(\Psi,\Psi_1,\Psi_n)]d\Psi = \frac{1}{2}di^2/dt\,, \qquad [A2]$$

with θ volumetric water content, $\theta_n = \theta(\Psi_n)$, and $F(\Psi,\Psi_1,\Psi_n)$ the dimensionless soil-water flux (Philip, 1973). The solution is completed by recalling (Knight, 1983)

$$t = \int_0^i \frac{1}{v_0}\,di' = \int_{\Psi_n}^{\Psi_1} \frac{1}{v_0(\Psi_1')}\,\frac{di}{d\Psi_1'}\,d\Psi_1'\,. \qquad [A3]$$

Equation [A1] gives v_0 as a function of Ψ_1 which, together

with [A2], gives $i(\Psi_1)$. Both combined in Eq. [A3] give $\Psi_1(t)$, and hence $i(t)$, $v_0(t)$, and di^2/dt.

It is more efficient to rewrite the solution in terms of the dimensionless variables

$$\Psi_* = \Psi/\lambda,\ t_* = t/\tau,\ v_{*_0} = v_0/K_0,\ i_* = i/\Delta\theta\lambda,$$

$$\text{and } \alpha_* = \alpha\lambda/K_0. \qquad [A4]$$

Here λ is given by Eq. [6], $\tau = \Delta\theta\lambda/K_0$ and $\Delta\theta = \theta_0 - \theta_n$.

In addition, we assume that $F(\Psi,\Psi_1,\Psi_n)$ in Eq. [A2] is given by

$$F(\Psi,\Psi_1,\Psi_n) = (\theta - \theta_n)/(\theta_1 - \theta_n) \qquad [A5]$$

with $\theta_1 = \theta(\Psi_1)$. We know that Eq. [5] represents a lower-bound estimate for F (Philip, 1973; White, 1979). This assumption gives directly (White and Sully, 1987):

$$\lambda = S_s^2/[2\Delta\theta_i K_s], \text{ and } \tau = \tfrac{1}{2}[S_s/K_s]^2 \qquad [A6]$$

with $S_s = S_0$ at $\Psi_n = 0$, and $\Delta\theta_i = \theta_i - \theta_n$ with $\theta_i = \theta(\Psi = 0)$.

Using Eq. [A5], the dimensionless variables Eq. [A4] and the exponential K, Eq. [5], the solutions Eq. [A1] and [A2] become in dimensionless form:

$$v_{*_0}^2/\alpha_* = \Psi_{*_0} - \Psi_{*_1} \qquad [A7]$$

and to a first approximation,

$$\frac{1}{2}\frac{di^2}{dt_*} \approx [\exp(\Psi_{*_1}) - \exp(\Psi_{*_0})]\Theta_* = i_* \cdot v_{*_0} \qquad [A8]$$

with $\Theta_* = (\theta_0 - \theta_n)/\Delta\theta$. Substituting Eq. [A7] in [A8] produces

$$\alpha_* i_* = 2[\exp(\Psi_{*_1}) - \exp(\Psi_{*_0})]/(\Psi_{*_0} - \Psi_{*_1}) \qquad [A9]$$

Using Eq. [A7] and [A9] in Eq. [A3] results in

$$\alpha_* i_* = \Theta_* \int_{\Psi_{*_0}}^{\Psi_{*_1}} \frac{(\Psi_{*_0} - \Psi_{*_1})\exp(\Psi_{*_1}) - \exp(\Psi_{*_0})]d\Psi_*}{(\Psi_{*_0} - \Psi_{*_1})^2}$$

Now for the exponential $K(\Psi)$ in Eq. [5] together with Eq. [A5] and taking $\Psi_* \to -\infty$, we can show that the ratio of sorptivity at any Ψ to that at $\Psi = 0$ is just

$$(S_s/S_0)^2 = \exp(\Psi_{*_1}) = \Theta_* \qquad [A10]$$

Integrating Eq. [A10] for $\Psi_{*_0} \to -\infty$ and using Eq. [A11] yields

$$\left[\frac{S_s}{S_0}\right]^2 \alpha_* i_* = \frac{1}{2}\left[\frac{\exp(-\Delta\Psi_*)}{\Delta\Psi_*}(1 - \Delta\Psi_*) - E_1(\Delta\Psi_*)\right] \qquad [A12]$$

and we may rewrite Eq. [A7] and [A9] as

$$v_{*_0} = \alpha_* \Delta\Psi_* = di_*/dt_* \qquad [A13]$$

and

$$(S_s/S_0)^2 \alpha_* i_* = \exp(-\Delta\Psi_*)/\Delta\Psi_*. \qquad [A14]$$

Here $\Delta\Psi_* = \Psi_{*_0} - \Psi_{*_1}$ and $E_1(x)$ is the exponential integral (Gautschc and Cahill, 1972). Substituting Eq. [A13] and [A14] in Eq. [A12], we arrive at

$$(S_s/S_0)^2 \alpha_* i_* = \frac{1}{2}\{(S_s/S_0)^2 \alpha_* i_*[1 + \alpha_*/(di_*/dt_*)] - E_1[(di_*/dt)/\alpha_*]\} \qquad [A15]$$

and [A13] to [A15] constitute the approximate, analytic solution that we seek.

REFERENCES

Ahuja, L.R., and D. Swartzendruber. 1973. Horizontal soil-water intake through a thin zone of reduced permeability. J. Hydrol. 19:71–89.

Beven, K., and P. Germann. 1982. Macropores and water flow in soils. Water Resour. Res. 18:1311–1325.

Bouwer, H. 1964. Unsaturated flow in ground-water hydraulics. J. Hydraul. Div. Proc. Am. Soc. Civ. Eng. 90(HY5):121–144.

Chong, S.K., and R.E. Green. 1983. Sorptivity measurement and its application. p. 82–91. *In* Advances in infiltration. Proc. Natl. Conf. Advances in Infiltration. Chicago, IL. 12–13 Dec. ASAE, St. Joseph, MI.

Clothier, B.E., and I. White. 1981. Measurement of sorptivity and soil water diffusivity in the field. Soil Sci. Soc. Am. J. 45:241–245.

Clothier, B.E., and I. White. 1982. Water diffusivity of a field soil. Soil Sci. Soc. Am. J. 46:155–158.

Clothier, B.E., I.White, and G.J. Hamilton. 1981. Constant-rate rainfall infiltration: Field experiments. Soil Sci. Soc. Am. J. 45:245–249.

Dirksen, C. 1975. Determination of soil water diffusivity by sorptivity measurement. Soil Sci. Soc. Am. Proc. 39:22–27.

Dixon, R.M. 1972. Controlling infiltration in biomodal porous soils: Air-earth interface concept. Proc. 2nd Symp. Fundam. Transp. Phenom. Porous Media. 1:102–117.

Dixon, R.M. 1975. Design and use of closed-top infiltrometers. Soil Sci. Soc. Am. Proc. 39:755–763.

Gautschi, W., and W.F. Cahill. 1972. Exponential integral and related functions. p. 227–254. *In* M. Abramowitz and I.A. Stegun, (ed.) Handbook of mathematical functions. Dover Publ. Inc., New York.

Hamilton, G.J., I. White, B.E. Clothier, D.E. Smiles, and I.J. Packer. 1983. The prediction of time to ponding of constant intensity rainfall. J. Soil Conserv. N.S.W. 39:188–195.

Knight, J.H. 1983. Infiltration functions from exact and approximate solutions of Richards' equation. p. 24–33. *In* Advances in infiltration. Proc. Natl. Conf. Advances in Infiltration. Chicago, IL. 12–13 Dec. ASAE, St. Joseph, MI.

Packer, I.J., G.J. Hamilton, and I. White. 1984. Tillage practices to conserve soil and improve soil conditions. J. Soil Conserv. N.S.W. 40:78–87.

Passioura, J.B. 1983. Roots and water economy of wheat. p. 185–196. *In* W. Day and R.K. Atkin (ed.) Wheat growth and modelling. Plenum Publ. Corp., New York.

Philip, J.R. 1957. The theory of infiltration. 4. Sorptivity and algebraic infiltration equations. Soil Sci. 84:257–264.

Philip, J.R. 1966. A linearization technique for the study of infiltration. p. 471–478. *In* R.E. Rijtema and H. Wassink (ed.) Water in the unsaturated zone. Proc. Int. Assoc. of Scientific Hydrologists/UNESCO Symp., Vol. 1., Wageningen, 19–23 June. UNESCO, Paris.

Philip, J.R. 1969. Theory of infiltration. Adv. Hydrosci. 5:215–296.

Philip, J.R. 1973. On solving the unsaturated flow equation: 1. The flux-concentration relation. Soil Sci. 116:328–355.

Philip, J.R. 1975. Stability analysis of infiltration. Soil Sci. Soc. Am. Proc. 39:1042–1049.

Philip, J.R. 1983. Infiltration in one, two, and three dimensions. p. 1–13. *In* Advances in infiltration. 12–13 Dec. Proc. Natl. Conf. on Advances in Infiltration. Chicago, IL. ASAE, St. Joseph, MI.

Philip, J.R. 1985. Reply to "Comments on steady infiltration from spherical cavities." Soil Sci. Soc. Am. J. 49:788–789.

Philip, J.R. 1987. The quasilinear analysis, the scattering analog, and other aspects of infiltration and seepage. p. 1–27. *In* Y.-S. Fok (ed.) Infiltration development and application. Water Resources Res. Centre, Honolulu.

Raats, P.A.C. 1973. Unstable wetting fronts in uniform and nonuniform soils. Soil Sci. Soc. Am. Proc. 37:681–685.

Smiles, D.E., and A.G. Harvey. 1973. Measurement of moisture diffusivity in wet swelling systems. Soil Sci. 116:391–399.

Smiles, D.E., J.H. Knight, and K.M. Perroux. 1982. Absorption of water by soil: The effect of a surface crust. Soil Sci. Soc. Am. J. 46:476–481.

Talsma, T. 1969. In situ measurements of sorptivity. Aust. J. Soil Res. 7:269–276.

Walker, J., and S.K. Chong. 1986. Characterization of compacted soil using sorptivity measurements. Soil Sci. Soc. Am. J. 50:288–291.

Watson, K.W., and R.J. Luxmoore. 1986. Estimating macroporosity in a forest watershed by use of a tension infiltrometer. Soil Sci. Soc. Am. J. 50:578–582.

White, I. 1979. Measured and approximate flux-concentration relations for absorption of water by soil. Soil Sci Soc. Am. J. 43:1074–1079.

White, I., and K.M. Perroux. 1987. Use of sorptivity to determine field soil hydraulic properties. Soil Sci. Soc. Am. J. 51:1093–1101.

White, I., and M.J. Sully. 1987. Macroscopic and microscopic capillary length and time scales from field infiltration. Water Resour. Res. 23:1514–1522.

White, I., B.E. Clothier, and D.E. Smiles. 1982. Pre-ponding constant-rate rainfall infiltration. p. 127–48. *In* V.P. Singh (ed.) Modeling components of hydrological cycle. Proc. Int. Symp. Rainfall-Runoff Modeling, Mississippi State, MS. 18–21 May 1981. Water Resources Publ., Littleton, CO.

Wilson, G.V., and R.J. Luxmoore. 1988. Infiltration, macroporosity, and mesoporosity distributions on two forested watershed. Soil Sci. Soc. Am. J. 52:329–335.